GRANT AGREEMENT N°223866

Deliverable	D05.03
Nature	Report
Dissemination	Public

D05.03 - Modulation and routing protocols for wireless control systems

Report Preparation Date	31/03/2011 Project month: 30
Authors	Juan Jiménez, David Muñoz de la Peña, Rafael Estepa, and Fabio Gómez-Estern US Jonathan Jaglin, Carlos Canudas de Wit, and Alireza Farhadi, INRIA Piergiuseppe Di Marco, KTH
Report Version **Doc ID Code**	V1 USIR_D5.3_310311_V1
Contract Start Date : **Duration :** **Project Coordinator :**	01/09/2008 41 months Carlos CANUDAS DE WIT, INRIA, France

Theme 3:

Information and Communication Technologies

SUMMARY

This document summarizes the progress made in four research lines related to modulation and routing protocols for wireless control systems with energy-limited resources.

First, a report entitled “Timely, reliable and energy efficient routing over wireless sensor networks” proposes an energy-efficient protocol for control applications over WSNs based on the IEEE 802.15.4 standard. This protocol allows the network to adapt dynamically to requirements variations typical of controllers.

The second section of this report, entitled “Energy efficient configuration of 802.11e networks subject to QoS requirements” deals with configuration of 802.11 MAC parameters with the aim of achieving maximal energy efficiency while minimum QoS requirements are satisfied.

The third part, “Min-Max Model Predictive Power Control Strategy for CDMA Cellular Networks” deals with the uplink power control problem within CDMA cellular networks and proposes a model predictive control (MPC) strategy to compensate the channel fading uncertainties.

The fourth part, entitled “Dwell-Time Adaptive Delta Modulation SignalCoding For Networked Controlled Systems” deals with the problem of control with limited data rates in the area of Networked Controlled Systems (NCS) and looks for a new adaptive quantization algorithm that reaches global stability for multivariable systems, while minimizing the required bandwidth, and has a smooth transient behavior.

Contents

1 Introducction **5**

2 Timely, reliable and energy efficient routing over wireless sensor networks **6**
2.1 Background 7
2.2 System Model 8
2.3 TREnD Protocol Stack 9
2.4 Protocol Optimization 11
2.4.1 Energy Consumption 12
2.4.2 Reliability Constraint 12
2.4.3 Latency Constraint 14
2.4.4 Protocol Optimization 14
2.5 Protocol Operation 15
2.6 Experimental Implementation and Validation 15
2.6.1 Performance Comparison 16
2.6.2 Dynamic Adaptation 17

3 Energy efficient configuration of 802.11e networks subject to QoS requirements **21**
3.1 Problem statement 22
3.1.1 Framework assumptions 23
3.2 Analytical model of 802.11 24
3.2.1 Power consumption 26
3.2.2 QoS Metrics 28
3.3 Model validation 29
3.3.1 Influence of background traffic on the real time application performance 30
3.4 Proposed algorithm 31
3.4.1 Estimator module 32
3.4.2 Calculator module 36
3.4.3 Decisor module 37
3.4.4 Algorithm summary 39
3.5 Numeric results 39

4 Min-Max Model Predictive Power Control Strategy for CDMA Cellular Networks **46**
4.1 Problem statement 47

4.1.1 Radio Link Model . . . 47
4.1.2 Radio Power Control Model for Prediction . . . 49
4.2 Min-Max MPC based power control . . . 50
4.2.1 Min-Max MPC Computation: a QP Formulation . . . 52
4.3 Simulations . . . 53
4.3.1 Uncertainty Bounds . . . 54
4.3.2 Benchmark Comparison . . . 54
4.3.3 Performance Assessment . . . 55
4.3.4 Results Analysis . . . 56

5 Dwell-Time Adaptive Delta Modulation SignalCoding For Networked Controlled Systems 61
5.0.5 Coding strategies . . . 61
5.0.6 Adaptive quantization . . . 62
5.0.7 Main contribution of the paper . . . 63
5.0.8 Paper organization . . . 66
5.1 Problem formulation . . . 67
5.2 The D-ZIZO algorithm for multivariable systems . . . 70
5.2.1 **The rotation matrix $\boldsymbol{T}(k)$** . . . 70
5.2.2 Further definitions for the D-ZIZO algorithm . . . 77
5.2.3 Description of the D-ZIZO . . . 79
5.3 Stability analysis: Without System Noise . . . 80
5.3.1 Standard mode transitions . . . 80
5.3.2 Transition to ZO due perturbations . . . 86
5.3.3 Main stability result . . . 87
5.4 The D-ZIZO algorithm in the presence of system noise . . . 88
5.4.1 Bounded noise . . . 89
5.5 Robustness to packet losses . . . 93

6 Conclusions and further work 96

A Refinement for energy expression 97
A.1 power consumption . . . 97
A.2 Energy efficiency . . . 98

B Modelling q under big buffer size assumption 100

1 Introducction

This report addresses four core issues related to the modulation and routing protocols for improving the energy efficiency in wireless networked control systems. The framework is that of a control system embedded in a wireless sensor network, where the sensors are assumed to be energy-limited, and hence the wireless transmission and routing policy must be optimally designed.

The fist part introduces a novel protocol for the class of industrial control applications in clustered multi-hop WSNs. TREnD is based on a simple algorithm that allows the network to adapt dynamically to requirements variations typical of controllers. It adopts a novel MAC solution based on sleeping discipline and a beacon mechanism, that offers high reliability and energy efficiency, and we assume a uniform distribution of sensing nodes throughout the network.

The second part proposes a centralized algorithm to maximize the energy efficiency in 802.11 wireless networks based on the dynamic tuning of the contention window size and the retry limit. Located at the Access Point (AP), the algorithm determines these optimal values and broadcast the result to stations so that they can update their configuration. Besides maximizing the energy efficiency, the joint control allows to meet QoS requirements. The benefits of this approach are especially significant in scenarios under limit load and noisy channel conditions.

The third part propose an open-loop min-max MPC strategy to the uplink radio power control problem for a CDMA cellular network assessed over time-varying channels. The new power control algorithm is shown to robustly compensate for channel fading uncertainty as well as to reduce the effect of interference. This is achieved by implementing a computationally efficient min-max MPC mechanism based on a simple model of the tracking error that is estimated at each sampling time from the local SINR.

The fourth part proposes a new adaptive differential coding algorithm for system controlled through digital networks with limited data rate. The proposed technique results in global stability for multivariable systems; while improves transient behavior and reaches the rate theoretical limits under constant length coding. These are achieved by introducing a Dwell-Time state in addition of Zoom-In and Zoom-Out classical modes. The Dwell-Time mechanism introduces a hysteretic effect that smooths out the periodic and oscillatory behavior observed in other approaches such as Zoom-In, Zoom-Out (ZIZO) quantizers

2 Timely, reliable and energy efficient routing over wireless sensor networks

Energy efficient wireless sensor networks (WSNs) are allowing us to exploit sensing, control, and actuation via wireless communication with potential significant effects in industrial and consumer applications. Designing WSNs for the class of control applications is challenging. Traditional applications (e.g., monitoring) need a high probability of success in the packet delivery (reliability). In addition to reliability, control applications ask also for timely packet delivery (latency). If reliability and latency constraints are not met, the correct execution of control actions concerning the phenomena sensed may be severely compromised, thus creating unstable control loops [44]. The protocol design is further complicated by the need of a parsimonious use of energy [105]. High reliability and low latency may demand significant energy expenditure, thus reducing the WSN lifetime. Controllers can usually tolerate a certain degree of packet losses and delay [101]: large delays are allowed for high reliable communication, low delays are instead required if the packet loss is high. In contrast to monitoring applications, for control applications there is no need to maximize the reliability. A trade-off between reliability and latency can be exploited to minimize the energy consumption.

we report the design of a routing protocol named TREnD. The acronym remarks the significant characteristics simultaneously embraced by the protocol as opposed to other solutions available from the literature: timeliness, reliability, energy efficiency and dynamic adaptation. TREnD is an energy-efficient protocol for control applications over WSNs. The distinctive property is that reliability and latency are flexible requirements incorporated in the design to boost the protocol performance. Control applications over wireless sensor networks (WSNs) require timely, reliable, and energy efficient communications. Cross-layer interaction is an essential design paradigm to exploit the complex interaction among the layers of the protocol stack and reach a maximum efficiency. Such a design approach is challenging because reliability and latency of delivered packets and energy are at odds, and resource constrained nodes support only simple algorithms. The TREnD protocol is a cross-layer protocol that embraces efficiently routing algorithm, MAC, data aggregation, duty cycling, physical layer aspects as existing modulation formats. The protocol parameters are adapted by an optimization problem, whose objective function is the network energy consumption, and the constraints are the reliability and latency of the packets. TREnD uses a simple algorithm that allows the network to meet the reliability and latency required by the control application while minimizing for energy consumption. TREnD is im-

plemented on a test-bed and compared to some existing protocols. Experimental results show good performance in terms of reliability, latency, low duty cycle, and load balancing for both static and time-varying scenarios.

2.1 Background

The standardization process for WSNs is ongoing and there is not any widely accepted complete protocol stack for WSNs [105], particularly concerning WSNs for control in industrial environments. The IEEE 802.15.4 protocol [48], which specifies physical layer and medium access control (MAC), is the base of recent solutions in industrial automation as WirelessHART and ISA100 [105]. Hence, we consider IEEE 802.15.4 as the reference standard in our investigation.

In Tab. 1, we summarize the characteristics of the main protocols for WSNs that may be used for control applications. From the table, we see that most of them (e.g., SPAN [24], GERAF [115], Dozer [14], ESRT [2], RMST [96], Flush [57], X-MAC [69], MMSPEED [36]) are designed mainly for monitoring applications, since do not support simultaneously energy efficiency, reliability and latency requirements. In standard solutions for industrial applications like WirelessHART [105], reliability and security are optimized but the energy efficiency is not a critical concern since nodes are fully powered. It follows that while all these solutions offer high performance in their class of application, they are not efficiently designed for the control problems we deal in this chapter.

In SERAN [1] and Breath [82] a relevant system-level design methodology has been presented for control application over WSNs. However, SERAN does not support average-high traffic regimes and tunable reliability requirements, which limits the performance of the protocol. Furthermore, load balancing and fair duty cycling are not taken into account in SERAN. On the other hand, Breath is limited to scenario with line topologies and source nodes at the edge of the network. We conclude that, to the best of our knowledge, there is no protocol from the literature suitable for control applications over WSNs, that is able to embrace all the techniques that concur to the energy efficiency (radio power control, MAC, routing, duty-cycling and load balancing) and, at the same time, able to guarantee reliability and latency constraints over multi-hop communication.

In this chapter we present TREnD, a novel protocol for the class of industrial control applications in clustered multi-hop WSNs. TREnD is based on a simple algorithm that allows the network to adapt dynamically to requirements variations typical of controllers. In contrast to SERAN and Breath, we adopt a novel MAC solution based on sleeping discipline and a beacon mechanism, that offers high

Table 1: Protocol Comparison - The letters **E**, **R**, and **L** denote energy, reliability and latency. The circle denotes that a protocol is designed by considering the indication of the column, but it has not been validated experimentally. The circle with plus denotes that the protocol is designed by considering the indication and experimentally validated. The dot denotes that the protocol design does not include indication and hence cannot control it, but simulation or experiment results include it.

Protocol	**E**	**R**	**L**	**Layer**
SPAN [24]	◯	·	·	MAC, routing
GERAF [115]	◯		◯	MAC, routing
Dozer [14]	⊕	⊕		MAC, routing
ESRT [2]		◯		MAC
RMST [96]		◯		MAC, transport
Flush [57]		⊕		MAC
XMAC [69]	⊕	·	·	MAC
MMSPEED [36]		◯	◯	Routing
SERAN [1]	◯		◯	MAC, routing
Breath [82]	⊕	⊕	⊕	Phy, MAC, routing
TREnD	⊕	⊕	⊕	Phy, MAC, routing

reliability and energy efficiency, and we assume a uniform distribution of sensing nodes throughout the network. An original analysis of the performance of TREnD is provided. Finally, TREnD is completely implemented on Tmote Sky sensors [75] by using TinyOS [40].

2.2 System Model

We consider a general scenario for an industrial control application: the state of a plant must be monitored at locations where electrical cabling is not available or cannot be extended, so that wireless sensor nodes are an appealing technology. The communication network must be energy efficient to guarantee long network lifetime. The sink of the network must receive packets from the single nodes with a desired probability of success and within a latency constraint demanded by the control application connected to the sink. Since control applications may need some reliability and delay during certain time interval, and a different pair

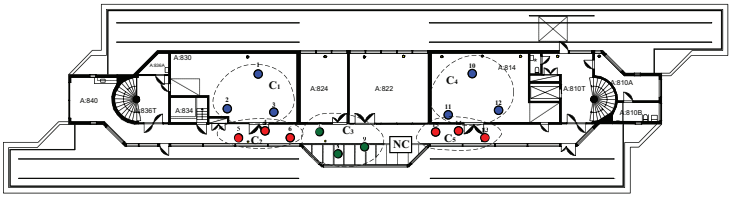

Figure 1: Experimental Setup.

of requirements during some other time interval, these reliability and latency requirements may change dynamically depending on the state of the plant and the history of the control actions.

Information taken by nodes, which are uniformly distributed in clusters, are sent to the sink node by multi-hop communication. The clustered topology is motivated by the energy efficiency, since transmitting data directly to the sink may consume more than routing through relays. The cluster formation problem has been thoroughly investigated in the literature and is out of the targets of this chapter (see, e.g., [79], [100]).

In Fig. 1, the system model is reported. Nodes are deployed in an indoor environment with rooms. Each dotted curve defines a cluster of nodes. Nodes of a cluster can send packets only to the nodes of next cluster toward the controller, which takes appropriate actions upon the timely and reliable reception of source information. Hence, nodes not only send their sensed data, but also forward packets coming from clusters further away from the sink. The network controller is the sink node, which, being a node of the networks, is equipped with light computing resources.

We assume that the controller knows cluster locations and the average number of nodes in each cluster, and nodes know to which cluster they belong. The controller can estimate the amount of data generated by each cluster, which is used to adapt the protocol to the traffic regime. These assumptions are reasonable in industrial environments [105].

2.3 TREnD Protocol Stack

In this section, we introduce the protocol stack of TREnD.

Similarly to SERAN [1], the routing algorithm of TREnD is hierarchically subdivided into two parts: a static route at inter clusters level and a dynamical routing algorithm at node level. this is supported at the MAC layer by an hybrid

time division multiple access and carrier sensing multiple access (TDMA/CSMA) solution.

The static schedule establishes which one is the next cluster to which nodes of a given cluster must send packets by calculating the shortest path from every cluster to the controller. The network controller runs a simple combinatorial optimization problem of latency-constrained minimum spanning tree generation [80]. Alternatively, if the number of clusters is large, the static routing schedule is precomputed off-line for a set of cluster topologies and stored in the sink node in a look-up array. No intra cluster packet transmission is allowed.

The static routing algorithm is supported at MAC level by a weighted TDMA scheme that regulates channel access among clusters. Nodes are awake to transmit and receive only during the TDMA-slot associated to the cluster for transmission and reception, respectively, thus achieving consistent energy savings. The organization of the TDMA-cycle must consider the different traffic regimes depending on the cluster location. Since clusters closer to the sink may experience higher traffic intensity, more than one transmitting TDMA-slot can be assigned to them. It is natural to first forward packets of clusters close to the controller, since this minimizes the storage requirement in the network. To minimize the global forwarding time, the evacuation of packets of a cluster is scheduled path-by-path. By following these rules, the controller is able to generate an appropriate TDMA scheduling table.

The dynamic routing is implemented by forwarding the packets to a node within the next-hop cluster in the path chosen at random, as proposed in [115] and [100]. In such an operation, no cluster-head node is needed within clusters, and nodes need to be aware only of the next-hop cluster connectivity. The procedure for random selection of next-hop node is performed by considering a duty cycling in the receiving cluster combined with beacon transmissions.

The communication stage between nodes during a TDMA-slot is managed at MAC layer by a *p*-persistent CSMA/CA scheme, to offer flexibility for the introduction of new nodes, robustness to node failures, and support for the random selection of next-hop node. As we will see in Sec. 2.6, in hybrid TDMA/CSMA solutions the *p*-persistent MAC gives better performance than the binary exponential backoff mechanism used by IEEE 802.15.4.

MAC operations of nodes are described in the following. Each node in the transmitter cluster having a packet to be sent wakes up in CSMA-slots with probability α and enters in listening state. At the receiver cluster, each node wakes up with probability β and multicasts a small length of beacon message to the nodes in the transmitter cluster. An awake node that correctly receives the beacon at the

transmitter side, senses the channel and, if clean, tries to unicast its packet to the beacon sender. An acknowledgement (ACK) may conclude the communication if a retransmission mechanism is implemented. If no beacon is sent or there is a collision, the awake nodes in the transmitter cluster keep on listening in the next CSMA-slot with probability α or go to sleep with probability $1 - \alpha$.

If we compare TREnD to SERAN [1], we see that SERAN has the drawback that nodes in the receiver cluster have to be listening for the overall TDMA-slot duration, due to a contention-based transmission of the ACKs. In TREnD, the selection of the forwarding nodes follows a random policy regulated by β. The main advantage of this novel solution is the absence of delays between packets exchange during a CSMA-slot. This allows TREnD to work with a much higher traffic regime when compared to SERAN.

TREnD offers the option of data aggregation to fairly distribute the traffic load and energy consumption among clusters. The aggregation has the advantage of reducing the number of TDMA-slots per cluster and of the traffic for clusters closer to the sink. However, packet aggregation gives significant advantages only when the traffic is sufficiently high, as we will see in Sec. 2.6, because nodes have to idle-listen longer to catch more than one packet per time and perform the aggregation, and idle-listening is energy inefficient.

2.4 Protocol Optimization

In this section, we pose and solve an optimization problem to select the TREnD protocol parameters by minimizing the overall energy consumption of the network under reliability and latency constraints:

$$\min_{S,\alpha,\beta} \quad E_{\text{tot}}(S,\alpha,\beta) \tag{1}$$

$$\text{s.t} \quad R(S,\alpha,\beta) \geqslant \Omega \tag{2}$$

$$\Pr[D(S,\alpha,\beta) \leqslant D_{\max}] \geqslant \Pi\,. \tag{3}$$

In this problem, $E_{\text{tot}}(S,\alpha,\beta)$ is the total energy consumption of the network and $R(S,\alpha,\beta)$ is the reliability constraint and Ω is the minimum desired reliability imposed by the control application. We denote by $D(S,\alpha,\beta)$ the random variable describing the distribution of the latency, by $D_{\max}$ the maximum latency desired by the control application, and by Π the minimum probability with which such a maximum latency should be achieved. The parameters Ω, $D_{\max}$, and Π are the requirements of the control application. The decision variables of the optimization problem are the TREnD parameters, namely the TDMA-slot duration S, the

access probability α and the wake up probability in reception β. In the following, we develop the expressions needed in the optimization problem, and derive the solution.

2.4.1 Energy Consumption

The total energy consumed by the network over a period of time is given by the combination of two components: listening and transmitting cost[1].

Listening for a time t gives an energy consumption that is the sum of a fixed wake up cost E_{w} and a time dependent cost $E_l t$. The energy consumption in transmission is given by four components: beacon sending E_{bc}, clear channel assessment E_{cca}, packet sending E_{pkt} and ACK sending E_{ack}.

Consider a general topology with N nodes per cluster and suppose that there are G paths in the static routing scheduling (recall Sec. 2.3). Let h_i be the number of clusters (hops) per path, we define $h_{\max} = \max_{i=1,\dots,G} h_i$. We define also W, as the number of listening TDMA-slots in a TDMA-cycle.

Recalling that the TDMA-cycle is $T_{\mathrm{cyc}} = SM_s$ where M_s is the number of TDMA-slots in a TDMA-cycle, we have the following result:

Claim 2.1 *Given traffic rate λ, the total energy consumed in a period T_{tot} is*

$$\begin{aligned} E_{\mathrm{tot}}(S,\alpha,\beta) =& \frac{T_{\mathrm{tot}}}{\gamma\, S} \sum_{j=1}^{\lambda T_{\mathrm{cyc}}} j\alpha\beta\, E_{\mathrm{cca}} + T_{\mathrm{tot}} M_s \lambda \left(E_{\mathrm{pkt}} + E_{\mathrm{ack}}\right) \\ &+ \beta\, \frac{N\, W\, T_{\mathrm{tot}}}{M_s} \left(\frac{E_{\mathrm{bc}}}{\delta} + \frac{E_{\mathrm{w}}}{S} + E_l\right) . \end{aligned} \tag{4}$$

Proof A proof is provided in [32].

2.4.2 Reliability Constraint

Considering the p-persistent slotted CSMA MAC and the duty cycling in reception, we have the following result:

Claim 2.2 *The probability of successful transmission in a CSMA-slot while there are k packets waiting to be forwarded in the cluster is*

$$p_k = \gamma\, p_{\mathrm{bc}} \left(1 - (1-\alpha)^k\right) (1 - p_{\mathrm{cl}})^{\alpha(k-1)} , \tag{5}$$

[1]Note that the costs for the initialization of the network are negligible in the energy balance

where $p_{\rm bc} = \gamma N \beta \, (1-\beta)^{N-1}$ *is the successful beacon probability and* $p_{\rm cl}$ *is the probability of an erroneous sensing of a node, when it competes with another node.*

Proof A proof is provided in [32].

In TREnD, a radio power control is implemented, so that the attenuation of the wireless channel is compensated by the radio power, which ensures a desired packet loss probability, as proposed in [82] and [70]. As a consequence of the power control, the channel can be abstracted by a random variable with good channel probability γ. Such a modelling has been adopted also in other related works (e.g., [1], [96]). Considering the collision probability $p_{\rm cl}$, we observe that for optimization purposes an upper bound suffices. Experimental results shows that a good upper bound is $p_{\rm cl} = 0.2$.

By using Claim 2.2, we can derive the following result:

Claim 2.3 *Let* $V(n) = \{1-p_n, 1-p_{n+1}, ..., 1-p_k\}$*, where* p_n *is the generic term given in Eq.* (5) *and* $A(n) = [a_{i,j}]_{M_c}^{S-k+n}$ *be a matrix containing all the* M_c *combinations with repetition of the elements in* $V(n)$*, taken in groups of* $S-k+n$ *elements. Let* $h_{\max}$ *be the maximum number of hops in the network. Then, the reliability of TREnD is*

$$R(S,\alpha,\beta) = \left(\sum_{n=0}^{k} \frac{k-n}{k} \prod_{l=n+1}^{k} p_l \left(\sum_{i=1}^{M_c} \prod_{j=1}^{S-k+n} a_{i,j} \right) \right)^{h_{\max}} . \tag{6}$$

Proof A proof is provided in [32].

With packet aggregation enabled, the following result holds:

Claim 2.4 *Let* h_i *be the number of hops in the path* i*. Let* R_z *be the reliability in a single hop when* z *packets are aggregated. The reliability of a packet that experiences* j *hops to the controller is*

$$R_j^{\rm ag}(S,\alpha,\beta) = R_{j-1}^{\rm ag} \, r_{B_i-j+1} \, , \tag{7}$$

where $r_j = \sum_{i=1}^{j} (1-r_{i-1}) \prod_{z=1}^{j-i+1} R_z$ *, with* $r_0 = 0$*.*

Proof A proof is provided in [32].

If the data aggregation is disabled or the size of aggregated packets does not change significantly, then we can simplify Eq. (7) and obtain the relation in Eq. (6). The previous claims are illustrated and verified by experiments in [32].

2.4.3 Latency Constraint

The furthest cluster from the controller is the one experiencing the highest latency. Therefore, the latency of packets coming from such a cluster must be less than or equal to a given value $D_{\max}$ with a probability Π.

Recalling that the maximum number of hops in the network is $h_{\max}$, an upper bound on the TDMA-slot duration S is $S_{\max} = D_{\max}/h_{\max}$. Then, we can provide the following result:

Claim 2.5 *The latency constraint in Eq.* (3) *is well approximated by*

$$\Pr[D(S,\alpha,\beta) \leqslant D_{\max}] \approx 1 - \frac{1}{2}\mathrm{erfc}\left(\frac{A-\mu}{\sigma}\right), \tag{8}$$

$$\text{where} \quad \mathrm{A} = \begin{cases} S & \text{if} \quad S \leqslant \frac{D_{\max}}{h_{\max}} \\ D_{\max} - (h_{\max}-1)S & \text{if} \quad S > \frac{D_{\max}}{h_{\max}} \end{cases}$$

$\mu = \sum_{j=1}^{k} 1/p_j$, *and* $\sigma^2 = \sum_{j=1}^{k}(1-p_j)/p_j^2$.

Proof A proof is provided in [32].

2.4.4 Protocol Optimization

In the previous subsubsection, we have established the expressions of the energy consumption in Eq. (4), the reliability in Eq. (7) and the latency constraint in Eq. (8). We observe that all this expressions are highly non-linear in the decision variables. Sensor nodes are not equipped with a high processing capacity to use these equations, therefore, we provide a computationally affordable sub-optimal solution to the optimization problem. In the following, we show that such a strategy still gives satisfactorily results.

First, we provide an empirical result on the access probability α and wake up probability β, for a given TDMA-slot duration S.

Claim 2.6 *Let N be the number of nodes is a cluster. Let λ be the traffic rate, the access probability α^* and the wake up probability β^*, that optimize the reliability in Eq.* (6)*, are*

$$\alpha^* = \frac{c_1}{\lambda\, S\, M_s + c_2} \qquad \beta^* = \frac{1}{N}\,. \tag{9}$$

with coefficients $c_1 = 2.17$, $c_2 = 1.81$.

Proof A proof is provided in [32].

We note here that such choices are sub-optimal because are limited to strategies with constant access and wake up probabilities per each node.

By using Eq. (9) for the access probability and wake up probability, and by assuming S as a real-valued variable, we can show that E_{tot}, given in Eq. (4), is a convex and monotonically decreasing function of S. It follows that a simple solution for the TDMA-slot duration, S^*, is given by the maximum integer value of S that satisfies one out of the two constraints in the problem (1), which are given explicitly by Eqs. (7) and (8), respectively. The search of the optimal S can be done by a simple additive increasing multiplicative decreasing algorithm, which we initialize by observing that $S^* \leqslant S_{\max}$. Indeed, as shown in Sec. 2.4.3, the maximum latency requirement $D_{\max}$ provides an upper bound for S, given by $S_{\max} = D_{\max}/h_{\max}$.

2.5 Protocol Operation

Suppose that the network user deploys a WSN of nodes implementing the TREnD protocol, and sets the desired control application requirements $\Omega, D_{\max}$ and Π. During an initial phase of operation the sink node retrieves the traffic and the cluster topology by the received packets. After computing or reading from a look-up array the static routing schedule and TDMA-cycle, the sink computes the optimal parameters as described in Sec. 2.4.4. Then, the sink communicates these values to the nodes of the network by tokens. Such a token passing procedure ensures synchronization among nodes and allows for initializing and self configuring of the nodes to the optimal working point of the protocol. The token are then forwarded by the nodes closer to the sink to other nodes of the clusters far away by using the ACK mechanism described in [1]. Such tokens need also to be updated so that our protocol adapts dynamically to new nodes added in the clusters, variations in the source traffic, control application requirements, and time drift of the clocks. We experienced that a 20 TDMA-cycles period for the refreshing procedure gives satisfactory performance to maintain an optimal network operation with negligible extra energy consumption.

2.6 Experimental Implementation and Validation

In this subsection, we present a complete implementation of TREnD by using TinyOS 2.x [40] and Tmote Sky nodes [75]. In order to benchmark our protocol, we implemented also SERAN [1] and IEEE 802.15.4 [48]. Recall that IEEE

802.15.4 is the base for WirelessHart and other protocols for industrial automation, and that there is no other protocol available from the literature that is energy efficient, and ensures reliable and timely packet transmission, as we summarized in Tab. 1. We used the default MAC parameters of IEEE 802.15.4 so that the protocol fits in the higher level TDMA structure and routing algorithm of SERAN and TREnD.

We reproduced the reference test-bed topology reported in Fig. 1, where clusters are placed in an indoor environment. Each cluster is composed by 3 sensors, deployed at random within a circle with one meter radius. We analyze different scenarios with different sets of traffic rate λ and control application requirements (Ω, $D_{\max}$, and Π), which we report in Tab. 2. For each scenario, Tab. 2 shows also the optimal TDMA-slot duration, access and wake up probabilities as obtained by the optimization in Sec. 2.4.4. We measured the duty cycle of nodes as indicator of the energy efficiency.

2.6.1 Performance Comparison

In the first set of experiments, we show the performance improvements in TREnD, when compared to SERAN. In Fig. 2, the reliability is reported as function of the traffic rate λ, by fixing $\Omega = \Pi = 95\%$, and $D_{\max} = 3,9$ s. TREnD has high reliability for all traffic rate conditions and SERAN is significantly outperformed. In particular with $D_{\max} = 3$ s, as traffic rate increases over $\lambda = 0.3$ pkt/s, the reliability of SERAN significantly decreases.

In Fig. 3 we compare the energy consumption of the two protocols, showing the average duty cycle of each node, for fixed $\Omega = \Pi = 95\%$, $D_{\max} = 3$ s and $\lambda = 0.3$ pkt/s. As discussed above, in this operative condition both SERAN and TREnD meet the reliability and latency constraints. By implementing TREnD with data aggregation, we observe a more balanced duty cycle among clusters, particularly for the last hop clusters. However, the price to pay for having a better load balancing is a slight increasing of the average duty cycle. In fact, TREnD presents a slightly higher duty cycle for most of the nodes, but it reduces of about 30% the energy consumption for nodes 7, 8 and 9 (cluster C_3), which are critical for the network operation since they also forward information from clusters C_1 and C_2. This suggests that packet aggregation is a viable choice only for the clusters supporting high traffic, as those next to the sink. Hence, it is recommended to implement packet aggregation only for those clusters, while for the others no aggregation is needed. In conclusion, TREnD ensures higher reliability, load balancing and a longer network lifetime than SERAN, without any significant difference in the complexity of the scheme.

Table 2: Application requirements and experimental results

Scenario	λ	$D_{\max}$	Π	Ω	S^*	α^*	β^*
$\mathcal{L}$	0.1 pkt/s	9 s	95%	95%	3.3 s	0.41	0.33
$\mathcal{H}$	0.3 pkt/s	3 s	95%	95%	1.2 s	0.43	0.33

Given these results, in the following performance evaluation of TREnD we disregard SERAN and consider IEEE 802.15.4. We present two sets of experimental results, evaluated for scenarios $\mathcal{L}$ and $\mathcal{H}$ as specified in Tab. 2. Fig. 4 reports the average values of reliability, latency and duty cycle as achieved by the experiments for TREnD and IEEE 802.15.4. Data of clusters belonging to the same paths are joined by lines. We see that TREnD always ensures the satisfaction of the reliability and latency constraints specified in Tab. 2. TREnD guarantees much better reliability, in particular for cluster C_1 (3 hops). In fact in C_1, IEEE 802.15.4 does not fulfill the requirement. The average latency of IEEE 802.15.4 is slightly lower than TREnD, but observe that the latency of IEEE 802.15.4 is computed only for packets arriving successfully at the sink. We observe similar behavior also for other scenarios.

Finally, we present some results about the duty cycle. According to the traffic load supported by the clusters and their allotted TDMA time slots, we observe that the duty cycle depends on the number of times a cluster wakes up for the forwarding procedure. The duty cycle is the same for the clusters far away from the sink (C_1 and C_4, see Fig. 1), but for all other clusters TREnD gives a consistent reduction of the duty cycle with respect to IEEE 802.15.4.

We remark here that the duty cycle strongly depends on the traffic load in the network. In Dozer [14], an average duty cycle 0.2% is achieved for a network of 40 nodes with a packet generation period of 120 s each (total traffic load $\simeq 0.3$ pkt/s). TREnD gives an average duty cycle 2.5%, but the total traffic load is much higher ($\simeq 5$ pkt/s) than Dozer.

2.6.2 Dynamic Adaptation

In the previous subsection, we used a static network topology where each node is placed at fixed position and the application requirements do not change with time. In this subsection, we show the dynamical behavior of the protocol. As we discussed before, no protocol in literature allows for a dynamical adaptation of the parameters to the application requirements.

We present the experimental results of dynamic changes between two scenar-

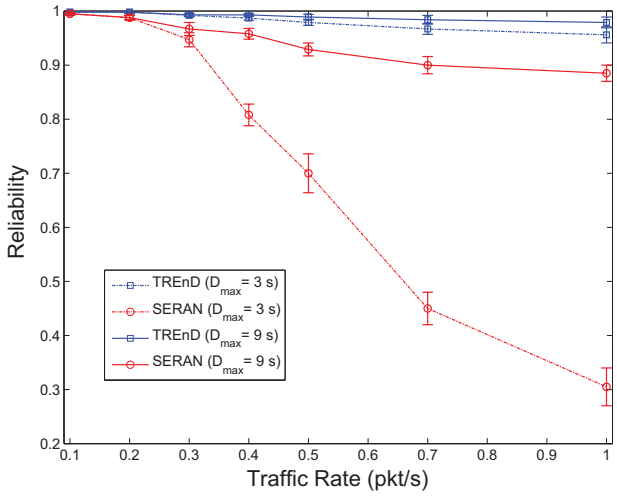

Figure 2: TREnD and SERAN: reliability vs. traffic rate λ, for $\Omega = \Pi = 95\%$.

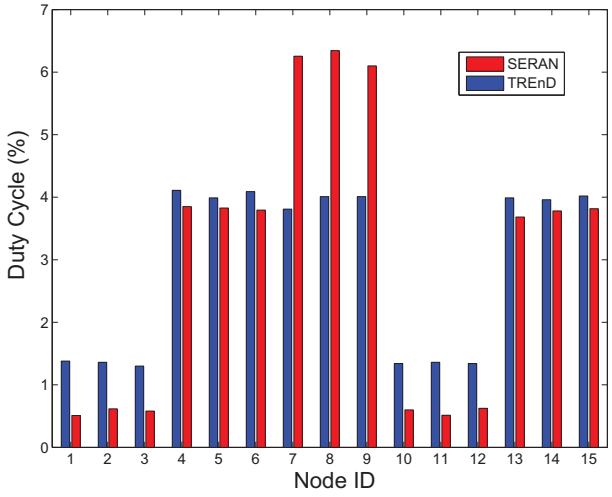

Figure 3: TREnD and SERAN: duty cycle distribution among nodes for $\lambda = 0.3pkt/s$, $\Omega = \Pi = 95\%$.

ios ($\mathcal{L}$ and $\mathcal{H}$ in Tab. 2) in static and time-varying channel conditions. A Rayleigh fading channel is obtained by moving the nodes around their initial position and also by placing metal obstacles in front of the source nodes so that the line-of-sight with the sink is lost. The network starts with scenario $\mathcal{L}$ and static channel, then after 20 TDMA-cycles we introduce a Rayleigh fading channel which per-

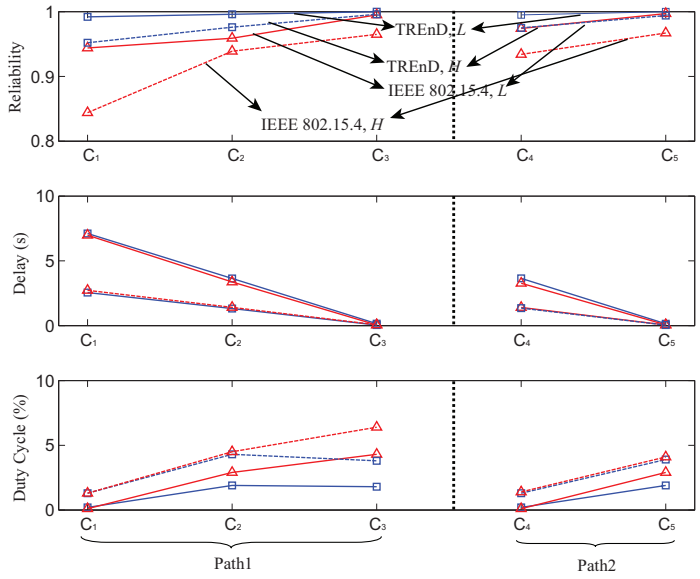

Figure 4: TREnD and IEEE 802.15.4: reliability, latency and duty cycle for scenarios $\mathcal{L}$ and $\mathcal{H}$.

sists until the TDMA-cycle 60. At TDMA-cycle 40, the application requirements change to scenario $\mathcal{H}$.

Figs. 5 and 6 report the resulting snapshot of the experiment in terms of reliability and latency. The reliability is measured at the sink node as average on each TDMA-cycle, while the latency is measured for each successfully received packet. In Fig. 5, we observe that TREnD guarantees the reliability requirement for both static and Rayleigh fading conditions, continuously adapting to the severe fading. The protocol is also robust to the change of scenario at TDMA-cycle 40. In Fig. 6 a snapshot of the latency is reported for clusters at different hops to the controller. We observe that the peaks of delay are limited due to the TDMA structure, the average and dynamics of the delay are slightly increasing in the time-varying stage but the latency constraint is fulfilled. Moreover, the protocol adapts well to the change of scenario at TDMA-cycle 40.

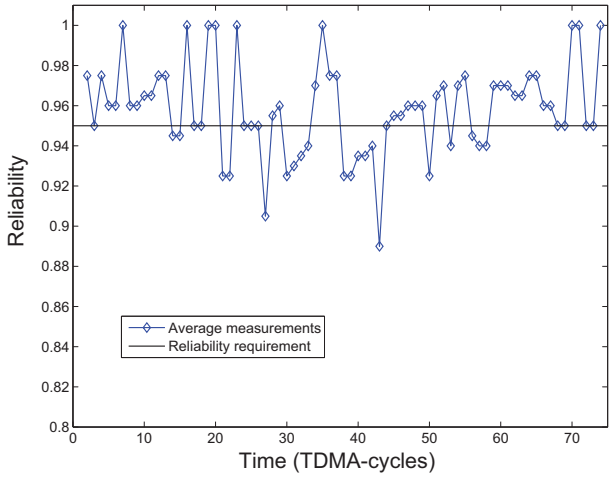

Figure 5: TREnD: Reliability trace given by the experiments.

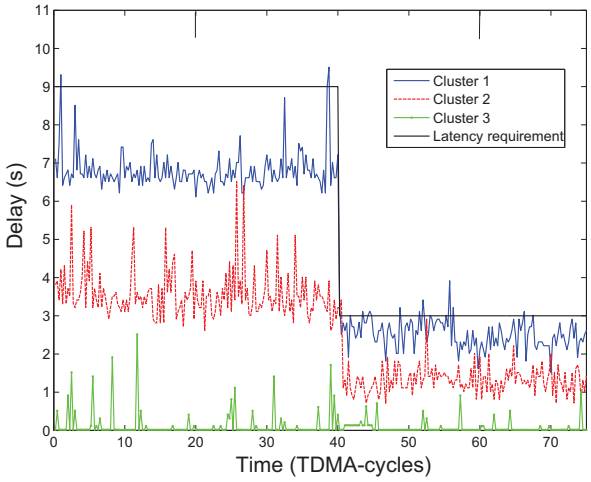

Figure 6: TREnD: Latency trace given by the experiments.

3 Energy efficient configuration of 802.11e networks subject to QoS requirements

Nowadays, IEEE 802.11 wireless networks can be used to provide real time services. While initial versions of 802.11 are not suitable to support real time applications with strict requirements of delay and packet loss, standard enhancements like QoS provisioning (802.11e) and MIMO technology (802.11n) become 802.11 an appropriate technology for such purpose [37, 85, 104, 106].

In wireless communications, energy is a valuable resource because devices are often powered by batteries. Therefore energy must be taken into account by the network designer in order to optimize its utilization. We are interested in extending the battery lifetime of wireless devices while maintaining a QoS level in communication. Since energy saving is at cross-purposes with QoS provisioning, we must analyze the tradeoff between both objectives. In this paper, we consider a scenario where wireless stations are attached to a central server and run VoIP applications demanding a constant bandwidth (generated by Constant Bit Rate codecs like G.711, G.729 and iLBC) and low packet loss and delay.

There are two complementary strategies to improve the energy efficiency of 802.11 networks. The first one is the use of the Power Saving Mode (PSM). This mechanism is adopted in several works that propose different adjustments of PSM parameters to reduce the power consumption of the stations. In [6] the authors find the listen Interval value which maximize the time that a station stay in sleep state while satisfying a certain quality of service. In [54] authors propose an adaptive mechanism to dynamically choose a suitable Ad hoc Time Message Interval (ATIM) window size, outperforming the default mechanism of power saving in terms of throughput and energy consumed. Unfortunately, PSM feature is not always available in 802.11 cards, hence an alternative mechanism to optimize the energy utilization should be considered. The second one is an appropriate setting of 802.11 MAC parameters like the contention window size and the retry limit, in order to maximize the energy efficiency in the wireless network. More precisely, in [67, 90, 103] authors derive the contention window size that maximizes the energy efficiency, applying dynamic contention window adjustment to achieve such optimal performance. Unfortunately, The analytical models of these works rely on a set of assumptions, such as saturation and ideal channel conditions, that result in a limited applicability to scenarios where the traffic has no packet loss and delay requirements.

The feasibility of 802.11 wireless networks constrained to real-time requirements (especially packet loss and delay) has been previously studied. Most of

works in the literature focus on tuning 802.11 parameters (especially the contention window) to increase the throughput performance. These strategies are based on either modifying the 802.11 standard behavior [11, 15, 31, 99, 102] or using the traffic priorization provided by 802.11e [8, 83]. Besides throughput, alternative performance metrics are also considered. In [25, 91, 109, 114] the packet delay metric is chosen and in [63, 113], packet losses are studied.

All of the above works use the contention window size as the exclusive control parameter, neglecting the advantages of adjusting the retry limit (which is set to its default value). The retry limit control is considered in [63] but the contention window tuning is not taken into account. We believe that the joint adjustment of both parameters could result in a better QoS performance, specially, under extreme load and channel noise conditions. The tradeoff between energy efficiency optimization and QoS level in communications is still an open challenge. In [20] the authors study the tradeoff between energy and delay but no optimization mechanism is proposed. To the best of our knowledge, there are no previous works that deal with the problem of optimizing the energy efficiency, considering the impact of the control decisions on the QoS performance.

In this work, we propose a centralized algorithm to maximize the energy efficiency in 802.11 wireless networks based on the dynamic tuning of the two main MAC parameters: contention window and retry limit. Thanks to the adjustment of both parameters, our algorithm maximizes the energy efficiency, and additionally allows the stations to achieve better QoS levels than other algorithms proposed in the literature controlling only one of the two parameters. Our algorithm is based on an analytical model that considers the extreme traffic load and non-ideal channel effects, and hence it can be applied under any network condition. We show the advantages of our approach by studying the results of energy efficiency and QoS level in a network scenario where stations run VoIP applications with CBR traffic, with variable channel conditions.

3.1 Problem statement

We deal with the energy management issue in a wireless network with the objective of finding the MAC parameter setting that optimizes the energy efficiency while a minimum QoS level is provided. With this aim, we propose a centralized algorithm (located at the AP) to adjust two MAC parameters, that is, the contention window and the retry limit.

Our optimization mechanism works as follows. The access point measures the level of congestion by running an estimation mechanism that calculates the prob-

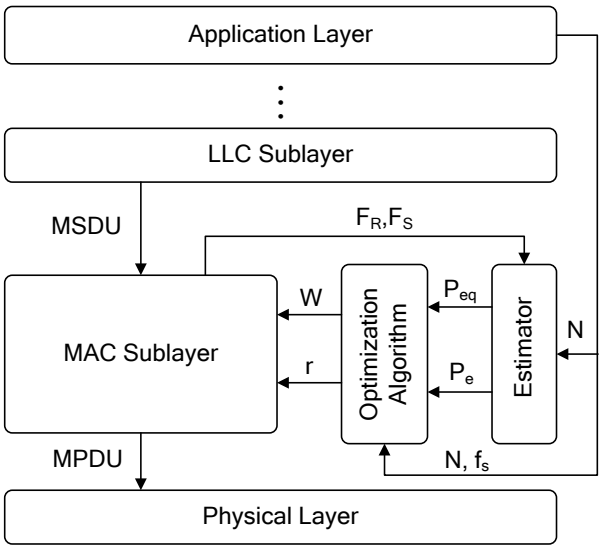

Figure 7: Modular architecture proposed for the access point.

ability of a station retransmitting a packet (due to collisions or channel errors). From that probability, along with the number of stations N and the station packet transmission rate f_s, our optimization algorithm computes the values of the contention window size and the retry limit that maximize the energy efficiency. The MAC layer of the access point receives the information and broadcasts it to the wireless stations, allowing them to read and update the new MAC parameters. Figure 7 shows the modules included in the access point architecture.

We will present now a detailed description of the context of this work.

3.1.1 Framework assumptions

The scope of this work is limited to wireless networks operating in infrastructure mode with a single access point. The scenario is composed of homogeneous wireless stations that periodically send packets to an access point which does not generate any data throughput. We assume that the number of stations N in the wireless network and the station's traffic rate f_s are known a priori. We set $W_{min} = W_{max}$ which is commonly used in scenarios where the number of stations is known [10, 91]. We assume that WLAN operates under 802.11e standard with one single traffic class and that ere are no hidden nodes. We contemplate

the use of both the active and power saving modes. When PSM is on, we suppose that stations stay in sleep mode since the end of transmission and until a new packet arrives. The RTS/CTS handshake mechanism is not considered because of its inefficiency in scenarios where stations send small packets [23] (Notice that the packet size of VoIP applications is usually between 10 and 80 bytes). Finally, we set the station buffers size to a small value in order to limit the packet delays.

3.2 Analytical model of 802.11

The analytical model of 802.11 allows deriving formulae for the power consumption, energy efficiency and parameters related to the quality of service (packet losses, throughput and packet delays). In addition, these formulae show the influence of the contention window size and retry limit on the energy efficiency and the level of QoS. We use an analytical model based on the bi-dimensional Markov chain model proposed by Bianchi in [9]. Bianchi assumes some unrealistic hypothesis to simplify the mathematical expressions which restrict the applicability of the model. Specifically, the model contains three assumptions which make it unsuitable for our study. First, it considers that the WLAN operates in saturation conditions, i.e. the transmission queue of each station is assumed to be always non-empty. Second, it assumes an error-free channel, i.e. packets are retransmitted only when they encounter collisions. Third, it assumes infinite retransmission attempts, i.e. packets are never dropped.

Fortunately, some authors have extended Bianchi's model to get rid of the above assumptions. Error-prone channels are considered in [22, 53, 78], non-saturated conditions are taken into account in [72] and the finite retry limit effect is considered in [21]. Some recent works include several features together. In [64], authors embed both the finite retry limit and non-saturation features in the model. In [28], the authors add channel errors and the non-saturation condition. Finally, papers [61, 93] propose a model including the three aspects.

In this work, we adopt the analytical model used in [93], as it includes the finite retry limit, channel errors, and extreme load conditions. These features are fundamental to our work. The model describes the 802.11 standard, but it can be directly applied to 802.11e when only one traffic class is considered. By properly choosing the network parameters, the analytical expression will be valid in both cases. Table 3 and 4 show the common network parameters used in 802.11 and 802.11e standards, together with their typical values. The first aim of the analytical model is to obtain the probability τ that a station transmits a packet in a random time slot. From that probability, it is possible to derive formulae for the

throughput, delay, packet loss, power consumption, and energy efficiency. The expression for the probability τ is obtained by solving the bi-dimensional Markov chain described in [93] and is presented in 10

$$\tau = \frac{2}{W + 1 + \frac{(1-q)(1-p_{eq})}{q(1-p_{eq}^{r+1})}} \tag{10}$$

Where W represents the contention window size, r denotes the retry limit, and q represents the probability that a station's buffer is not empty. If we assume saturation condition $q = 1$, our expression matches the Bianchi's one [10]:

$$\tau = \frac{2}{W + 1} \tag{11}$$

We also define the following probabilities:

p_{eq}: the probability that a packet fails due to collision or channel errors. It can also be seen as the probability that a packet must be retransmitted.

$$p_{eq} = p_c + p_e - p_c p_e \tag{12}$$

p_c: pc is the probability that a packet transmission fails due to collision.

$$p_c = 1 - (1 - \tau)^{n-1} \tag{13}$$

p_t: represents the probability that at least one station transmits in a random time slot. It can be seen as the probability that the channel is busy.

$$p_t = 1 - (1 - \tau)^n \tag{14}$$

p_s: represents the probability that only one station transmits in a random time slot. It can be seen as the probability that a station transmits without collisions.

$$p_s = \frac{n\tau(1-\tau)^{n-1}}{1 - (1-\tau)^n} \tag{15}$$

Additionally, we need to define the average length of a time slot which is given by:

$$E[S_{ts}] = (1 - p_t)\sigma + p_t(1 - p_s)T_c + p_t p_s(1 - p_e)T_s + p_t p_s p_e T_e \tag{16}$$

Here σ is the duration of a empty slot time, T_s is the average time the channel is sensed busy due to a collision, T_s is the average time the channel is sensed busy because of a successful transmission, and T_e is the average time the channel is sensed busy due to a packet transmission with errors. We use the definition for T_s, T_c, and T_e as proposed in [28].

According to [72], it is possible to relate the probability q to the load offered at the station load as:

$$q = f_s E[S_{ts}] \tag{17}$$

This expression is valid under small buffer and periodic traffic-pattern conditions. In Appendix B, we develop an alternative expression for q which can be used if such conditions are not met.

All these equations describe a nonlinear system of equations that can be numerically solved, obtaining values for τ and the rest of probabilities. Therefore, we are ready to calculate some useful metrics such as packet losses, delays, power consumption, and energy efficiency.

3.2.1 Power consumption

Although different expressions to compute the energy consumption have been proposed in the literature, they are been derived under the assumption of saturation [18, 19, 34, 47, 111, 112] or ideal channel conditions in [89]. In order to include the extreme load and erroneous cannel effects, we extended the formulae given in [34] for computing the power consumption. Fist, we must rewrite the average energy that a station consumes per time slot $E[J_{st}]$, as given in (18).

$$\begin{aligned} E[J_{ts}] = (1-\tau)^n J_\sigma + (1-p_e)\tau(1-\tau)^{n-1} J_s^{rx}(l) + p_e\tau(1-\tau)^{n-1} J_e^{rx} \\ + (1-p_e)(n-2)\tau(1-\tau)^{n-1} J_s^{rx}(\sim l) + p_e(n-2)\tau(1-\tau)^{n-1} J_e^{rx} \\ + (1-\tau)(p_c - (n-1)\tau(1-\tau)^{n-2}) J_c^{rx} + 1 - p_e)\tau(1-p_c) J_s^{tx} + p_e\tau(1-p_c) J_e^{tx} \\ + \tau p_c J_c^{tx}, \end{aligned} \tag{18}$$

being J_σ, $J_s^{rx}(l)$, $J_s^{rx}(\sim l)$,J_c^{rx}, J_s^{tx}, J_c^{tx}, J_e^{tx} y J_e^{rx} the energy consumed by each kind of slot. A detailed explanation of slot types and the formulae are given in Appendix A. From $E[J_{st}]$, we now derive formulae for the power consumption under active and power saving modes.

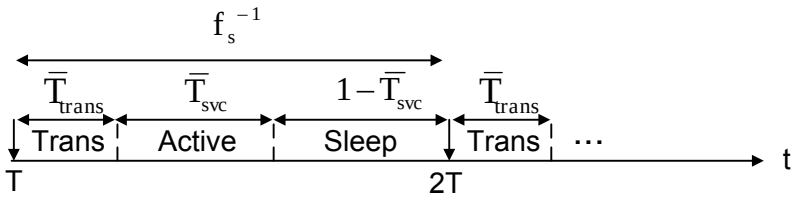

Figure 8: Simplified PSM mechanism.

Power consumption in active mode: The power consumption is defined as the energy consumed per time unit so it possible to obtain the average power consumption from (18) and (16) as:

$$\overline{P} = \frac{E[J_{ts}]}{E[S_{ts}]} \tag{19}$$

Power consumption in power saving mode: In IEEE 802.11 PSM, a node can be in one of the two power modes, that is, the active mode when a node can receive and transmit frames at any time, and the power saving mode when a node a node cannot transmit or receive and consumes very little power. In the power saving mode, all nodes in the network are synchronized to wake up periodically to listen to beacon messages. If a node has a packet aimed at another node, it will send an ATIM packet, and the receiver acknowledges that it will stay awake. If a node has neither a packet to send nor it receives an ATIM packet, it goes to sleep at the end of the ATIM window. In this work we assume that wireless stations do not receive any traffic. This allows us to consider a simplified PSM where a station only wakes up when receives a new packet and stays awake until such packet is either successfully transmitted or dropped. After finishing its transmission, the station enters into sleep mode again. The transition from sleep-to-active state is not immediate so we consider an intermediate state, denoted as transition state [2]. Fig. 8 illustrates the phases of our simplified PSM as well as their duration and associated consumption. Each state has a different duration and associated consumption. Typical values for the duration $\overline{T}_{trans}$ and consumption ρ_{trans} of the transition state can be found in [54]. The average duration of active state can be obtained from the average service time expression $\overline{T}_{svc}$ given by (20) and the

[2]The active-to-sleep state is not taken into account due to its impact on the energy consumption is negligible [43]

average consumption is given in (19). Once we know the duration of the transition state and active state, the duration of the sleep mode can be computed just by taking into account that the time between two transitional states is equal to the station interarrival time $1/f_s$. The consumption of this phase is determined by ρ_{sleep}. Hence, we can write the average power consumed by a station in PSM as:

$$\overline{T}_{svc} = \left\{ \sum_{i=0}^{r} p_{eq}^{i} \left(iT_c + \sum_{j=0}^{i} \overline{W}_j E[S_{ts}] + T_s \right) + p_{eq}^{r+1} \left[(r+1)T_c + \sum_{j=0}^{r} \overline{W}_j E[S_{ts}] \right] \right\} / \sum_{j=0}^{r+1} p_{eq}^{j} \quad (20)$$

We can also rewrite the average energy consumption per slot for PSM by using the Eqs. (16) and (21) as:

$$\overline{P}^{psm} = \overline{P} \cdot f_s \overline{T}_{svc} + (\rho_{trans} - \rho_{sleep}) f_s \overline{T}_{trans} + \rho_{sleep}(1 - f_s \overline{T}_{svc}) \quad (21)$$

$$E[J_{ts}]^{psm} = E[J_{ts}] \cdot f_s \overline{T}_{svc} + E[S_{ts}](\rho_{trans} - \rho_{sleep}) \cdot f_s \overline{T}_{trans} + \rho_{sleep} E[S_{ts}](1 - f_s \overline{T}_{svc}) \quad (22)$$

Energy efficiency: We define the energy efficiency E_{ef} as the ratio between the bits transmitted and the energy consumed in a time slot:

$$E_{ef} = \frac{p_t p_s (1 - p_e) E[P]}{E[J_{ts}]} \quad (23)$$

For PS mode, the energy efficiency can be rewritten as:

$$E_{ef}^{psm} = \frac{p_t p_s (1 - p_e) E[P]}{E[J_{ts}]^{psm}} \quad (24)$$

3.2.2 QoS Metrics

Here we compute the two most important quantities to measure the level of QoS for real-time applications, i.e. the average packet delay and the average packet loss rate.

Packet delay: The average packet delay can be related to the average service time seen in (20). The first term in the summation represents the average time

that a station spends through the backoff stages before transmitting a packet, i.e., the so-called MAC access time. The second term of the summation takes into account the average duration of a packet drop. The time spent in transmitting packets which are finally dropped should not be included in the calculation of the average packet delay. Hence, we only consider the first term of the summation. The average packet delay can be computed as

$$\overline{D} = \frac{\sum_{i=0}^{r} p_{eq}^{i}(iT_c + \sum_{j=0}^{i} \overline{W}_j E[S_{ts}] + T_s)}{\sum_{j=0}^{r+1} p_{eq}^{j}} \tag{25}$$

Where the average contention window size for the j-th backoff stage, $\overline{W}_j$ is defined as

$$\overline{W}_j = \frac{2^{\min(j,m)} W_0 - 1}{2}.$$

Packet loss rate: We derive the expression for the average packet loss rate from the throughput expression as

$$S = \frac{p_t p_s (1 - p_e) E[P]}{(1 - p_t)\sigma + p_t(1 - p_s)T_c + p_t p_s (1 - p_e)T_s + p_t p_s p_e T_e}, \tag{26}$$

where $E[P]$ is the average packet size and S represents the system throughput, which can be obtained as

$$P_{loss} = 1 - \frac{S}{n f_s E[P]}. \tag{27}$$

3.3 Model validation

We will validate our analytical model through OPNET simulations [81]. We choose OPNET simulator as validation tool because it offers an accurate implementation of the 802.11 standard. Besides, OPNET results are widely accepted by the research community. Despite of the original implementation accuracy, it has been necessary to carry out several modifications to extend it to our requirements. A new energy consumption module has been developed to compute the energy consumed by each station. The module considers both the active and power saving modes. We have also implemented a simple power saving mode mechanism that works according to the description given in section 3.2.1. Since we focus on the study of the energy consumption in PSM rather than on the PSM mechanism itself, this simplified implementation is adequate for our purposes. Finally,

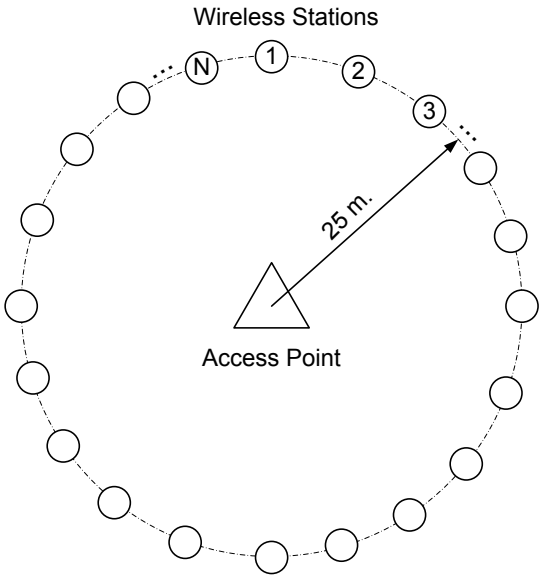

Figure 9: Simulation scenario.

we perform a little modification to set the buffer size in packet units instead of bit units. The topology of our scenario is presented in Fig. 9, while the network parameters used in simulations are listed in Table 3.

Fig. 10 shows a comparison between simulated and analytical results for power consumption (Active and PS mode), packet delays, and packet loss rate. The analytical results are close to the simulation experiments and provide a significant level of accuracy. Hence, we conclude that the analytical expressions derived in previous sections properly describe the 802.11 behavior and can be used as a basis for our optimization algorithm.

3.3.1 Influence of background traffic on the real time application performance

In this section we study the influence of the background traffic on the real-time application performance in a 802.11e network that operates in EDCA mode. For this purpose, we run a batch of simulations and then compare the real-time application

[3]This packet results from a VoIP application using the G.729 codec with four frames per packet over the RTP/UDP/IP protocol .

Table 3: MAC parameters for simulation of IEEE 802.11b standard

Parameter	Value
PL	80 Bytes[3]
f_s	25 pkt/s
Buffer size (k)	1
R_b	1 Mb/s.
PHY	192 μs
MAC	28 Bytes
ACK	14 Bytes
SLOT	20 μs
DIFS	50 μs
SIFS	10 μs
EIFS	364 μs
ρ_σ, ρ_{rx}, ρ_{tx} and ρ_{psm}	0.11, 0.9, 2.5 and 0.02 W
r	5
m	5

performance in the absence and presence of background traffic. The simulation scenario is composed of N stations running VoIP applications and another station running a non real-time application. We set VoIP traffic to higher priority than background traffic. Fig.11 shows that VoIP traffic is weakly affected by the presence of background traffic thanks to the priorization mechanism provided by the 802.11e standard. It can be seen that the packet loss rate and delays are similar in both cases. Therefore, the analytical expressions for delays and losses are still valid, although there is more than one traffic class.

3.4 Proposed algorithm

We propose an algorithm to maximize the energy efficiency. As we will see later, there exists an optimal value for the transmission probability τ, denoted as τ^e_{opt}, maximizing the energy efficiency [4]. The probability τ depends on two MAC parameters, the contention window size and the retry limit. Hence, we can find a proper pair (W, r) that maximizes the energy efficiency. In fact, the optimal probability τ^e_{opt} can be achieved by only tuning W. However, we propose a joint control of W and r since an appropriate adjustment of the retry limit parameter

[4] To minimize the energy consumption means that stations do not transmit any packets.

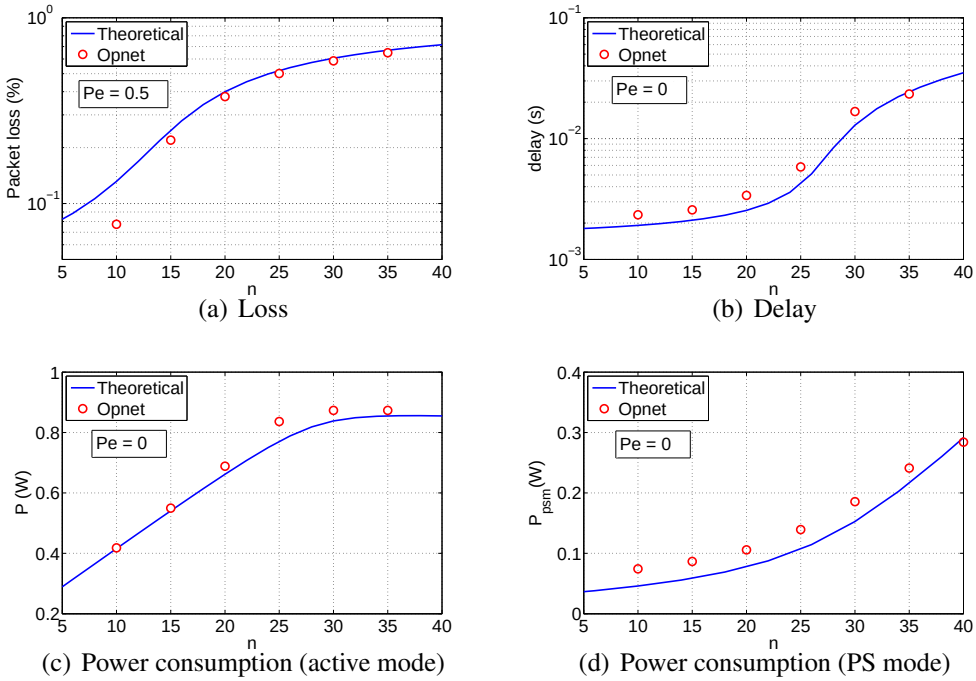

(a) Loss (b) Delay

(c) Power consumption (active mode) (d) Power consumption (PS mode)

Figure 10: Analytical and simulation results of 802.11b network performance.

reduces the packet delay and improves the QoS level.

The algorithm architecture consists of three modules. First, the estimation block which estimates the probabilities p_e and p_{eq} by sensing the channel state and monitoring the received frames for the AP. Our algorithm needs to know these probabilities to adjust the contention window size and the retry limit. The second module computes the probability that optimizes the energy efficiency. The third module is the decision block, which computes the pair (W, r) that makes the network operate at its optimal point in terms of energy efficiency. The algorithm has four input parameters: the number of stations N, the packet rate f_s , the number of frames received by the AP F_s and the number of retransmitted frames F_r received by the AP. Fig. 12 shows the modular architecture described above.

3.4.1 Estimator module

Our algorithm is based on a set of analytical formulae that contains the probability p_{eq} and p_e. Because of both probabilities are unknown, it is necessary to estimate

Table 4: MAC parameters for simulation of IEEE 802.11e standard

Parameter	Value
PHY	192 μs.
MAC	30 bytes
ACK	14 bytes
AIFS[Best effort]	70 μs.
AIFS[Voip]	80 μs.
TXOP[Best effort]	1 MSDU
TXOP[Voip]	1 MSDU
r[Best effort]	5
m[Best effort]	5
r[Voip]	2
m[Voip]	2

them. In the literature, we can find different approaches to achieve such purpose. Papers [71, 98] estimate the probabilities that a station detects a collision (p_c) and transmits an error affected frame (p_e) by monitoring the channel sate continuously in each station. Due to the fact that our algorithm follows a centralized estimation approach, these strategies are not suitable for us. In [83], authors suggest estimating the collision probability by analyzing the retry bit field of the frame received at the AP. This approach is centralized and provides an estimation of the collision probability, but no mechanism is proposed to estimate the probability p_e, as the authors assume ideal channel conditions. We propose to extend the latter estimation mechanism so that it can be applied to scenarios with channel errors.

Estimation of p_{eq}: The quantity p_{eq} represents the probability that a packet transmission fails due to a collision or external noise. Alternatively it can be seen as the probability that a packet must be retransmitted. Our AP-located algorithm obtains the probability p_e from the ratio between the number of retransmitted frames and the total number of received frames. Let be $F_s(k)$ the number of frames received by the AP in a estimation interval with the retry bit unset, and $F_r(k)$ the number of frames received with the retry bit set. Then, we can write

$$\frac{F_s(k)}{F_s(k)+F_r(k)} = \frac{1-\widetilde{p}_{eq}(k)}{1-\widetilde{p}_{eq}^{r+1}(k)}, \tag{28}$$

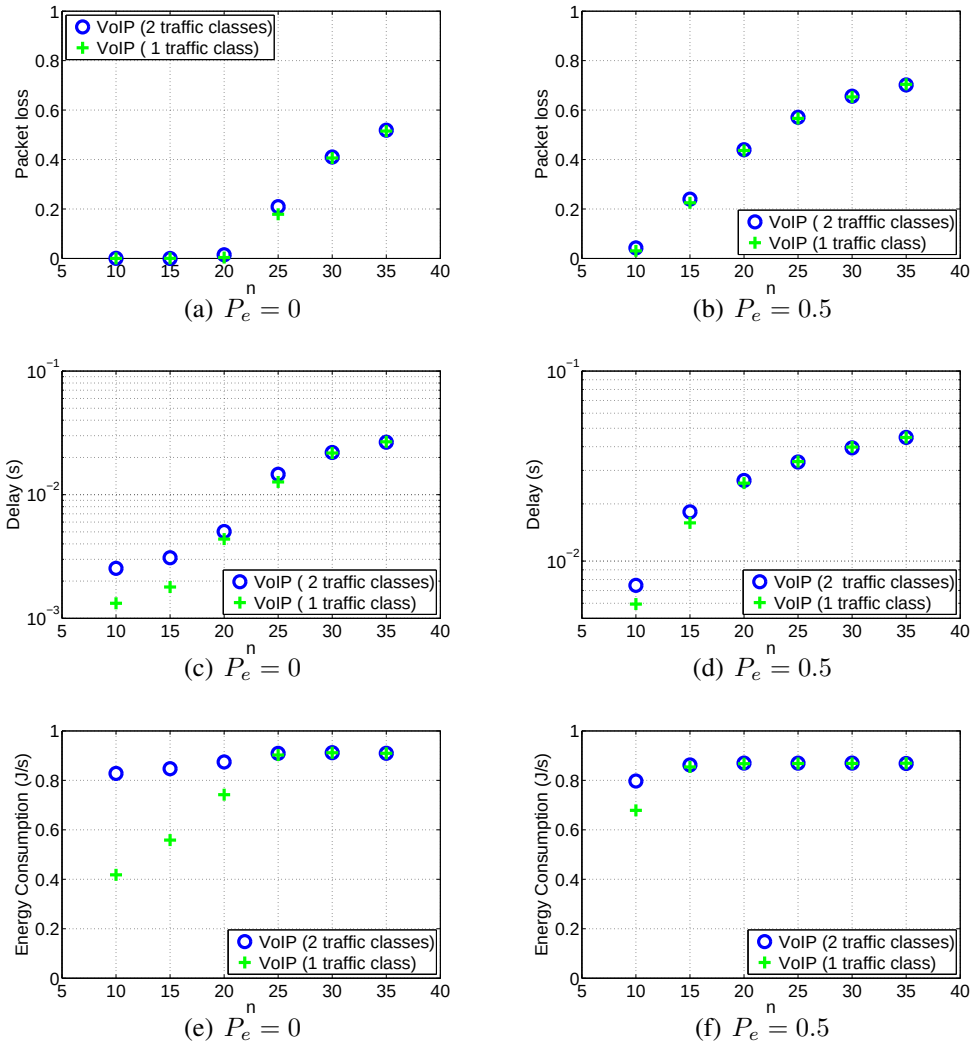

Figure 11: Packet loss rate, delays and power consumption for 802.11e stations under the presence and absence of background traffic. The left column plots show the results under ideal channel conditions ($p_e = 0$) whereas the right column plots depict results under noisy channel conditions ($p_e = 0.5$).

where $\widetilde{p}_{eq}(k)$ represents the equivalent error probability measured in the interval k. From now on, we will denote the measure of $x(k)$ in the estimation interval k as $\widetilde{x}(k)$, and the estimation of x as $\widetilde{x}(k)$. We can rewrite (28) as a $r+1$ order

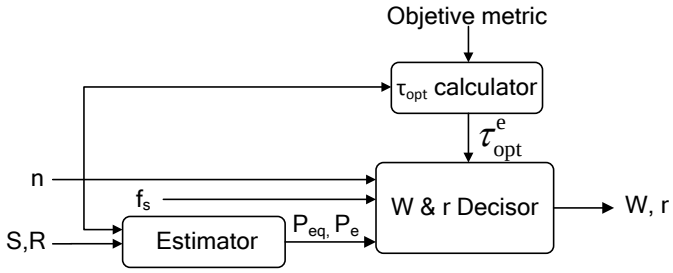

Figure 12: Modular architecture proposed for the optimization algorithm.

equation:

$$\frac{F_s(k)}{F_s(k)+F_r(k)}\widetilde{p}_{eq}(k)^{r+1} - \widetilde{p}_{eq}(k) + \frac{F_r(k)}{F_r(k)+F_s(k)} = 0 \tag{29}$$

Note that the probability that a packet is dropped decreases as the retry limit increases. In practice, our algorithm sets the retry limit to values which allows us to disregard the influence of packet dropping. If we neglect this effect, we can simplify (29) as

$$\widetilde{p}_{eq}(k) = \frac{F_r(k)}{F_r(k)+F_s(k)}, \tag{30}$$

which coincides with the expression given in [83]. If stations never drop packets because of reaching the retry limit attempts, the estimated p_{eq} and the real one are matched exactly. Otherwise, the estimated p_eq is slightly lower than real one. We obtain the run-time estimation of probability p_{eq} by applying an ARMA (Auto Regressive Moving Average) filter.

$$\widehat{p}_{eq}(k) = \widehat{p}_{eq}(k-1) + \frac{\widetilde{p}_{eq}(k) - \widetilde{p}_{eq}(k-M)}{M} \tag{31}$$

where M represents window size.

Estimation of p_e: In order to estimate the error probability p_e, we express it as a function of p_{eq} y p_c:

$$p_e = \frac{p_{eq} - p_c}{1 - p_c} \tag{32}$$

Since the probability p_{eq} is already known , we can compute the error probability p_e by estimating the collision probability p_c. The collision probability only depends on the number of stations, which is known, and the transmission probability τ, which can be estimated by monitoring the channel state. We use the estimation mechanism proposed in [45] based on the measurement of consecutive idle slots between packet transmissions.

Let be n_{idle}, a random variable representing the number of consecutive idle slots between two packet transmissions. Its expected value of n_{idle} depends on the probability p_t in the following way:

$$\overline{n}_{idle} = \frac{1}{p_t} - 1 = \frac{(1-\tau)^n}{1-(1-\tau)^n} \tag{33}$$

Solving (33) for τ yields:

$$\tau = 1 - \left(\frac{\overline{n}_{idle}}{1+\overline{n}_{idle}}\right)^{1/n} \tag{34}$$

Note that the collision probability p_c can be rewritten as a function of n_{idle} by substituting (34) in (13). Finally, substituting (13) and (34) in (32, we compute the estimation of p_e as

$$\widetilde{p}_e(k) = \frac{\widehat{p}_{eq}(k) + \left(\frac{\overline{n}_{idle}}{1+\overline{n}_{idle}}\right)^{\frac{n-1}{n}} - 1}{\left(\frac{\overline{n}_{idle}}{1+\overline{n}_{idle}}\right)^{\frac{n-1}{n}}} \tag{35}$$

3.4.2 Calculator module

This module computes the optimal probability τ^e_{opt}, maximizing the energy efficiency which can be obtained by solving the equation $dE_f/d\tau = 0$. This optimal probability has been previously obtained in [90] but the authors assumes the unrealistic hypothesis that frames are always successfully transmitted in order to simplify the expression of τ^e_{opt}. This expression cannot be used in scenarios under high noise conditions, and hence we propose a more generic expression which is suitable under any situation. Solving the equation $dE_f/d\tau = 0$, and after some

algebra we get,

$$\tau_{opt}^{e} = \frac{1}{n + \frac{\sqrt{J_\sigma(n-1)(2J_c^{tx} + (n-2)J_c^{rx} - 2nJ_\sigma)}}{\sqrt{2}J_\sigma}}. \tag{36}$$

A comparison between our proposed expression and the expression described in [90] as well as a more detailed calculation of the optimal probability τ_{opt} can be found in Appendix A.

3.4.3 Decisor module

This module represents the core of our optimization strategy. It computes the pair (W, r) that maximizes the energy efficiency in the network, given a number of stations N and packet rate f_s. Solving (10) for W, we get an expression that gives the optimal contention value as a function of N, f_s, p_{eq} and r. Note that the number of stations and the packet rate are known, the probability p_{eq} has been estimated, and the retry limit is a free parameter which can be tuned to meet an additional condition.

$$W_{opt} = \max\left(W_{min}, \frac{2}{\tau_{opt}} - 1 - \frac{2(1-q)(1-p_{eq})}{q(1-p_{eq}^{r+1})}\right) \tag{37}$$

From Eq. (37) we can note that the optimal point of energy efficiency is only achievable from a minimum packet rate, denoted f_{min}. For achieving maximal energy efficiency at a lower packet rate, the contention window size should be set to a negative value, which makes no sense. When the packet rate of stations is below f_{min}, the network is lightly loaded and collisions rarely happen. In these cases we set the contention size to its minimal value, denoted as W_{min}, in order to increase the station aggressiveness as much as possible[5]. The minimum packet rate f_{min} at which energy efficiency optimization can be performed is obtained by solving (37) for f_s.

$$f_{min} = \frac{2(1-p_{eq})}{E[S_{ts}] \cdot \left((1-p_{eq}^{r+1})(2\tau_{opt}^{-1} - W_{min} - 1) + 2(1-p_{eq})\right)} \tag{38}$$

In (38) we can observe that the minimum packet rate f_{min} decreases as the

[5]the minimal contention window size ensuring that two or more stations don't collide indefinitely is given by $W_{min} = 2$.

retry limit increases. It means that the energy efficiency optimization can be achieved at lower rates by increasing the retry limit parameter. However, this effect becomes insignificant once the retry limit approaches $p_e^{r+1} \approx p_e^r$. In this case, keeping increasing the retry limit stops being useful and has a negative impact on the packet delay. In order to avoid an inappropriate selection of the retry limit, we establish a threshold Δ_{min} which represents the minimum difference between p_{eq}^r and p_{eq}^{r+1} (denoted as Δ from now on) that allows us to keep increasing the retry limit. Then, our algorithm selects the retry limit value thought an iterative process designed as follows:

Algorithm 1 computation of r_{max}

1: **while** $(\Delta > \Delta_{min})$ **do**
2: $\quad r_{max} = r_{max} + 1$
3: **end while**

As stated above, when networks operate under light traffic load, i.e $f_s < f_{min}$, stations should increase their aggressiveness as much as possible with the aim of improving the energy efficiency in the network. In this case, our algorithm chooses the most aggressive configuration of MAC parameters given by (W_{min}, r_{max}). This setting results in better energy efficiency and smaller packet losses than alternative configurations that only tune the contention window size. In addition, the packet delay remains approximately the same in both configurations.

When the traffic load is higher enough to meet $f_s \geqslant f_{min}$, the optimal probability τ can be obtained for different values of the pair (W,r). As seen above, the retry limit is a free parameter that can be used to satisfy an additional requirement besides energy efficiency optimization. In this work, we choose the packet delay as the extra goal so we select the pair (W, r) that maximizes the energy efficiency, achieving a lower packet delay. The rety limit satisfying such requirement is given by,

$$r_{min} = \left\lceil \frac{\ln\left(1 - \dfrac{2(1 - f_s \cdot E[S_{ts}])(1 - p_{eq})}{f_s \cdot E[S_{ts}](2\tau_{opt}^{-1} - W_{min} - 1)}\right)}{\ln(p_{eq})} - 1 \right\rceil \tag{39}$$

Then, the retry limit value must set to r_{min} o higher values in order to energy efficiency optimization.

3.4.4 Algorithm summary

After describing the modules included in our optimization architecture, we will summarize the behavior of our algorithm (see Algorithm 2). First, the estimator module estimates the probabilities p_{eq} and p_e from the measurement of F_s and F_r. Meanwhile, the calculator module obtains the optimal probability τ^e_{opt} which only depends on N as showed in (36). Then, the maximum retry limit, which depends on the threshold and the probability p_{eq} is calculated. Once we get r_{max}, the minimum packet rate f_{min} can be obtained since all parameters involved in (38) are known. Finally, we check the operation region and set the contention window size and the retry limit accordingly. Our algorithm runs this process every estimation period, which itself can be adjusted depending on the time-varying channel conditions.

Algorithm 2 Pseudocode of the proposed algorithm

Input: n, f_s, S, R and the objective metric
Output: W, r

// We first estimate the probability p_{eq}
Compute $\widehat{p}_{eq}$ from (30)
// Compute the optimal operation point τ_{opt} for the energy efficiency optimization
Compute τ^e_{opt} from (36)
//Compute the retry limit
while $(\Delta > \Delta_{min})$ (1) **do**
    $r_{max} = r_{max} + 1$
end while
Compute f_{min} from (38)
// Select r depending on the operation region
if $(f_s > f_{min})$ **then**
    $r = r_{max}$
else
    $r = r_{min}$ from (39)
end if
Compute W_{opt} from (37)

3.5 Numeric results

This section provides some numerical results for the energy efficiency, packet losses, packet delay and other QoS metrics when different MAC configuration

mechanisms are applied. We have used Matlab to solve the nonlinear system of equations describing the behavior of 802.11 protocols. We compare our optimization strategy against the default configuration and the mechanism proposed in [90]. We compare the strategies for different numbers of stations (2-35), and varying packet error probabilities (0.1-0.8). We also take into account both the active and the power saving mode in the analysis.

Results for delays and packet losses We first compare the strategies in terms of energy efficiency, packet delays and packet losses under both light and heavy load conditions. As showed in Fig. 13 the packet loss rate and delays achieved by our algorithm are always lower. Under light load conditions, our algorithm sets the contention window to W_{min} and the retry limit to r_{max}. This setting allows stations to be more aggressive than other configurations, and reduce their packet loss rate. Under heavy load conditions, our algorithm achieves smaller packet delays than the rest of strategies because the retry limit is set to its minimum value r_{min} which is usually lower than the default value.

As plotted in Fig.14, the average power consumption for various numbers of stations and error probabilities. In active mode, our optimization mechanism leads to slightly higher consumption when the network operates under limited load (linear region) and achieves lower consumption under saturated conditions (flat region). In power saving mode, our algorithm saves energy due to the reduction of the packet delays which allow stations spend more time in sleep state.

Results for VoIP peformance Besides optimizing the energy efficiency, we are interested in studying the feasibility of 802.11 networks to support real time services such as VoIP. The E-model [27] is widely used for measuring and assessing the conversational speech quality for VoIP applications. It takes into account a wide range of telephony-band impairments, in particular the impairment due to low bit-rate coding devices and one-way delay, as well as the classical telephony impairments of loss, noise and echo. The primary output of the E-model calculations is a scalar quality rating value known as the Transmission Rating Factor, R. which can be directly related to network parameters as packet delays and losses. The expression of R includes several parameters which depend on the voice codec. As an example, when codec G.729b is chosen, the R factor yields:

$$R = 94.2 - 0.24d - 0.11(d - 177.3)\mathrm{H}(d - 177.3) - 11 - 40\ln(1 + 10e) \quad (40)$$

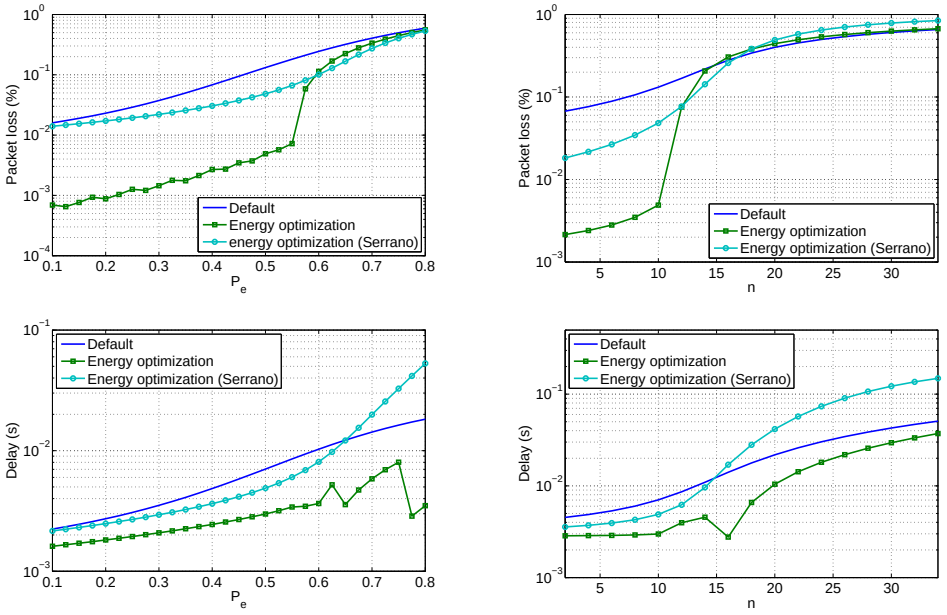

Figure 13: Packet losses and delays obtained with different configuration mechanisms. Plots on the left column show the results for 10 stations when the error probability varies. Plots on the right column show the results for different numbers of stations when the error probability is 0.5

where d represents the end-to-end delay, e is the packet loss percentage and $\mathrm{H}(x)$ is the Heavyside function.

Factor R can be transformed into other quality measures such as Mean Opinion Score (MOS). Table 5, taken from ITU-T Rec. G.109 [88], relates the E-model Ratings R to categories of speech transmission quality and to user satisfaction. Fig. 15 shows the MOS results for the different strategies under study. Our strategy always obtains better MOS results because it achieves smaller packet loss rate and similar packet delays than the rest of strategies. In a network scenario with 10 nodes, our algorithm provides high speech quality, i.e. MOS between 4.03 and 4.34 as long as the packet error probability p_e is below 0.55 whereas the other strategies never achieve such level of speech quality.

Tradeoff between energy consumption and QoS level We define a joint cost function J_e that represents the trade-off between power consumption and QoS level. This performance metric encourages the QoS in communications while

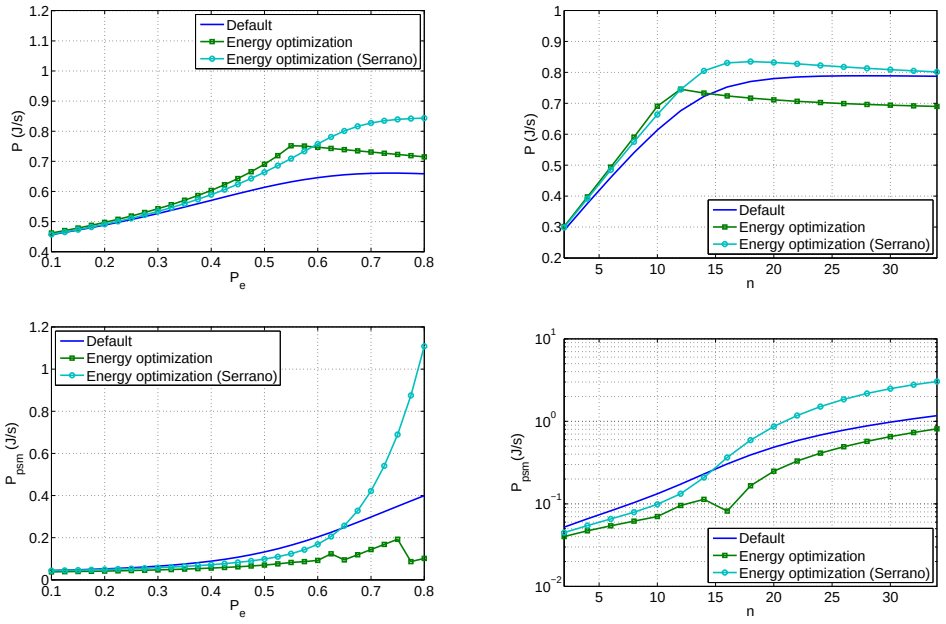

Figure 14: Power consumption (active and PS mode) obtained with different configuration mechanisms. Plots on the left column show the results for 10 stations when error probabilitiy varies. Plots on the right column show the results for various number of stations when error probability is 0.5.

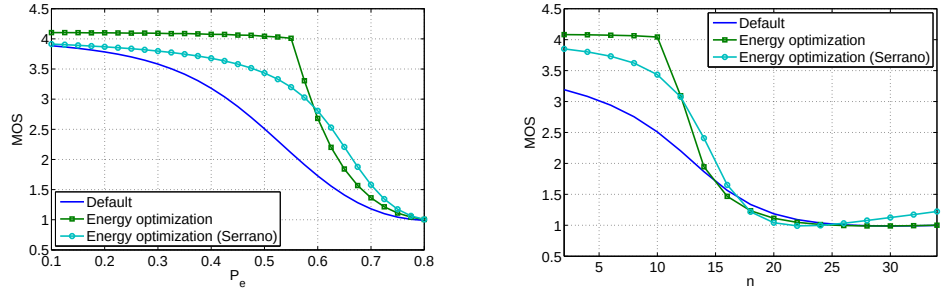

Figure 15: MOS obtained with different configuration mechanisms. Plots on the left column show the results for 10 stations when error probability varies. Plots on the right column show the results for various number of stations when error probability is 0.5.

Table 5: R factors, speech quality rating and associated MOS

Factor R	Quality ratings	MOS
$90 < R < 100$	Best	4.34 - 4.5
$80 < R < 90$	High	4.03 - 4.34
$70 < R < 80$	Medium	3.60 - 4.03
$60 < R < 70$	Low	3.10 - 3.60
$50 < R < 60$	Poor	2.58 - 3.10

discouraging the power consumption.

$$J_e = \alpha E_n + (1 - \alpha) J_{QoS}$$

In this equation, E_n is the normalized power consumption and J_{QoS} is a cost function indicating the impairment of QoS for the VoIP application. The weight factor α is introduced to control the relative importance of the power consumption and QoS terms in the formula. We define the R function given in (40) as the complementary function of the QoS cost function. Then, we can rewrite the joint cost function in terms of power consumption and MOS as $J = 1 - MOS_n$, where MOS_n represents the normalized MOS. Figs.16 and 17 shows the joint cost function when station operates in active and power saving mode, respectively. Again, our strategy performs better than the rest of approaches for most situations. Specifically, we focus on evaluating the strategy within the region which allows the network to provide minimum QoS levels. This region is determined by the network load and can be easily identified by looking at the MOS results given in Fig. 15). WLAN can only provide QoS requirements under non saturated conditions. Under saturated conditions, packet delay and losses make the network performance unacceptable for real-time applications. Note that our algorithm always performs well in the region of interest, specially, when the QoS term has a greater weight in the joint function cost, i.e., smaller α. The utility of the joint tuning of W are r is more remarkable when the network operates under limited load and channel error conditions.

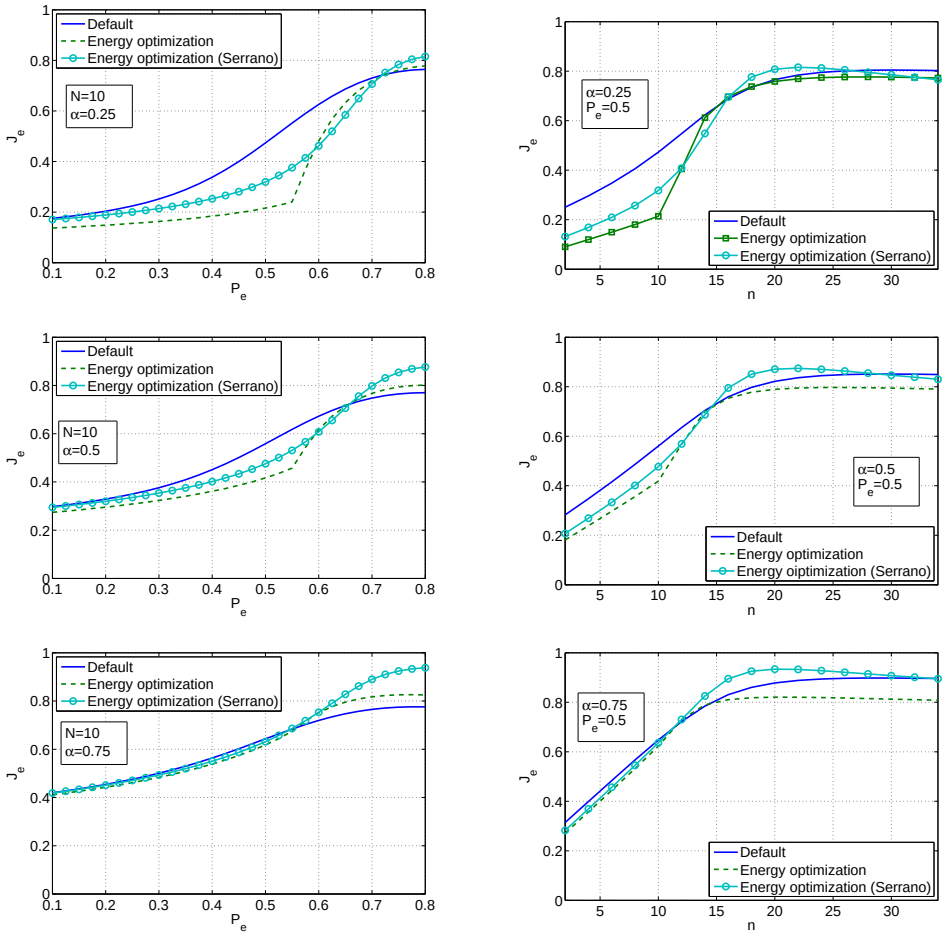

Figure 16: Joint cost function obtained with different configuration mechanisms for various α and stations operating in active mode. Plots on the left column show the results for 10 stations and variable packet error probability. Plots on the right column show the results for various number of stations and fixed packet error probability.

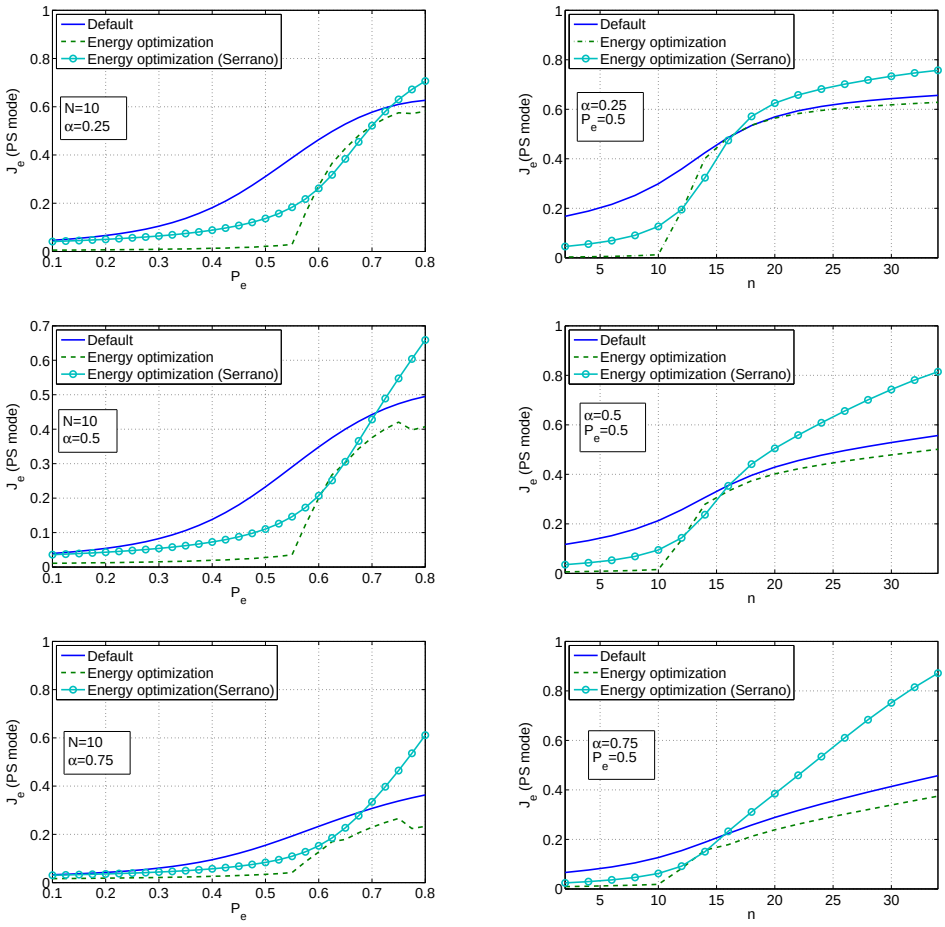

Figure 17: Joint cost function obtained with different configuration mechanisms for various values of α and stations operating in PS mode. Plots on the left column show the results for 10 stations and variable packet error probabilities. Plots on the right column show the results for various numbers of stations and fixed packet error probability.

4 Min-Max Model Predictive Power Control Strategy for CDMA Cellular Networks

In general, wireless power control systems are typically subject to external disturbances due to radio channel fading and multiple access interference (MAI) that cause a significant degradation in communication quality, hence network performance, [42]. Moreover, when mobility is introduced, the problem becomes more difficult to solve. The problem is characterised by time varying attenuation in the received signal strength, thereby causing significant perturbations in the received signal-to-noise-plus-interference ratio (SINR). In this paper, the focus is on the uplink power control problem within a typical code-division multiple-access (CDMA) system, emphasising the utility of a model predictive control (MPC) strategy in compensating for the aforementioned uncertainties, so that an acceptable SINR level is achieved for all users, hence maximising the global system capacity. Here, outage probability, [55], is taken into account as a supplementary quality of service (QoS) type performance metric. Thus, power control can play a crucial role not only in satisfying the target SINR, but also in maintaining a level of SINR that is just above a prescribed threshold so that the base station can stay connected with the mobile user without unnecessary interference being generated across the network.

Transmit power control schemes can be classed as either centralised or decentralised. In the centralised scheme, a controller requires complete information of all the channel gains and interferences in the system to calculate appropriate power levels for all users. Conversely, a decentralised controller utilises only locally available information such as the measured SINR as a feedback signal. For a comprehensive survey please consult [60].

A decentralised approach is adopted in this work. Early work focussed on a fixed-step size power control algorithm as a solution, [4]. Some decentralised power control mechanisms have also been successfully used in cellular networks, see e.g., [38, 60, 110].

Recent studies of the power control problem have focused on a satisfactory assessment of the influence of time-varying radio channel gain, interference, or noise on performance. In [50], an estimation based decentralised power control that assumes slow channel variation was presented. Based on this assumption, the channel gain has been accurately estimated, and power control has been implemented. In [62], a robust power controller has been designed that uses a $\mathcal{H}_\infty$ filtering algorithm to minimise the worst-case effects of interference and noise regardless of the information that is being transmitted along the channel.

In [26], a queue-based power control scheme cast as an optimal control problem was considered. The algorithm features include fast on-line implementation, good performance and has exhibited significant power saving. However, a certain level of robust performance with respect to any or all of the aforementioned uncertainties has not been properly characterised thus far. In practical systems, the link information is not readily available. To address this limitation, a robust MPC is taken into account in this paper that applies a readily implementable open-loop min-max MPC algorithm, [84]. Such an approach explicitly takes into account the constrained SINR tracking error dynamics, and treats such uncertainties as bounded additive disturbances. In the decentralised framework that is formulated, the complex network dynamics of power control are represented by a simple state-space model of the SINR tracking error of each user, thus making the on-line optimisation problem tractable. In fact, given that in CDMA systems the power update rate tends to be very low, implementing the proposed min-max MPC by an explicit computation of the quadratic program (QP) that naturally arises, [84], is also shown to be quite feasible. As a result, this facilitates every mobile user to operate robustly at an acceptable SINR, while jointly satisfying a useful QoS requirement. The resulting controller is numerically evaluated via a radio network simulation model developed in [3] to demonstrate the feasibility and efficiency of this particular approach.

4.1 Problem statement

In order to implement a MPC, we need a reduced complexity model of the CDMA power control process. In this subsection, we present a linear state-space tracking error model that we will use to design a controller to robustly maintain the SINR around a target value, while preserving a satisfactory QoS for all mobiles.

Throughout the paper, the logarithmic (e.g., dB) value of a variable x is denoted by $\bar{x}$, namely, $\bar{x} = 10 \log_{10} x$.

4.1.1 Radio Link Model

We consider a single-cell CDMA uplink of n mobiles, labeled $1, \ldots, n$ and the base station. Assuming that the user i is transmitting using the power level $p_i > 0$, the corresponding connected base station will experience a received signal power given by $s_i(k) = g_i(k)p_i(k)$. The term g_i, which is positive, represents the time-varying path gain from the i-th user to the base station. Correspondingly, this gain

can be modeled as the product of different time-varying random quantities,

$$g_i(k) = g_{p,i}(k)g_{s,i}(k)g_{f,i}(k), \tag{41}$$

where $g_{p,i}$, $g_{s,i}$, and $g_{f,i}$ represent path loss, log-normal shadowing, and Rayleigh fading, which limit the network performance during the transmission and can be determined according to

$$g_{p,i}(k) = \frac{A_p}{r^{\alpha}_{p,i}(k)}, \tag{42}$$

$$g_{s,i}(k) = 10^{0.1\xi_{s,i}(k)}, \tag{43}$$

$$g_{f,i}(k) = X^2. \tag{44}$$

In the path loss model (42), $r_{p,i}$ is the distance from i-th mobile to the base station, α the typical path loss exponent ranging from 2 (free-space propagation) to 5 (dense urban area), and A_p is a constant that depends on the antenna characteristics and the average channel attenuation. Note that $A_p = 1$ has been adopted in this work. For shadow fading, empirical studies have shown that $g_{s,i}$ follows a log-normal distribution, [87], hence implying $g_{s,i}$ is Gaussian. A simple and realistic model of $g_{s,i}$ can be given by (43) that incorporates the mobile velocity v and the decorrelation distance X_c, where $\xi_{s,i}$ is a Gaussian random variable with zero mean and variance $\sigma^2_{\xi_{s,i}} = (1 - a^2_{s,i})\sigma^2_{s,i}$. The term $\sigma_{s,i}$ denotes the log-standard deviation, and the coefficient $a_{s,i}$ is given by $a_{s,i} = \exp(-vT_s/X_c)$, where T_s denotes the sampling period, [87]. In a Rayleigh fading environment, the received signal envelope due to channel fading typically has a Rayleigh distribution, [87]. It is typical to model this fast power fluctuation as (44), where X is a random variable with Rayleigh distribution.

Due to the fact that many users quite naturally simultaneously compete for bandwidth and transmit over the same physical channel using a specific spread spectrum code for each user, the interference plus noise power caused to user i at its assigned base station is given by $I_i(k) = \sum_{\forall j \neq i} g_j(k)p_j(k) + \eta_0$, where $\eta_0 > 0$ assumed to be additive white Gaussian (AWG) denotes the noise power at the receiver of the base station. The achieved SINR for user i is given by

$$\gamma_i(k) = \frac{s_i(k)}{I_i(k)}. \tag{45}$$

For signal reception to occur, the SINR must exceed a given threshold γ^{th}, reflect-

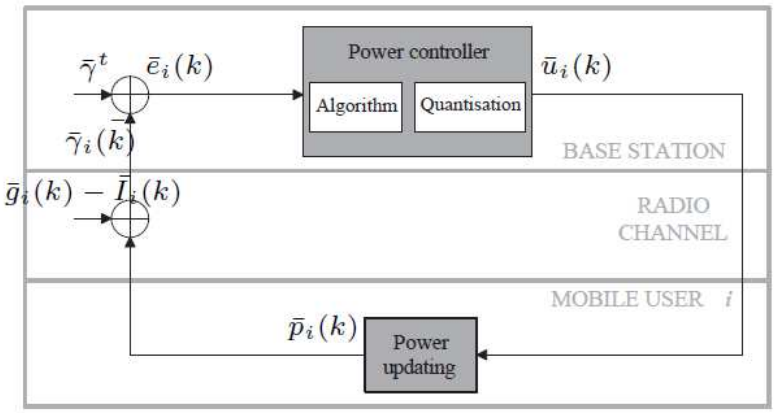

Figure 18: A closed-loop decentralised radio power control

ing a certain QoS requirement, i.e., the outage probability.

4.1.2 Radio Power Control Model for Prediction

A closed-loop SINR-based radio power control system in the logarithmic domain is depicted in Fig. 18. Note that in a decentralised power control framework, only local SINR measured at the base station (i.e., minimal feedback information) is required.

At sampling instant k at the base station, the measured SINR is compared to the target SINR $\bar{\gamma}^t$ for each user. This measurement can be written as

$$\bar{\gamma}_i(k) = \bar{p}_i(k) + \bar{g}_i(k) - \bar{I}_i(k), \tag{46}$$

and the SINR tracking error $\bar{e}_i$ can be expressed as

$$\bar{e}_i(k) = \bar{\gamma}^t - \bar{\gamma}_i(k). \tag{47}$$

The control error will be fed into the power controller, thereby generating the power control update command $\bar{u}_i$. Then the quantised power control command is transmitted via the downlink to the mobile. With $\bar{u}_i$, the power $\bar{p}_i$ to transmit

data packets is updated according to the power control mechanism,

$$\bar{p}_i(k+1) = \bar{p}_i(k) + \bar{u}_i(k). \tag{48}$$

Next, the mobile transmits with this adjusted transmit power on the uplink, wherein it is corrupted by time varying uncertain interference, noise, and channel gain.

From (46)-(48), the next-step SINR tracking error can be derived as the following error dynamic equation,

$$\bar{e}_i(k+1) = \bar{e}_i(k) - \bar{u}_i(k) + \bar{w}_i(k), \tag{49}$$

where $\bar{w}_i$ denotes the uncertain interference, fading, and noise. This allows the complex network dynamics of power control to be simplified, and then represented by using a state-space model applied for each mobile,

$$\bar{x}_i(k+1) = \bar{x}_i(k) - \bar{u}_i(k) + \bar{w}_i(k) \tag{50a}$$

$$\bar{e}_i(k) = \bar{x}_i(k), \tag{50b}$$

with $\bar{x}_i$ representing the state of the SINR tracking error. The model is clearly decentralised and has less complexity than the centralised model, whose dimension depends on the number of users in the cell. In the next subsection, a decentralised robust MPC controller is presented based on the model of the SINR tracking error for a given agent. For simplicity of the notation, the subscript i will now be suppressed.

Remark 1: All computations in MPC are based on a prediction model, and the cost function to be minimised is typically quadratic in the state and in the control input. From (50), the dimension of state and input is small (say, each equal to 1), thus largely reducing the complexity of the optimisation problem.

4.2 Min-Max MPC based power control

In order to deal with the additive uncertainty taken into account in the derived SINR tracking error model (50), we propose to use min-max MPC, [107]. In this paradigm, the objective function is minimised for the worst possible realisation of the uncertainty. In particular, we consider open-loop min-max MPC with state feedback control law and quadratic cost function, [84]. In what follows, we revise the formulation of this class of controllers presented here. In this paper, it was shown that this class of controllers can be implemented by solving a QP problem.

System (50) belongs to the following class of discrete linear time-invariant

system with bounded uncertainty,

$$\bar{x}(k+1) = A\bar{x}(k) + B\bar{u}(k) + D\bar{w}(k), \tag{51}$$

where $\bar{x}(k) \in \mathcal{R}^{n_{\bar{x}}}$ is the state, $\bar{u}(k) \in \mathcal{R}^{n_{\bar{u}}}$ the control input, $\bar{w}(k) \in \mathcal{R}^{n_{\bar{w}}}$ the bounded uncertainty, that is $\bar{w}(k) \in W$, where W is a closed polyhedron that contains the origin.

In order to introduce the effect of feedback in the predictions, we assume that the control input is defined as follows,

$$\bar{u}(k) = -K\bar{x}(k) + \bar{v}(k), \tag{52}$$

where K is a linear gain. This implies that the control moves $\bar{u}(k)$ for updating the transmit power, are corrected by $\bar{v}(k)$ that will be computed by the MPC controller.

The constrained min-max predictive power control problem considered here is

$$\begin{aligned} J^*(\bar{x}) = & \min_{\bar{\mathbf{v}}} \max_{\bar{\mathbf{w}} \in W_{N_p}} V(\bar{x}, \bar{\mathbf{v}}, \bar{\mathbf{w}}) \\ \texttt{s.t.} \quad & \bar{x}(k+j|k) \in \bar{X}, \ \forall \bar{\mathbf{w}} \in W_{N_p}, \ j = 0, \cdots, N_p \\ & \bar{u}(k+j|k) \in \bar{U}, \ \forall \bar{\mathbf{w}} \in W_{N_p}, \ j = 0, \cdots, N_p - 1, \end{aligned} \tag{53}$$

where N_p is the prediction horizon, $\bar{x}(k|k) = \bar{x}$ is the initial state, $\bar{x}(k+j|k)$ and $\bar{u}(k+j|k)$ are the predicted state and control input, respectively, $\bar{\mathbf{v}} = [\bar{v}(k|k)^T, \cdots, \bar{v}(k+N_p-1|k)^T]^T$ is the sequence of correction control inputs, $\bar{\mathbf{w}} = [\bar{w}(k)^T, \cdots, \bar{w}(k+N_p-1)^T]^T$ represents a possible sequence of input disturbances to the system, $W_{N_p} \subseteq \mathcal{R}^{N_p \cdot n_{\bar{w}}}$ denotes the set of possible disturbance sequences of length N_p, $W_{N_p} = W \times W \times \cdots \times W$, where $\times$ denotes the cartesian product, $\bar{X}$ and $\bar{U}$ are polyhedra defined by the state and input constraints respectively and $V(\bar{x}, \bar{\mathbf{v}}, \bar{\mathbf{w}})$ is the objective function defined as

$$\begin{aligned} V(\bar{x}, \bar{\mathbf{v}}, \bar{\mathbf{w}}) \quad = \quad & \sum_{j=0}^{N_p-1} [\bar{x}(k+j|k)^T Q \bar{x}(k+j|k) \\ & + \bar{u}(k+j|k)^T R \bar{u}(k+j|k)] \\ & + \bar{x}(k+N_p|k)^T P \bar{x}(k+N_p|k)], \end{aligned} \tag{54}$$

with $Q \geqslant 0$, $P \geqslant 0$, and $R > 0$.

4.2.1 Min-Max MPC Computation: a QP Formulation

Min-max optimisation problems in general exhibit a very high computational complexity. In [84], it was shown that the optimisation problem (53) can be reformulated into a QP problem. We review in what follows the equivalent QP formulation.

Taking into account (51) and (52), as the predictions $\bar{x}(k+j|k)$ and $\bar{u}(k+j|k)$ depend linearly on $\bar{x}$, $\bar{\mathbf{v}}$, and $\bar{\mathbf{w}}$, the constraints of (53) can be written as $F\bar{x} + G\bar{\mathbf{v}} \leqslant m + M\bar{\mathbf{w}}$, $\forall \bar{\mathbf{w}} \in W_{N_p}$. It follows that the robust constraints of the problem (53) are equivalent to $F\bar{x} + G\bar{\mathbf{v}} \leqslant d$, where d is a vector such that its i-th entry satisfies $d_i = m_i + \max_{\bar{\mathbf{w}} \in W_{N_p}} M_i \bar{\mathbf{w}}$, and m_i and M_i are the i-th element and row of m and M, respectively.

In addition, taking into account (54), matrices $H_{\bar{x}}$, $H_{\bar{v}}$, and $H_{\bar{w}}$ can be found in [16], in such a way that the cost function $V(\bar{x}, \bar{\mathbf{v}}, \bar{\mathbf{w}})$ can be evaluated as the following quadratic function,

$$V(\bar{x}, \bar{\mathbf{v}}, \bar{\mathbf{w}}) = \|H_{\bar{x}} x + H_{\bar{v}} \bar{\mathbf{v}} + H_{\bar{w}} \bar{\mathbf{w}}\|_2^2. \tag{55}$$

As the function $V(\bar{x}, \bar{\mathbf{v}}, \bar{\mathbf{w}})$ is convex in $\bar{\mathbf{w}}$, the maximum can be obtained by evaluating the cost function at the set of *vertices* of the polyhedron W_{N_p}, denoted by $\mathcal{V}(W_{N_p})$. As a result, the problem (53) can be rewritten as

$$\begin{aligned} J^*(\bar{x}) = \min_{\bar{\mathbf{v}}} \max_{\bar{\mathbf{w}} \in \mathcal{V}(W_{N_p})} & V(\bar{x}, \bar{\mathbf{v}}, \bar{\mathbf{w}}) \\ \texttt{s.t.} \quad & F\bar{x} + G\bar{\mathbf{v}} \leqslant d. \end{aligned} \tag{56}$$

If $V(\bar{x}, \bar{\mathbf{v}}, 0)$ is added and subtracted from the cost function $V(\bar{x}, \bar{\mathbf{v}}, \bar{\mathbf{w}})$, the min-max problem can be expressed as the following quadratic optimization problem using the epigraph approach to evaluate the maximum of a set of linear functions,

$$\begin{aligned} J^*(\bar{x}) = \min_{\bar{\mathbf{v}}, \gamma} & V(\bar{x}, \bar{\mathbf{v}}, 0) + \gamma \\ \texttt{s.t.} \quad & F\bar{x} + G\bar{\mathbf{v}} \leqslant d \\ & \gamma \geqslant V(\bar{x}, \bar{\mathbf{v}}, \bar{\mathbf{w}}) - V(\bar{x}, \bar{\mathbf{v}}, 0), \\ & \qquad \forall \bar{\mathbf{w}} \in \mathcal{V}(W_{N_p}), \end{aligned} \tag{57}$$

with

$$\begin{aligned} & V(\bar{x}, \bar{\mathbf{v}}, \bar{\mathbf{w}}) - V(\bar{x}, \bar{\mathbf{v}}, 0) \\ & \quad = \bar{\mathbf{w}}^T H_{\bar{w}}^T H_{\bar{w}} \bar{\mathbf{w}} + 2\bar{\mathbf{w}}^T H_{\bar{w}}^T (H_{\bar{x}} \bar{x} + H_{\bar{v}} \bar{\mathbf{v}}). \end{aligned} \tag{58}$$

In order to obtain an equivalent problem to (57) in which the functional does not depend on the state vector, the following variable change is introduced,

$$\bar{\mathbf{z}} \triangleq \bar{\mathbf{v}} + [H_{\bar{v}}^T H_{\bar{v}}]^{-1} H_{\bar{v}}^T H_{\bar{x}} x. \tag{59}$$

As a result, the min-max problem (53) is now equivalent to

$$J^*(\bar{x}) = \bar{x}^T Y \bar{x} + \min_{\bar{\mathbf{z}},\gamma} \frac{1}{2} \bar{\mathbf{z}}^T H \bar{\mathbf{z}} + \gamma \tag{60}$$

$$\texttt{s.t.} \quad G_m \bar{\mathbf{z}} + g_m \gamma \leqslant W_m + S_m \bar{x} \tag{61}$$

$$G_c \bar{\mathbf{z}} \leqslant W_c + S_c \bar{x}. \tag{62}$$

The constraints (21) described by matrices G_m, g_m, W_m, and S_m correspond to the maximisation of the functional, while (22) defined by G_c, W_c, and S_c represent the robust constraints of the problem. All these matrices can be obtained from the system model and the cost function.

Therefore, the application of the min-max MPC to the radio power control system can be written as:

Algorithm:

1. At sample k, solve the optimisation problem (20)-(22).
2. Obtain $\bar{\mathbf{v}}$ from the variable change defined in (59).
3. Then, set $\bar{v}(k) = \bar{\mathbf{v}}(0)$, and apply $\bar{u}(k) = -K\bar{x}(k) + \bar{v}(k)$ for the power control update command.
4. Get new SINR tracking error measurement, and repeat the optimisation at sample $k+1$.

4.3 Simulations

The min-max MPC based power control algorithm described in the previous subsection has been numerically studied by using the CDMA network simulation model developed in [3]. This provides a benchmark simulation platform for the evolution of this class of network. The simulation parameters to form the network can be summarised as follows. In this scenario, a single-cell uplink CDMA system has been simulated with 10 mobile users. The hexagonal cell with radius of 1 km is controlled by one base station centred at the origin. The mobile users are randomly distributed over this area according to a Gaussian distribution. The

mobility of each user is arbitrarily chosen at the beginning of the simulation to create several test situations. The simulations have been performed based on the operating frequency of 900 MHz and the bandwidth B_w of each channel assumed to be 1.23 MHz. The data bit rate R_b is set at 9.6 kbps. For simplicity, perfect SINR measurement is supposed and the target SINR $\bar{\gamma}^t$ is set to be -10 dB for all users. Moreover, the standard deviation of noise power at the base station has been selected as a random value between 0.5 and 1. An urban area setting has been taken into account for the operational environment. The parameters settings of the radio link propagation employed in the simulation model that follows in such a circumstance is:- path loss exponent $\alpha = 4$, log-standard deviation of shadowing $\sigma_{s,i} = 2.7$, and the Rayleigh distribution parameter has been set to 0.5.

4.3.1 Uncertainty Bounds

To apply the min-max MPC, the uncertainty bounds have been set according to the error computed using the predicted state which came from the prediction model (49) with $\bar{w}_i(k) = 0$. The errors computed using this model are shown in Fig. 19. The uncertainty bounds have been set to -2.5 and 2.5, since 95.13% of the errors are within these bounds.

4.3.2 Benchmark Comparison

To benchmark the advantages of the proposed algorithm, the min-max MPC is compared with other existing control laws.

Power control with fixed-step size: In this technique, [4], the base station transmits the control decision to the mobile to either up or down its power by a typical fixed-step size of 1 dB, i.e., if the measured SINR is above the target, then the update command is to decrease power by -1 dB, otherwise the control action taken is to increase power by 1 dB.

Power control with robust $\mathcal{H}_\infty$: In [62], a robust $\mathcal{H}_\infty$ power controller with fixed state feedback gain K_∞ was proposed to minimise the worst-case effects of interference and noise on SINR variance by solving an $\mathcal{H}_\infty$ optimal tracking problem, $\frac{\sum_{k=0}^{k_f} \bar{e}(k)^T R_1 \bar{e}(k)}{\sum_{k=0}^{k_f} \bar{w}(k)^T R_2 \bar{w}(k)} < \gamma^2$, subject to some linear matrix inequality (LMI) constraints. Here, R_1 and R_2 are respectively positive weighting factors for tracking and disturbance rejection, and γ is a prescribed value. With this method, a resulting optimal $\mathcal{H}_\infty$ gain (K_∞) of 1 has been obtained for the case studied.

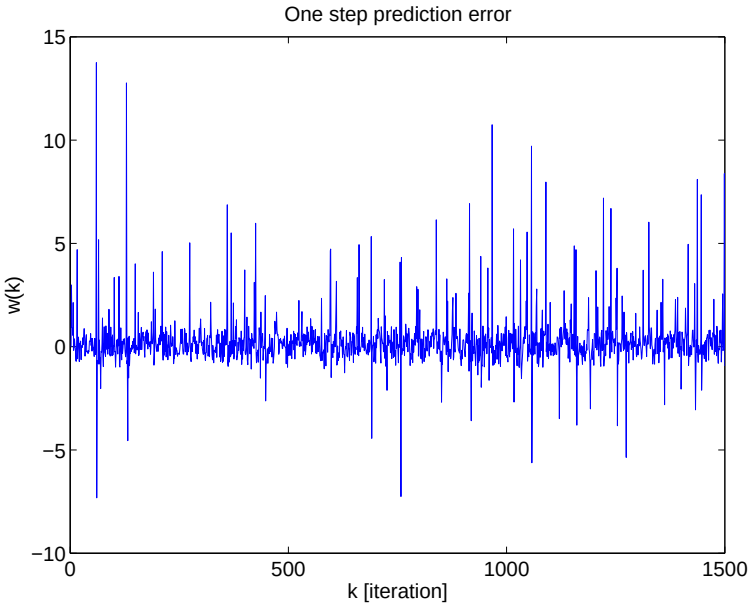

Figure 19: One-step prediction error

Power control with nominal MPC To test the robustness of the proposed strategy, a nominal MPC has also been considered in this benchmark comparison. The settings of the controller parameters have been reasonably well tuned: $N_p = 3$, $Q = P = 2$, and $R = 1$.

Power control with min-max MPC The following tuning and weighting factors have been used during the application of the proposed min-max MPC scheme: $N_p = 2$, $Q = P = R = 1$, and $K = -0.618$. The min-max MPC optimisation problem (20)-(22) to be solved at each sample k is subject to the state constraint $\|\bar{x}(k)\|_\infty \leqslant 4$, corresponding to the SINR threshold value, and the input constraint $|\bar{u}(k)| \leqslant 10$. Note that these constraints have also been set for the nominal MPC.

Both the nominal MPC and the min-max MPC quadratic optimisation problems have been solved using Matlab's `quadprog`.

4.3.3 Performance Assessment

In order to compare the performance of the proposed min-max MPC control strategy with the other controllers, several simulation test scenarios that include vari-

able mobile speeds for each user in the range 20-100 km/h have been considered. For each scenario, the simulation has been iteratively performed for 10 runs with a duration of 200 samples in each run. Note that for consistency the type of motion for each user was randomly determined at the beginning of each simulation and not changed when an experiment is conducted for each controller. During the simulation, dynamic data of all users were stored, and at the end the mean measured values were produced according to the following two performance criteria:

- Outage probability, [55]:

$$P_{o_i} = \text{Prob}\{\bar{\gamma}_i < \bar{\gamma}^{\text{th}}\}, \tag{63}$$

  where $\bar{\gamma}^{\text{th}}$ denotes the SINR threshold, a minimum value required for signal reception to occur. The SINR threshold is given by $\bar{\gamma}^{\text{th}} = (\frac{E_b}{I_o})(\frac{R_b}{B_w})$, where E_b denotes the energy dissipated per information bit and I_o the total interference and noise power spectral density. In order to achieve an acceptable bit error rate (BER) of $< 10^{-3}$, the target $\frac{E_b}{I_o} = 7$dB is required for every user, which results in $\bar{\gamma}^{\text{th}} = -14$dB.

- Standard deviation of the SINR tracking error:

$$\bar{\sigma}_{e_i} = \left(\frac{1}{N}\sum_{k=1}^{N}(\bar{\gamma}^t - \bar{\gamma}_i(k))^2\right)^{\frac{1}{2}}, \tag{64}$$

  where N is the total number of samples.

4.3.4 Results Analysis

Impact of channel uncertainty (one user case): To investigate the system performance in the presence of channel fading, only one user is considered. The results shown in Fig. 20 and 21 illustrate the evolution of the achieved SINR level and the transmission power in each iteration for a user (traveling at 100 km/h) using the different controller designs. It is readily observed that in this highly uncertain environment the min-max MPC offers a significant improvement in respect of maintaining the SINR above a threshold value, (i.e., the number of measurements that violate the SINR floor constraint is much lower in the min-max MPC case than for other competing strategies). The min-max MPC approach also exhibits the lowest average transmission power in these experiments.

Effect of increasing number of users: In this scenario, the effect of 10 users utilising the network simultaneously is considered. Figure 22 and 23 depict the evolution of SINR and transmission power for a randomly observed user traveling at 100 km/h in such a scenario. As expected, the min-max MPC approach provides the best robust tracking performance with the smallest variations in the received SINR, thus resulting in the least number of samples in which the threshold value has been crossed. Furthermore, Fig. 23 suggests that the effect of induced MAI causes the overall power consumption to be much better in the min-max MPC case, in particular with respect to the robust $\mathcal{H}_\infty$ design. This suggests that the use of a min-max MPC approach avoids an unnecessarily high user (or link) cost, and will thereby result in a (much) improved battery lifetime.

Effect on P_o and $\bar{\sigma}_e$: In this example, the effect of variable mobile velocity ranging from 20-100 km/h on both the outage probability and tracking performance is addressed. As mobility increases, the fluctuation in channel gain becomes more rapid. The results are aggregated for the performance criteria (63) and (64) in Fig. 24 and 25, respectively. It is clear from Fig. 24 that transmit power control using the min-max MPC performs best with a significant enhancement in a certain level of robustness to outage events with respect to the other methods over the set of mobile velocities considered. Figure 25 demonstrates the fact that the min-max MPC approach exhibits smaller standard deviation with respect to SINR tracking error than the other schemes over the test set.

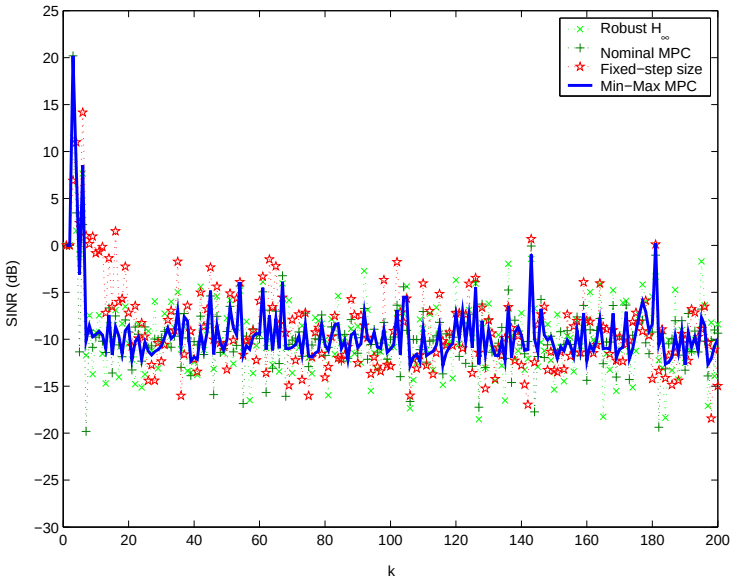

Figure 20: Evolution of the SINR for one mobile user traveling at 100 km/h. (Scenario 1)

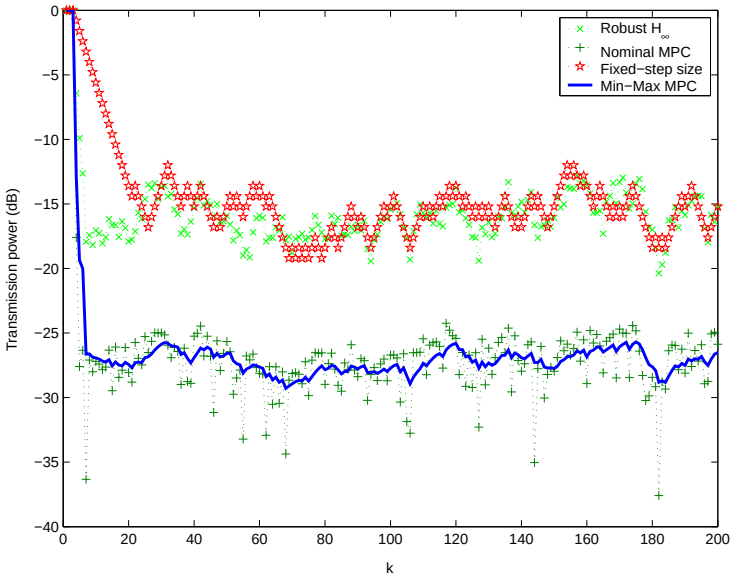

Figure 21: Evolution of the transmission power for one mobile user traveling at 100 km/h. (Scenario 1)

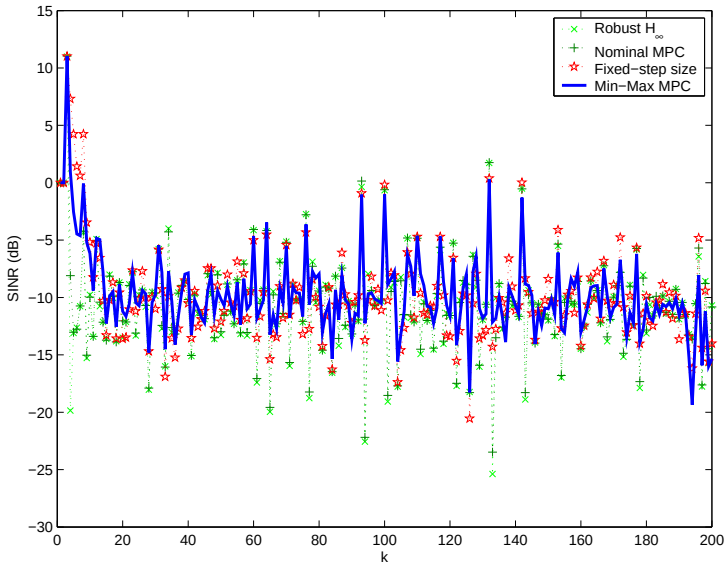

Figure 22: Evolution of the SINR for a randomly selected mobile user traveling at 100 km/h. (Scenario 2)

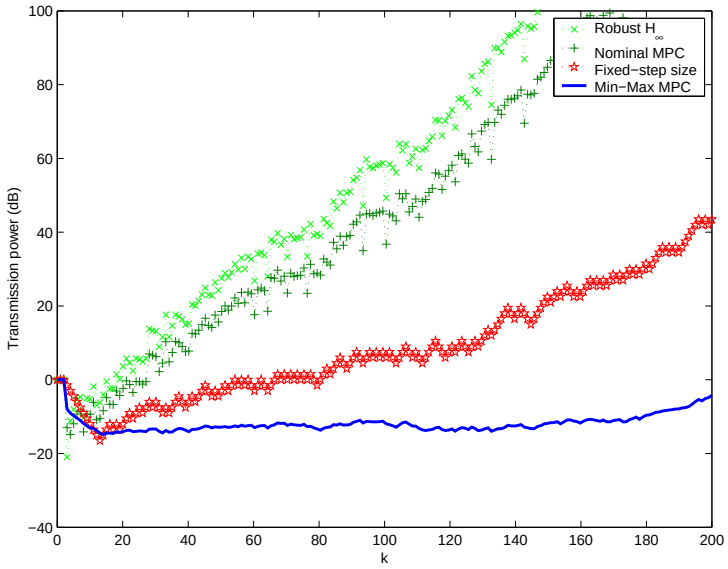

Figure 23: Evolution of the transmission power for a randomly selected mobile user traveling at 100 km/h. (Scenario 2)

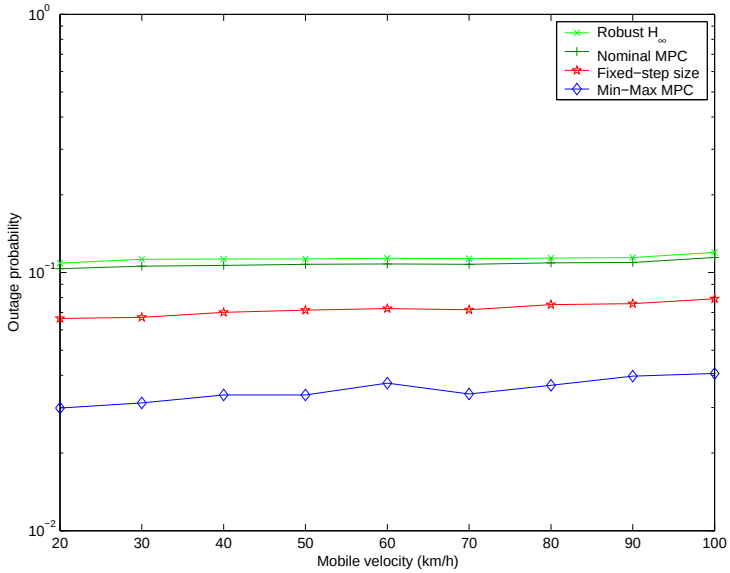

Figure 24: Outage probability with varying mobile velocity for 10 mobile users

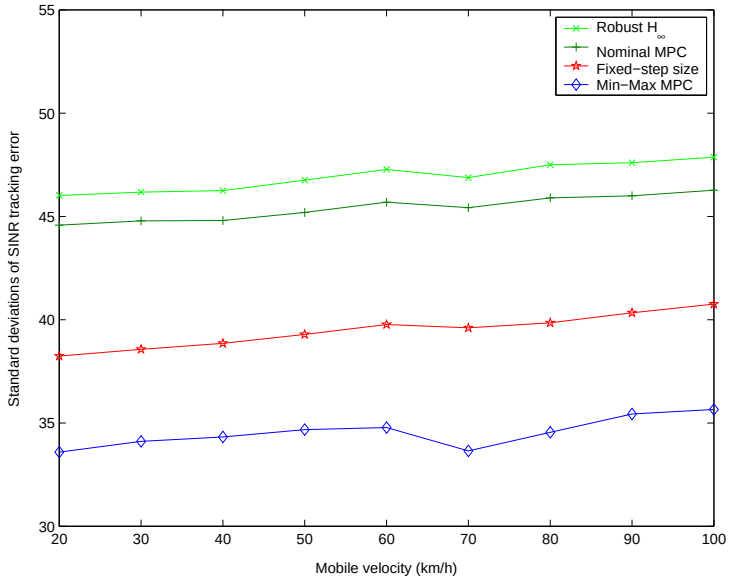

Figure 25: Standard deviations of the SINR tracking error with varying mobile velocity for 10 mobile users

5 Dwell-Time Adaptive Delta Modulation SignalCoding For Networked Controlled Systems

This paper deals with the problem of control with limited data rates in the area of Networked Controlled Systems (NCS). Limited data rates impose a tradeoff between the communication bandwidth and the amount of information required for stabilization. Large quantization errors and instability of the system may be observed when this tradeoff is not handled properly (in particular for open-loop unstable systems). It has been shown in [76], [35] [49] and in [97], [13] or more recently in [74] that the required number of bits per sample is related to the open-loop eigenvalues. For instance, in the scalar case, the available theorem provides the condition $R > \log_2 |\lambda|$ bits per sample, where R is the data rate and λ is the open-loop eigenvalue. This result is a consequence of Kolmogorov-Sinai theorem introduced in the fifties, [59] [95]. This was the first time that a theoretical measure for entropy was defined. Interested readers can also refer to [77] and [7] where a complete overview is given. The objective of this paper is then to look for a new adaptive quantization algorithm that reaches global stability for multivariable systems, while minimizing the number of required bits, and has a smooth transient behavior.

5.0.5 Coding strategies

There is a large variety of coding (quantization) strategies in the context of NCS. Quantization can be *uniform or not*. The typical example for non uniform quantization is the logarithmic quantization, where the resolution is high if the quantized signal is close to the reference signal; but coarse otherwise. In [33], the authors show that the coarsest quantizer that quadratically stabilizes a single input linear discrete time invariant system is logarithmic. With a finite number of quantization levels, the authors obtain local practical stability for the closed-loop system. In [56], [39] this analysis is generalized to multivariable systems. And in those contributions, they find an optimal logarithmic base that can be exclusively written in terms of the unstable eigenvalues of the system.

Quantization can be performed in the *absolute or differential* signal frame. In *absolute* coding, the outputs are directly quantized, and no past information is kept in memory (memoryless coding). In the case of static quantization, only local practical stability could be obtained and the performance depends on the number of words used to code the signal and the corresponding size of the quantization step Δ. A pioneer work on that type of coding is [29]. Since then, several other

extensions have been published along that idea; [108], [12] and [30]. On the other hand, *differential* quantization codes the signals differences (or rate) instead. The signals are then compared to a memory value and then its variation is quantized. Differential coding is well adapted to reduce at maximum the amount of information to be transmitted, as it includes local memory (dynamic coding). [94] presents a dynamic coding using noise shaping quantization ideas to take quantization effects into account. Using linear time invariant system theoretical tools, the authors design a noise shaping quantizer that minimizes the impact of quantization noise on loop performance, as measured by the tracking error variance due to quantization. On the other hand, in [86], the basic grounds for differential coding (delta modulation) are well described. Differential coding with uniform quantization was studied in [17], [52]. In [17] the authors provides one-bit delta modulation for scalar systems. This result was extended for arbitrary-dimension multivariable linear systems in [52], where a new centralized vector coding algorithm is proposed, and two tuning methods for selecting the quantization steps were presented. Other alternatives have been presented in [13], [65], [66], [92], [5]. In [5], an optimal dynamic quantizer for a class of linear multivariable time - invariant system actuated by discrete - valued signals are presented. The quantizer considered in [5] is in the form of a linear difference equation.

Quantization steps could also be *constant or adaptive*. Constant quantization results, at best, in local practical stability. Inversely, adaptive coding algorithms allows to devise globally and asymptotically stable systems.

Because of its nature of encoding differences rather than absolute values, differential coding may suffer from loss of synchronization [73] between the sender and the receiver. Hence, some additional mechanisms, such as feedback from receiver to sender, may be necessary to overcome data loss due to the channel erasure. An example of such mechanisms has been proposed in [68].

5.0.6 Adaptive quantization

The literature of adaptive quantization in NCS is very rich. A good starting points is the work [13], where a globally stable adaptive quantization algorithm was proposed. The main idea here is to increase the value of the quantization steps when the signal is large (“Zoom - Out") and to decrease it otherwise (“Zoom - In"). In practice, this method offers similar advantages as the logarithmic quantization, though this method uses a small data rate (the resolution is high if the quantized signal is close to the reference signal; but coarse otherwise). In adaptive quantization, some works have focused their attention mainly on the Zoom-In process (e.g., [97], [49]). In these works, the stability results are limited to semi-global

stability. More recent works in [41], [66], [92], [77], have improved the issue of semi - global stability by introducing diverse types of new mechanisms.

Adaptive differential coding combines the two advantage mentioned before (minimum bits and good stability properties). Differential coding with uniform quantization was studied in [17], [52], [41]. In [41], the authors have presented a quantization method based on a one-bit-adaptive delta modulation. The benefits of this idea is that it provides global stability in the scalar case (under the conservative condition that the open-loop eigenvalue, λ, is $|\lambda| < 1.3$). Natural directions for improvements are thus, the extension to multivariable systems, and the algorithm re-design to reach stability conditions closer to the theoretical limits under fixed-length coding algorithms[6]. These are the objective of this paper. Note that in this paper, we use fixed length coding schemes. The motivation for using fixed length coding techniques is the simplicity of the modulation/de-modulation schemes. If we use variable length coding schemes, the receiver must be able to distinguish between three modes: “0", “1", and “idle: When the channel is not being used". But, if we use fixed length coding schemes, the receiver only needs to distinguish between two modes: “0" and “1".

5.0.7 Main contribution of the paper

In this paper, we propose a new adaptive differential coding algorithm for multivariable state-space systems, with global exponential stability and improved transient behavior. The algorithm reaches the rate theoretical limits (the algorithm is coded with the minimum number of possible bits under fixed-length coding). The idea is to introduce a new *Dwell-Time* state in addition of the classical Zoom-In and Zoom-Out. This yields a better estimate of the transition condition between Zoom-In and Zoom-Out states, and thereby its transition improves the global behavior of the algorithm. The Dwell-Time mechanism introduces a hysteretic effect that smoothes out the periodic and oscillatory behavior observed in [92], and [66]. During Dwell-Time state, past coded information is collected and kept in memory for a finite time. This information is used to predict the moment when the reconstructed state error leaves a threshold indicating to which state (Zoom-In, or Zoom-Out) the transition should be enabled. Because of this behavior the algorithm is named *Dwell-Time Zoom-In/Zoom-Out* (D-ZIZO).

[6]For the stability of linear time invariant systems over digital channels, the minimum bit rate is equal to the eigenvalue rate: $\sum_{\{l=1,|\lambda_l|>1\}} \log|\lambda_l|$ (λ_ls are the eigenvalues of the system). Most of the time, the eigenvalue rate is not an integer number; and we are restricted to use a fixed length coding. For this case, the best we can do is to reach a bit rate equals to the smallest integer bigger than the eigenvalue rate.

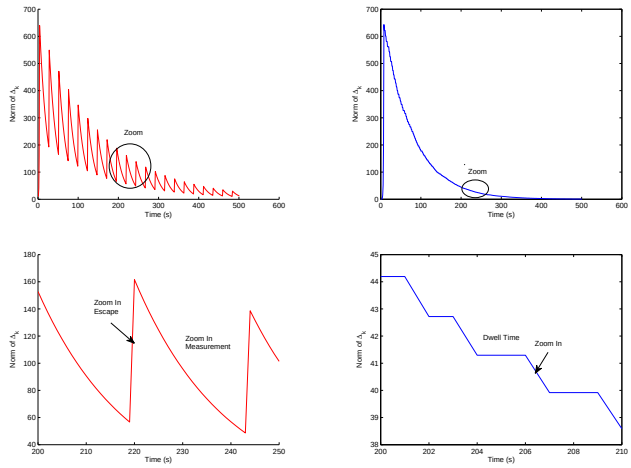

Figure 26: Comparison between the evolution of the norm of the quantization step $\Delta(k)$ for both adaptive quantization algorithms: ZIZO is presented in the left side and D-ZIZO in the right side. We clearly see that with ZIZO, the norm of $\Delta(k)$ increases during the ZIE phase and in D-ZIZO the norm of $\Delta(k)$ remains constant. The simulation is for the scalar case (the case study presented in [51]) with $\lambda = 2.1$ and the duration of Dwell - Time $\nu = 3$. The parameters are constrained by the following conditions: $C_{in} = 0.96$, $C_{out} = 2.7$, $\Theta_{out} = 2.7$, $\Theta_{in,m} = 0.96$, $\Theta_{in,e} = 2.7$, and the duration of Zoom In Measurement $p = 22$ with $\Theta_{in,m}^{p}\Theta_{in,e} < 1$. The initial conditions are $\Delta(0) = 0.1$ and $\tilde{x}(0) = 2$.

In Fig. 26, we compared the evolution of the norm (i.e., transient behavior) of the quantization step $\Delta(k)$ for both adaptive quantization algorithms: ZIZO [92] and D-ZIZO. Note that as the quantization step $\Delta(k)$ affects the estimation error and subsequently the control signal; and therefore, the states of the system (see Fig. 28), the evolution of the norm of the quantization step can represent the transient control performance. In the ZIZO algorithm of [92], the behavior of the adaptive quantization law after the first Zoom-Out stage, is composed of two parts: Zoom-In Measurement (ZIM), in which the quantization steps decrease, and Zoom-In Escape (ZIE) used for robustness purposes, where the quantization steps increase. As shown in Fig. 26, this process is periodic and introduces oscillations that are reflected in the state estimation; and hence into the regulation quality of the closed-loop system. However, in the D-ZIZO algorithm, the ZIM-ZIE steps are replaced by a Dwell- Time, and a Zoom-In stage. During Zoom-In stage, the quantization steps decrease, whereas during Dwell-Time, the quantiza-

tion steps remain constant. The result of this modification, as can be seen in Fig. 26, is that the oscillations can be canceled. As clear from Fig. 26, the evolution of the norm of the quantization step of the D-ZIZO algorithm is much smoother than the one from the ZIZO structure. The non - smooth evolution of the norm of the quantization step associated to the ZIZO algorithm [92] results in exciting the unmodeled high frequency part of the system dynamics, friction between mechanical components, fast aging, etc. The smooth evolution of the norm of D-ZIZO algorithm overcomes these drawbacks.

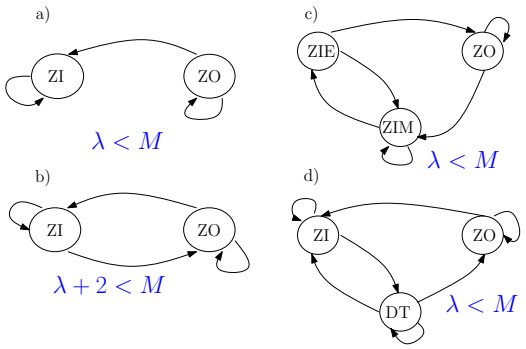

Figure 27: For the scalar case, figure a) is associated to the algorithm of [97], figure b) is associated to the algorithm of [13], figure c) is associated to the algorithm of [92] and figure d) is associated to the D-ZIZO algorithm. The condition below each graph represents the maximal value for the eigenvalue λ such that the system is stabilized.

In Fig. 27, different algorithms proposed in the literature are presented using finite-state machine graphs. This type of representation captures some of the main properties of each algorithm. For instance, works in [97], [49], [13], [65] belong to the class represented by Fig. 27 a), where we clearly see that once the algorithm enters in the Zoom-In stage, there is no way to go back to Zoom-Out stage. So, the algorithm cannot be robust with respect to unmodeled disturbances. Works like [66] (scalar case), enter into the classification of algorithms represented by the graph in Fig. 27 b), where the closed-loop system is stable under the condition $\lambda + 2 < M$ ($M \geqslant 3$ is the number of words/quantization levels used to quantize the signal). Belonging to the same class, the work in [77], proposes an adaptive quantization law for scalar case. The quantization levels are the same as [66]; but the coded information is decomposed in M signal words and one alarm bit.

Improvement in terms of approaching the theoretical rate limits are reached in more recent works of [92], which are captured by the 3-state finite machine graph as shown in Fig. 27 c). In this category, the adaptive quantization law is robust to disturbances under the condition $\lambda < M$. This result holds for multivariable systems with a diagonalizable open-loop matrix. Note that the approach of [92] does not verify the data rate theorem for $\lambda < 2$ because the algorithm needs at least $M = 3$ words per signal.

The work proposed in this paper has also 3-states (modes in the sequel); but with different functionalities (the ZIE and ZIM modes are replaced by ZI and DT modes) as shown in Fig. 27 d). The adaptive algorithm satisfies the minimal value of the data-rate theorem, and applies for all classes of linear systems. As mentioned before, it presents a smoother behavior than the class in Fig. 27 c).

Compared with the algorithm of [92], we can underline the following potential improvements: a) The D-ZIZO algorithm reaches the theoretical rate limit for scalar and multivariable systems, and, b) Due to the hysteretic effect introduced by the Dwell-Time mechanism, the transient behavior (in terms of high-frequency component) of the D-ZIZO is improved over the ones from the ZIZO structure. The behavior improvement is shown in Fig. 26, where the evolution of the quantization steps $\Delta(k)$ for D-ZIZO and ZIZO algorithms are shown.

5.0.8 Paper organization

The aim of the paper is to present an adaptive quantization algorithm that provides exponential stability for controllable linear systems; while reaching the data-rate theoretical limits and displaying a smooth transient behavior. Section 5.1 of the paper formulates the problem and presents the architecture of the adaptive quantization. In that section, we also present a detailed description of each block composing the whole algorithm. This includes: The model-based predictor, the quantizer; and in particular, the change of coordinates, via the dynamic matrix $\boldsymbol{T}(k)$, that allows us to treat the general case of multivariable linear systems. In Section 5.2, we present the adaptive quantization law for general multivariable case. The extension from scalar systems to multivariable systems is possible due to the introduction of matrix $\boldsymbol{T}(k)$.

The last part of the paper deals with robustness issues: Section 5.4 extends the analysis to systems with bounded input disturbances, and new data-rate conditions are derived for stabilization, in terms of the noise upper bound. Finally, Section 5.5 analyzes the system behavior in the presence of packet losses, and proposes a recovery procedure to resynchronize the estimators at the sender and the receiver when packet losses have biased them.

5.1 Problem formulation

The following conventions will be used throughout the paper:

- **N** denotes the set of positive integers.
- $\boldsymbol{I}_m$ denotes the identity matrix of dimension $m \times m$.
- T_s is the sampling period.
- n is the state dimension that corresponds to the number of sensors,
- m is the number of control inputs,
- $x(k) = [x_1(k), \ldots, x_n(k)]^T \in \mathbf{R}^{(n\times 1)}$ is the n-dimensional state vector at instant kT_s (each $x_i(k)$ corresponds to the ith sensor) ;
- $u(k) = [u_1(k), \ldots, u_m(k)]^T \in \mathbf{R}^{(m\times 1)}$, is the m-dimensional control input vector at instant kT_s.
- $\boldsymbol{A}$ is the open-loop matrix and $\boldsymbol{B}$ is the matrix associated to the control inputs with $\boldsymbol{A} \in \mathbf{R}^{(n\times n)}$ and $\boldsymbol{B} \in \mathbf{R}^{(n\times m)}$. The pair $(\boldsymbol{A}, \boldsymbol{B})$ is controllable.
- $\hat{x}(k)$ is an estimation of $x(k)$ and, more generally, for a given signal $q(k)$, $\hat{q}(k)$ represents an estimated value of $q(k)$.
- $\tilde{x}(k)$ denotes the estimation error: $\tilde{x}(k) = x(k) - \hat{x}(k)$, and $\tilde{q}(k)$ represents the error $q(k) - \hat{q}(k)$.

The problem considered is the stabilization of a multivariable system, in which sensor signals are centralized, and then transmitted through a digital communication link to a remote controller. In a normal situation, the communication link is the digital noiseless channel; while, in an abnormal case, it is subject to packet losses.

The discretized system is given by:

$$x(k+1) = \boldsymbol{A}x(k) + \boldsymbol{B}u(k) + s(k), \tag{65}$$

where $|s(k)| \leqslant S$ is the additive bounded noise. The controller law is given by:

$$u(k) = -\boldsymbol{K}\hat{x}(k) \tag{66}$$

with $\boldsymbol{K} \in \mathbf{R}^{(n\times m)}$ such that the matrix $\boldsymbol{A} - \boldsymbol{B}\boldsymbol{K}$ is Schur (the module of $\boldsymbol{A} - \boldsymbol{B}\boldsymbol{K}$'s eigenvalues are strictly inferior than 1).

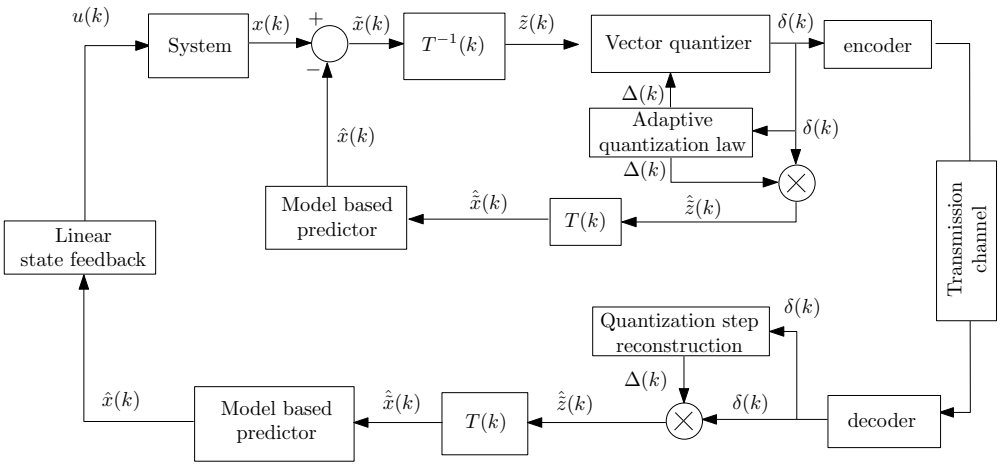

Figure 28: Closed-loop system with Dwell-Time delta modulation.

Fig. 28 illustrates the general architecture of the proposed differential coding algorithm. It is composed of four main blocks, as described below:

1. **The rotation matrix $\boldsymbol{T}(k)$** which transforms the estimation error $\tilde{x}(k) = [\tilde{x}_1(k), \ldots, \tilde{x}_n(k)]^T$ into a new set of coordinates $\tilde{z}(k) = [\tilde{z}_1(k), \ldots, \tilde{z}_n(k)]^T$. The aim of this matrix is to reduce the complexity of the analysis and design (originally in dimension n) to a set of several independent subsystems with smaller dimension than the original system. Specific details on the construction of this matrix will be given latter in Section 5.2.1.

2. **The quantizer block** which transforms the error $\tilde{z}(k)$, using the adaptive quantization steps $\Delta(k) = [\Delta_1(k), \ldots, \Delta_n(k)]^T$ to the codeword $\delta(k) = \delta(\tilde{z}(k)) = [\delta_1(k), \ldots, \delta_n(k)]^T$, by using the following map:

$$\delta_i(k) = \begin{cases} (M_i - 1)/2 & \text{if } \mathcal{C}^+, \text{ holds} \\ N_j & \text{if } \mathcal{C}_j, \text{ holds} \\ -(M_i - 1)/2 & \text{if } \mathcal{C}^-, \text{ holds} \end{cases} \tag{67}$$

with

$$N_j = \frac{M_i - j}{2}, \quad \forall j = 3, 5, 7, 9, \ldots, (2M_i - 3)$$

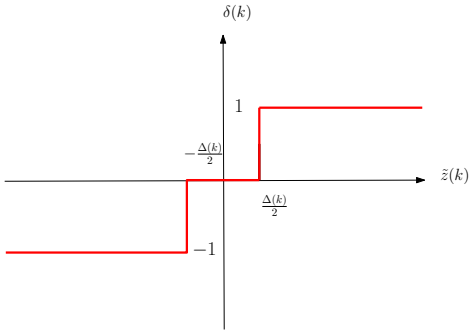

Figure 29: Example of quantization of one state variable with 3 words per signal.

where the set of conditions $\mathcal{C}_j$ are defined as follows:

$$\begin{aligned} \mathcal{C}^+ &: \tilde{z}_i(k) \geqslant (M_i - 2)\Delta_i(k)/2 \\ \mathcal{C}_j &: (N_j - 1/2)\Delta_i(k) \leqslant \tilde{z}_i(k) < (N_j + 1/2)\Delta_i(k), \\ \mathcal{C}^- &: \tilde{z}_i(k) < -(M_i - 2)\Delta_i(k)/2 \end{aligned}$$

Note that Fig. 29 illustrates the quantization policy for the scalar case using $M = 3$ words (quantization levels) per signal.

3. **Adaptive quantization law** which maps the codeword $\delta(k)$, to the adaptive quantization steps $\Delta(k)$. The precise equations and the associated stability properties will be detailed in Section 5.2. The adaptation law will be of the following general form:

$$\Delta(k+1) = \Phi(\Delta(k), \delta(k), ..., \delta(k - \nu + 1)), \tag{68}$$

where ν is the size of the adaptation law window, which will be related to the system eigenvalue structure (i.e. the number of similar poles, etc.). It will be also directly related to the Dwell-Time state defined for our proposed algorithm.

4. **The model based predictor** which transforms back the codeword, $\delta(k)$, to the system state estimation $\hat{x}(k)$, by using the following predictor equation:

$$\hat{x}(k+1) = (A - BK)\hat{x}(k) + AT(k)\hat{\tilde{z}}(k) \tag{69}$$

with $\hat{\tilde{z}}(k) = [\hat{\tilde{z}}_1(k), \ldots, \hat{\tilde{z}}_n(k)]^T$, where $\hat{\tilde{z}}_i(k) = \Delta_i(k) \cdot \delta_i(k), \;\; 1 \leqslant i \leqslant n.$

In this paper, we attempt to find a suitable function Φ, in (68) under which the closed-loop system is globally stable with smooth transient behavior and reaches the rate theoretical limits under constant length coding.

5.2 The D-ZIZO algorithm for multivariable systems

The D-ZIZO algorithm for scalar systems with three quantization levels/words (i.e., $M = 3$) was introduced in [51]. In this section we generalize it to the case of multivariable systems with arbitrary quantization levels. The main ideas for this extension involve:

- Using a transformation matrix $\boldsymbol{T}(k)$ (Section 5.2.1), which reduces the complexity of the analysis and design to a set of several independent subsystems with smaller dimension.
- Suitably initializing the quantization steps $\Delta_i(0)$
- Extending the results of [51] to a system with μ number of quantization levels per signal.
- Defining a condition $\mathcal{C}_{\mathcal{T}}$ to switch from DT to ZO in the case that unexpected time-limited disturbances cause quantizer overload. If condition $\mathcal{C}_{\mathcal{T}}$ does not hold, Zoom-In always occurs after Dwell-Time.
  The condition $\mathcal{C}_{\mathcal{T}}$; and in particular, the value of the Dwell-Time period ν are chosen such that they provide enough samples to form a robust criterion (i.e., $\mathcal{C}_{\mathcal{T}}$) to decide to switch ZO mode only if strictly necessary (i.e., a large disturbance occurs).
- As in the scalar case [51], the stability analysis will be based on the dynamics of the error-to-quantizer ratio, which for multivariable systems is defined as follows,

$$y(k) \stackrel{\triangle}{=} [\tilde{z}_1(k)/\Delta_1(k), \tilde{z}_2(k)/\Delta_2(k), \ldots, \tilde{z}_n(k)/\Delta_n(k)]^T.$$

5.2.1 The rotation matrix $\boldsymbol{T}(k)$

For simplicity of the analysis, we require the dynamic equations of $y(k)$ to have a particular structure. However, in order to preserve the generality of the algorithm,

we will describe a time-varying linear coordinate change $\boldsymbol{T}(k)$ that transforms any linear state-space system into the required form.

To understand the advantage of the change of coordinates with a matrix $\boldsymbol{T}(k)$, consider the following two examples which involve pairs of complex conjugate eigenvalues with magnitude $|\lambda|$.

Example 1. Consider a system of the form (65), with

$$\boldsymbol{A} = |\lambda|\boldsymbol{R}(\pi/4)$$

where $\boldsymbol{R}(\pi/4) = \begin{pmatrix} cos(\pi/4) & sin(\pi/4) \\ -sin(\pi/4) & cos(\pi/4) \end{pmatrix}$, and $\boldsymbol{B}$ is such that the pair $(\boldsymbol{A}, \boldsymbol{B})$ is controllable. This system involves a pair of complex conjugate eigenvalues with magnitude $|\lambda|$. Let $y_1(k) = \tilde{z}_1(k)/\Delta_1(k)$, $y_2(k) = \tilde{z}_2(k)/\Delta_2(k)$ and

$$\mathcal{B}^{ext} = \{\begin{pmatrix} y_1(k) \\ y_2(k) \end{pmatrix} : |y_i(k)| \leqslant M_i/2, \;\; 1 \leqslant i \leqslant 2\}, \tag{70}$$

where M_i is the number of words/quantization levels used to quantize the error signal $y_i(k)$.

Suppose that we take $\boldsymbol{T}(k) = \boldsymbol{I}_2$, which gives $\tilde{x}(k) = \tilde{z}(k)$, and consequently

$$\tilde{z}(k+1) = |\lambda|\boldsymbol{R}(\pi/4)(\tilde{z}(k) - \hat{\tilde{z}}(k))$$

Let us choose $M_i = 3$ subdivisions per signal, with quantization steps $\Delta_1(k)$,$\Delta_2(k)$. We suppose that the initial condition at $k = 0$ is such that $y(0) \in \mathcal{B}^{ext}$. It can be easily shown that for $\Delta_1(k) = \Delta_2(k) = \Delta$ we obtain $y(1) \in \mathcal{B}^{ext}$ provided $|\lambda| < \frac{3}{\sqrt{2}}$. This condition is more conservative than $|\lambda| < 3$. But, it is possible to retrieve a less conservative result by redefining the transform matrix $\boldsymbol{T}(k)$ as follows:

$$\boldsymbol{T}(k) = \boldsymbol{R}(k\pi/4).$$

Then, for $\tilde{z}(k) = \boldsymbol{R}(-k\pi/4)\tilde{x}(k)$ we obtain

$$\begin{aligned} \tilde{z}(k+1) &= \boldsymbol{R}(-(k+1)\pi/4)|\lambda|\boldsymbol{R}(\pi/4)\boldsymbol{R}(-k\pi/4)^{-1}(\tilde{z}(k) - \hat{\tilde{z}}(k)) \\ &= |\lambda|\boldsymbol{R}(-(k+1)\pi/4)\boldsymbol{R}(\pi/4)\boldsymbol{R}(k\pi/4)(\tilde{z}(k) - \hat{\tilde{z}}(k)) \\ &= |\lambda|\boldsymbol{I}_2(\tilde{z}(k) - \hat{\tilde{z}}(k)) \end{aligned}$$

Let $D(k) = diag(\Delta_1(k), \Delta_2(k))$, $F(|\lambda|) = |\lambda|\boldsymbol{I}_2$, $\delta(k) = [\delta_1(k), \delta_2(k)]^T$ and

$G(|\lambda|) = D^{-1}(k+1)F(|\lambda|)D(k)$. Consequently, we have the following error equation:

$$y(k+1) = G(|\lambda|)(y(k) - \delta(k)), \;\; G(|\lambda|) = diag(|\lambda|\frac{\Delta_1(k)}{\Delta_1(k+1)}, |\lambda|\frac{\Delta_2(k)}{\Delta_2(k+1)}),$$

which is a fully decoupled system; and therefore, the stability analysis presented in the previous section for scalar systems is directly applied for this system. Note that by a straightforward calculation, it can be easily shown that if $y(0)$ begins in the set $\mathcal{B}^{ext}$, then for $|\lambda| < 3$ and an independent choice of $\Delta_1(k) = \Delta_1$ and $\Delta_2(k) = \Delta_2$, we have $y(1) \in \mathcal{B}^{ext}$. That is, using the above transformation, the invariance property of the algorithm holds for a larger class of systems. ■
The generalization of this result needs another transformation to have the same properties as real eigenvalues system. This is illustrated in the following example.
Example 2. Again consider a system of form (65), with

$$\boldsymbol{A} = \begin{pmatrix} |\lambda|\boldsymbol{R}(\pi/4) & \boldsymbol{I}_2 \\ \boldsymbol{0} & |\lambda|\boldsymbol{R}(\pi/4) \end{pmatrix} \tag{71}$$

This system involves a pair of complex conjugate eigenvalues with multiplicity 2. Suppose that we take

$$\boldsymbol{T}(k) = \begin{pmatrix} |\lambda|\boldsymbol{R}((k+1)\pi/4) & \boldsymbol{0} \\ \boldsymbol{0} & \boldsymbol{R}((k+2)\pi/4) \end{pmatrix}.$$

Then, for $\tilde{z}(k) = \boldsymbol{T}^{-1}(k)\tilde{x}(k)$, we obtain

$$\tilde{z}(k+1) = \begin{pmatrix} |\lambda|\boldsymbol{I}_2 & \boldsymbol{I}_2 \\ \boldsymbol{0} & |\lambda|\boldsymbol{I}_2 \end{pmatrix} (\tilde{z}(k) - \hat{\tilde{z}}(k)). \tag{72}$$

Subsequently, considering separately odd indices and even indices, i.e., $\tilde{z}^o(k) = [\tilde{z}_1(k), \tilde{z}_3(k)]^T$ and $\tilde{z}^e(k) = [\tilde{z}_2(k), \tilde{z}_4(k)]^T$, we obtain the following:

$$\tilde{z}^o(k+1) = \begin{pmatrix} |\lambda| & 1 \\ 0 & |\lambda| \end{pmatrix} (\tilde{z}^o(k) - \hat{\tilde{z}}^o(k)), \tag{73}$$

where $\hat{\tilde{z}}^o(k) = [\Delta_1(k)\delta_1(k), \Delta_3(k)\delta_3(k)]^T$ and

$$\tilde{z}^e(k+1) = \begin{pmatrix} |\lambda| & 1 \\ 0 & |\lambda| \end{pmatrix} (\tilde{z}^e(k) - \hat{\tilde{z}}^e(k)), \tag{74}$$

with $\hat{\tilde{z}}^e(k) = [\Delta_2(k)\delta_2(k), \Delta_4(k)\delta_2(k)]^T$.
Now, consider one of these systems, for instance, consider system (73), and let $y(k) = [\tilde{z}_1(k)/\Delta_1(k),$
$\tilde{z}_3(k)/\Delta_3(k)]^T$, $D(k) = diag(\Delta_1(k), \Delta_3(k))$, $F(|\lambda|) = \begin{pmatrix} |\lambda| & 1 \\ 0 & |\lambda| \end{pmatrix}$, $\delta(k) = [\delta_1(k), \delta_3(k)]^T$, and $G(|\lambda|) = D^{-1}(k+1)F(|\lambda|)D(k)$. Then, we have the following error equation for system (73)

$$y(k+1) = G(|\lambda|)(y(k) - \delta(k)), \quad G(|\lambda|) = \begin{pmatrix} |\lambda|\frac{\Delta_1(k)}{\Delta_1(k+1)} & \frac{\Delta_3(k)}{\Delta_1(k+1)} \\ 0 & |\lambda|\frac{\Delta_3(k)}{\Delta_3(k+1)} \end{pmatrix}$$

Now, we extend this idea to the general form of multivariable systems. For the general multivariable systems, the rotational matrix $\boldsymbol{T}(k)$ is obtained by a) Applying the real Jordan canonical transformation (Lemma 1) and b) A transformation that transforms a Jordan block associated with complex conjugate eigenvalues to a form similar to the Jordan blocks associated with the real valued eigenvalues (Lemma 2) .

Lemma 1 *[46] For $\boldsymbol{A} \in \boldsymbol{R}^{n\times n}$ there exists a real valued nonsingular matrix $\boldsymbol{\Lambda}$ and a real valued matrix $\boldsymbol{\Gamma}$ such that $\boldsymbol{\Lambda A \Lambda}^{-1} = \boldsymbol{\Gamma} = diag(J_{\lambda_1}, ..., J_{\lambda_\gamma})$, where for the multi-valued real eigenvalue λ_l with multiplicity μ_l, the matrix $\boldsymbol{J}_{\lambda_l}$, for $1 \leqslant l \leqslant \alpha \leqslant \gamma$, are of the following form:*

$$\boldsymbol{J}_{\lambda_l} = \begin{pmatrix} \lambda_1 & 1 & & \\ & \lambda_l & 1 & \\ & & \vdots & \\ & & & \lambda_l \end{pmatrix} = F(\lambda_l) \in \boldsymbol{R}^{\mu_l \times \mu_l}. \tag{75}$$

And for the multi-valued complex conjugate eigenvalues $\lambda_l = |\lambda_l|(\cos(\theta_l) \mp \sin(\theta_l))$ with multiplicity μ_l, the matrix $\boldsymbol{J}_{\lambda_l}$, are, for all $\alpha + 1 \leqslant l \leqslant \gamma$, of the

form

$$\boldsymbol{J}_{\lambda_l} = \begin{pmatrix} |\lambda_l|\boldsymbol{R}(\theta_l) & \boldsymbol{I}_2 & & \\ & |\lambda_l|\boldsymbol{R}(\theta_l) & \boldsymbol{I}_2 & \\ & & \vdots & \\ & & & |\lambda_l|\boldsymbol{R}(\theta_l) \end{pmatrix} \in \boldsymbol{R}^{2\mu_l \times 2\mu_l}, \tag{76}$$

where $\boldsymbol{R}(\theta_l)$ *is the rotation matrix given by*

$$\boldsymbol{R}(\theta_l) = \begin{pmatrix} \cos(\theta_l) & \sin(\theta_l) \\ -\sin(\theta_l) & \cos(\theta_l) \end{pmatrix}. \tag{77}$$

Above lemma implies that we can always express the system matrix $\boldsymbol{A}$ of system (65) in its real Jordan form. That is, $\boldsymbol{A}$ can be written in the form of $\boldsymbol{A} = diag(J_{\lambda_1}, ..., J_{\lambda_\gamma})$. Thus, without loss of generality, it is assumed that $\boldsymbol{A} = diag(J_{\lambda_1}, ..., J_{\lambda_\gamma})$.
As shown in previous examples, it is desirable to transform the Jordan blocks associated with complex conjugate eigenvalues to a form similar to the case of real valued eigenvalues. For the multi-valued complex conjugate eigenvalues, we introduce a change of coordinate with a dynamic matrix $\boldsymbol{T}(k)$ to transform the associated Jordan block to a form similar to (75). This transformation is discussed in the following lemma.

Lemma 2 *Consider the Jordan block* J_{λ_l}*, which corresponds to the complex conjugate eigenvalues* $\lambda_l = |\lambda_l|(\cos(\theta_l) \mp \sin(\theta_l))$ *with multiplicity* μ_l*. Let us introduce matrices* $\boldsymbol{W}(\theta_l) \in \boldsymbol{R}^{2\mu_l \times 2\mu_l}$ *and* $\boldsymbol{Q}(\theta_l) \in \boldsymbol{R}^{2\mu_l \times 2\mu_l}$ *as follows:*

$$\boldsymbol{W}(\theta_l) = \begin{pmatrix} \boldsymbol{R}(\theta_l) & & & \\ & \boldsymbol{R}(\theta_l) & & \\ & & \vdots & \\ & & & \boldsymbol{R}(\theta_l) \end{pmatrix}, \tag{78}$$

$$\boldsymbol{Q}(\theta_l) = \begin{pmatrix} \boldsymbol{R}(\theta_l) & & & \\ & \boldsymbol{R}(2\theta_l) & & \\ & & \vdots & \\ & & & \boldsymbol{R}(\mu_l\theta_l) \end{pmatrix}. \tag{79}$$

Then, under the transformation $\tilde{z}(k) = \bar{\boldsymbol{T}}^{-1}(k)\tilde{x}(k)$, $\bar{\boldsymbol{T}}(k) = \boldsymbol{W}(k\theta_l)\boldsymbol{Q}(\theta_l)$, *we have a similar form as in the case of real valued eigenvalues.*

Proof Under the above transformation, it can be shown after a few calculations that

$$\tilde{z}(k+1) = \check{\boldsymbol{J}}_{\lambda}(\tilde{z}(k) - \hat{\tilde{z}}(k)), \tag{80}$$

where

$$\check{\boldsymbol{J}}_{\lambda_l} \triangleq \boldsymbol{Q}^{-1}(\theta_l)\boldsymbol{W}^{-1}((k+1)\theta_l)\boldsymbol{J}_{\lambda_l}\boldsymbol{W}(k\theta_l)\boldsymbol{Q}(\theta_l) = \begin{pmatrix} |\lambda_l|\boldsymbol{I}_2 & \boldsymbol{I}_2 & & \\ & |\lambda_l|\boldsymbol{I}_2 & \boldsymbol{I}_2 & \\ & & \vdots & \\ & & & |\lambda_l|\boldsymbol{I}_2 \end{pmatrix}.$$

Let $F(|\lambda_l|)$ be a matrix with $|\lambda_l|$ on the diagonal and 1 on the superior diagonal. Then, considering separately even indices and odd indices, we exactly recover the results of the case of real valued eigenvalues. In fact, if we denote $\tilde{z}^e(k) = [\tilde{z}_2(k), \tilde{z}_4(k), \ldots, \tilde{z}_{2\mu}(k)]^T$ and $\tilde{z}^o(k) = [\tilde{z}_1(k), \tilde{z}_3(k), \ldots, \tilde{z}_{2\mu-1}(k)]^T$, we have

$$\tilde{z}^e(k+1) = F(|\lambda_l|)(\tilde{z}^e(k) - \hat{\tilde{z}}^e(k)); \quad \tilde{z}^o(k+1) = F(|\lambda_l|)(\tilde{z}^o(k) - \hat{\tilde{z}}^o(k)). \tag{81}$$

Consequently, the change of coordinates with a dynamic matrix $\bar{\boldsymbol{T}}(k)$ allows us to reduce the study to the following class of systems:

$$\tilde{z}(k+1) = \underbrace{\begin{pmatrix} |\lambda| & 1 & & \\ & |\lambda| & 1 & \\ & & \vdots & \\ & & & |\lambda| \end{pmatrix}}_{F(|\lambda|)\in\boldsymbol{R}^{\mu*\mu}} (\tilde{z}(k) - \hat{\tilde{z}}(k)) \tag{82}$$

for both systems of (81).

For the simplicity of presentation from now on let $\lambda_l = \lambda$ and $\mu_l = \mu$. From above lemmas it follows that the change of coordinates allows us to reduce the study to

the following class of systems:

$$\tilde{z}(k+1) = \underbrace{\begin{pmatrix} \lambda & 1 & & \\ & \lambda & 1 & \\ & & \vdots & \\ & & & \lambda \end{pmatrix}}_{F(\lambda)=F_r(\lambda)\in \boldsymbol{R}^{\mu*\mu}} (\tilde{z}(k) - \hat{\tilde{z}}(k))$$

for real valued eigenvalues; and

$$\tilde{z}(k+1) = \underbrace{\begin{pmatrix} |\lambda| & 1 & & \\ & |\lambda| & 1 & \\ & & \vdots & \\ & & & |\lambda| \end{pmatrix}}_{F(\lambda)=F_c(|\lambda|)\in \boldsymbol{R}^{\mu*\mu}} (\tilde{z}(k) - \hat{\tilde{z}}(k))$$

for complex conjugate eigenvalues.
For these systems let the vector $y(k)$ include components $y_i(k) = \tilde{z}_i(k)/\Delta_i(k)$ $(1 \leqslant i \leqslant \mu)$ and let $D(k) = diag(\Delta_i(k))$ where $\Delta_i(k)$'s are the quantization steps. Then, we obtain the following error equation:

$$y(k+1) = G(\lambda)(y(k) - \delta(k)), \tag{83}$$

where:

- for real valued eigenvalues:

$$G(\lambda) = G_r(\lambda) =$$

$$D^{-1}(k+1)F_r(\lambda)D(k) = \begin{pmatrix} \frac{\lambda\Delta_1(k)}{\Delta_1(k+1)} & \frac{\Delta_2(k)}{\Delta_1(k+1)} & & \\ & \frac{\lambda\Delta_2(k)}{\Delta_2(k+1)} & \frac{\Delta_3(k)}{\Delta_2(k+1)} & \\ & & \vdots & \\ & & & \frac{\lambda\Delta_\mu(k)}{\Delta_\mu(k+1)} \end{pmatrix},$$

and

- for complex conjugate eigenvalues:

$$G(\lambda) = G_c(|\lambda|) =$$

$$D^{-1}(k+1)F_c(|\lambda|)D(k) = \begin{pmatrix} \frac{|\lambda|\Delta_1(k)}{\Delta_1(k+1)} & \frac{\Delta_2(k)}{\Delta_1(k+1)} & & \\ & \frac{|\lambda|\Delta_2(k)}{\Delta_2(k+1)} & \frac{\Delta_3(k)}{\Delta_2(k+1)} & \\ & & \ddots & \\ & & & \frac{|\lambda|\Delta_\mu(k)}{\Delta_\mu(k+1)} \end{pmatrix}.$$

5.2.2 Further definitions for the D-ZIZO algorithm

Starting from the previous matrices, some definitions and arrangements will be instrumental for the algorithm specification and analysis. First, we will benefit from the previous variable change to consider every subsystem derived from an eigenvalue of multiplicity μ, (2μ if complex conjugate) as a unique system evolving independently of the rest (two systems in the case of complex conjugate pairs), with their own $(F(\lambda), G(\lambda))$. For a μ-dimensional system of that type, consider the vector of quantization steps,

$$\Delta(k) = [\Delta_1(k),\ \Delta_2(k),\ \ldots,\ \Delta_\mu(k)]^T.$$

As the initial state estimation error is a freely assigned quantity for all variables, it might be appealing to choose all $\Delta_i(0)$ equal; however, as it will be shown later, this would have a negative effect on the transient performance as the errors propagate from one signal to the next in a cascade, due to the upper triangular structure of matrix $F(|\lambda|)$. Subsequent calculations will show that an homogeneous $\Delta(0)$ would also impose suboptimal bandwidth assignment (via M). A choice that does not add conservativeness to our results while it still guarantees a tractable analysis is the following

$$\Delta(0) = \Delta_1(0) \cdot [1, \kappa,\ \kappa^2, \ldots,\ \kappa^\mu]$$

where $\Delta_1(0) > 0$ and $0 < \kappa < 1$ are freely chosen scalars. From the fact that the ZO-ZI-DT machine state is unique (not element-wise), and assuming that C_{out} and C_{in} are the same for all element i of the state vector, we have that this proportion

will hold along time, yielding the following simple matrices:

$$G(\lambda) = \frac{1}{C_m}\begin{bmatrix} |\lambda| & \kappa & 0 & \dots & 0 \\ 0 & |\lambda| & \kappa & \dots & 0 \\ & & & \vdots & \\ 0 & 0 & 0 & \dots & \kappa \\ 0 & 0 & 0 & \dots & |\lambda| \end{bmatrix} \quad D(k) = \Delta_1(k) \cdot diag(1, \kappa, \ \kappa^2, \dots, \ \kappa^\mu),$$

where C_m stands for the Zoom factor corresponding to the current mode of operation, namely C_{out}, 1 or C_{in} for the respective ZO, DT and ZI modes. Under this assumption, it is clear that the $||G(\lambda)||_\infty = (|\lambda| + \kappa)/C_m$ which can be made arbitrarily close to $|\lambda|/C_m$. The main consequence is that the rate-condition for stability of the algorithm can be minimized with the appropriate choice of κ, as it will be shown in the subsequent analysis. From the previous definitions, it is also convenient to define the following,

Definition The error-dynamics norm is defined as

$$\rho(k) = ||G_r(\lambda)||_\infty = ||G_c(|\lambda|)||_\infty,$$

which, using the fact that the zoom factor is unique for all states anytime, and with the above choice of $\Delta(k)$, turns into

$$\rho(k) \quad = \quad \begin{cases} \max_{1 \leqslant i \leqslant \mu}(|\lambda| + \kappa)/C_{out} < 1 (\Delta_{\mu+1}(0) = 0) & \text{if ZO} \\ \max_{1 \leqslant i \leqslant \mu}\{|\lambda| + \kappa\} & \text{if DT} \\ \max_{1 \leqslant i \leqslant \mu}(|\lambda| + \kappa)/C_{in} > 1 & \text{if ZI} \end{cases} \tag{84}$$

From Lemma 1, Lemma 2 and the above results, it follows that for the stability analysis, it is enough to focus only on the error equation (83). Note that for $|\lambda| < 1$, $\lim_{k\to\infty} \tilde{z}(k) = 0$. Consequently, in what follows, without loss of generality, we assume that $|\lambda| > 1$.

5.2.3 Description of the D-ZIZO

Definition The stability analysis and the full description of the complete D-ZIZO algorithm, requires the following set definitions:

$$\begin{aligned}
\mathcal{B}^o &= \{y(k) : 1 \leqslant i \leqslant \mu : |y_i(k)| \leqslant \frac{(M_i - 2)}{2}\} \\
\mathcal{B}^{ext} &= \{y(k) : 1 \leqslant i \leqslant \mu : |y_i(k)| \leqslant \frac{M_i}{2}\} \\
\mathcal{B}^{\text{int}} &= \{y \in \mathbf{R}^\mu : |y_i| \leqslant \frac{|\lambda| + \kappa}{2C_{in}} \forall i : 1 \leqslant i \leqslant \mu - 1 \text{ and } |y_\mu| \leqslant \frac{|\lambda|}{2C_{in}}\} \\
\mathcal{B}^u &= \{-\frac{\min_{1\leqslant i\leqslant \mu} M_i - m}{2}, ..., \frac{\min_{1\leqslant i\leqslant \mu} M_i - m}{2}, \ \ m = 3, 5, ..., \min_{1\leqslant i\leqslant \mu} M_i\}.
\end{aligned}$$

The operation of the adaptive quantization multivariable D-ZIZO law is described by Fig. 30. The algorithm switches between the following states:

- **"Zoom-Out" state** activates the capture mode where $\Delta(k)$ increases with a rate $\Delta(k+1) = C_{out}\Delta(k)$, where $C_{out} > 1$. The precise value of C_{out}, given later, will depend on the initial condition of $\Delta(0)$ and on the system matrix $\boldsymbol{A}$. Then, by monitoring $\delta(k)$ the algorithm will switch to Zoom-In mode, and hence $y(k) \to \mathcal{B}^o \subset \mathcal{B}^{ext}$, in finite time.

- **"Zoom-In" state** makes $\Delta(k)$ decrease with a rate $\Delta(k+1) = C_{in}\Delta(k)$, where $C_{in} < 1$. The precise value of C_{in}, given later, will depend on the initial condition of $\Delta(0)$ and on the system matrix $\boldsymbol{A}$. Then, by monitoring $\delta(k)$ the algorithm will switch to Dwell-Time mode.

- **"Dwell-Time" state** freezes the evolution of $\Delta(k)$. That is, $\Delta(k+1) = \Delta(k)$. Let k_{DT} be the time when the algorithm enters in Dwell-Time state. Using the information collected during the time period of $[k_{DT}, k_{DT}+\nu-1]$, the algorithm is able to determine whether $y(k_{DT}) \in \mathcal{B}^{ext}$; or $y(k_{DT}) \notin \mathcal{B}^{ext}$. Then, the algorithm backs to "Zoom-In" mode if $y(k_{DT}) \in \mathcal{B}^{ext}$. Otherwise; if $y(k_{DT}) \notin \mathcal{B}^{ext}$, then the algorithm moves to "Zoom-Out" mode. The duration in Dwell-Time mode is finite and bounded by a parameter ν which depends only on the open loop system eigenvalues, the number of words $(M_1, ..., M_\mu)$ and the initial values of the quantization steps $(\Delta_1(0), ..., \Delta_\mu(0))$.

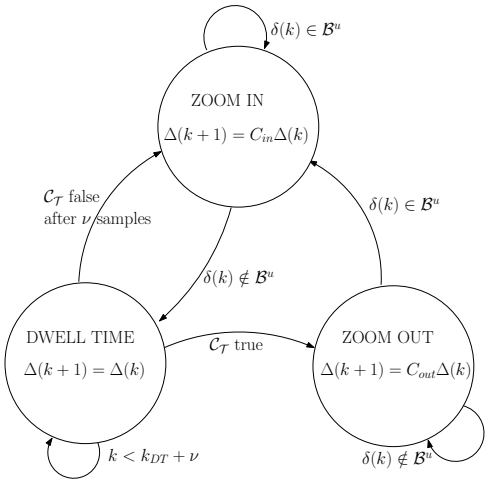

Figure 30: D-ZIZO state machine for multivariable systems and $M_i \geqslant 3$.

5.3 Stability analysis: Without System Noise

In this section, the stability of the D-ZIZO algorithm will be analyzed, without system noise (i.e., $S = 0$), throughout the following steps:

- Capture and transition from Zoom-Out to Zoom-In (Lemma 3),
- Invariance property of $\mathcal{B}^{ext}$ during Zoom-In mode (Lemma 4),
- Transition from Zoom-In to Dwell-Time (Lemma 5),
- Definition of the transition condition $\mathcal{C}_\mathcal{T}$ (Lemma 6)
- Stability of the closed-loop system (Theorem 5.1).

5.3.1 Standard mode transitions

We start this section with the following lemma, which shows that if the algorithm is initialized in Zoom-Out mode, then there exists a finite time k_{catch}, at which the algorithm switches to Zoom-In mode. Note that for $M_i \geqslant 3$, the condition for switching is that $\delta(k_{catch}) \in \mathcal{B}^u$; and for $M_i = 2$, the condition is that the sign of each components of vector $\delta(k_{catch})$ has been changed.

Lemma 3 (Capture and Transition from ZO to ZI) *Assume that initially, the algorithm is in Zoom-Out mode, and let the initial values of the quantization steps be constrained by*

$$|\lambda| + \kappa \leqslant M_i,\ 1 \leqslant i \leqslant \mu,\ \ \Delta_{\mu+1}(0) = 0,\ \ \Delta_1(0) \neq 0,\ \ 1 \leqslant i \leqslant \mu. \tag{85}$$

And $C_{out} > 0$ *satisfies*

$$\max_{1 \leqslant i \leqslant \mu} (|\lambda| + \kappa) < C_{out}. \tag{86}$$

Then, there exists a finite time, $k_{catch} > 0$*, after which the algorithm reaches in Zoom-In mode. That is, for any arbitrary initial condition* $y(0)$*, we have:*

$$\begin{array}{rcll} y(k_{catch}) & \in & \mathcal{B}^o \subset \mathcal{B}^{ext}, & \forall M_i \geqslant 3, \\ y(k_{catch}) & \in & \mathcal{B}^{ext}, & M_i = 2. \end{array}$$

or, equivalently $y(k_{catch}) \in \mathcal{B}^{ext}, \quad \forall M_i \geqslant 2.$

Proof The analysis is done for two separate cases: $M_i \geqslant 3$ and $M_i = 2$.

- **Case** $M_i \geqslant 3$. Without loss of generality, assume that $y(0) \notin \mathcal{B}^o$. With the adaptive quantization rule $\Delta_i(k+1) = C_{out}\Delta_i(k)$, from the error equation (83) we have:

$$\rho = ||G(\lambda)\|_\infty = \max_{1 \leqslant i \leqslant \mu} (|\lambda| + \kappa)\, \frac{1}{C_{out}}$$

$$\begin{array}{rcl} \|y(k+1)\|_\infty & \leqslant & \rho\|y(k) - \delta(k)\|_\infty \leqslant \rho\|y(k)\|_\infty \\ \|y(k+1)\|_\infty & \leqslant & \rho^{k+1}\|y(0)\|_\infty \end{array}$$

  If $\rho < 1$, then the sequence $\rho^{k+1}\|y(0)\|_\infty$ is contractive. $\rho < 1$ is satisfied if

$$\max_{1 \leqslant i \leqslant \mu} (|\lambda| + \kappa) < C_{out} \tag{87}$$

  Therefore, under the assumption of (87), for all initial conditions $y(0)$ there exists a $k_{catch} \geqslant \ln((M_i - 2)/(2\|y(0)\|_\infty))/\ln(\rho)$ such that $\|y(k_{catch})\|_\infty \leqslant (M_i - 2)/2 > 0, \forall 1 \leqslant i \leqslant \mu$. This completes the proof because $||y(k_{catch})||_\infty \leqslant \frac{M_i - 2}{2}, \forall i$ implies that $\delta(k_{catch}) \in \mathcal{B}^u$.

- **Case** $M_i = 2$

  The main idea here is to show that the sign of each signal $\delta_i(k)$ changes. Inspired by the analysis obtained for the scalar case in [41], we propose

the following: Without loss of generality, we can assume that $y_\mu(0) > 0$ (the case of $y_\mu(0) < 0$ follows from the same analysis); and subsequently, $\delta_\mu(0) > 0$ (due to the quantization rule given earlier). During Zoom-Out state, we have

$$y_\mu(k) = \frac{|\lambda|}{C_{out}}(y_\mu(k) - \underbrace{\delta_\mu(k)}_{<0}) \tag{88}$$

As long as $y_\mu(k) > 0$, we have $\delta_\mu(k) = 1/2$. Subsequently,

$$\begin{aligned} y_\mu(k) &= \left(\frac{|\lambda|}{C_{out}}\right)^k y_\mu(0) - \sum_{i=0}^{k-1} \frac{|\lambda|}{C_{out}} \left(\frac{|\lambda|}{C_{out}}\right)^i \delta_\mu(k-i-1) \\ &= \underbrace{\left(\frac{|\lambda|}{C_{out}}\right)^k \left(y_\mu(0) + \frac{|\lambda|/(2C_{out})}{1-|\lambda|/C_{out}}\right)}_{\to 0 \text{ when } k\to+\infty} \underbrace{- \left(\frac{|\lambda|/(2C_{out})}{1-|\lambda|/C_{out}}\right)}_{<0} \end{aligned}$$

So $\exists k_\mu \in \mathbf{N}$ such that $y_\mu(k_\mu) < 0$ (and subsequently $\delta_\mu(k_\mu) < 0$); and therefore using (88), we can conclude that $|y_\mu(k)| \leqslant 1$ for all $k \geqslant k_\mu$ until the D-ZIZO state machine is in Zoom-Out state.

Now, we will show that if we have the above property for $y_\mu(k)$, then this property also holds for $y_{\mu-1}(k), ..., y_1(k)$. So we suppose that for $k \geqslant k_{i+1}$, we have $|y_{i+1}(k)| \leqslant 1$ and also $y_i(k_{i+1}) > 0$ (and subsequently $\delta_i(k_{i+1}) > 0$). Now, we show that the same holds for $y_i(k)$.
During Zoom-Out state we have

$$\begin{aligned} y_i(k+1) &= \frac{|\lambda|}{C_{out}}(y_i(k) - \delta_i(k)) + \frac{\kappa}{C_{out}}(y_{i+1}(k) - \delta_{i+1}(k)), k \geqslant k_{i+1} \\ &\leqslant \underbrace{\left(\frac{|\lambda|}{C_{out}}\right)^{k-k_{i+1}} \left(y_i(k_{i+1}) + \frac{(|\lambda|-\kappa)/(2C_{out})}{1-|\lambda|/C_{out}}\right)}_{\to 0 \text{ when } k\to+\infty} \\ &\quad \underbrace{- \left(\frac{(|\lambda|-\kappa)/(2C_{out})}{1-|\lambda|/C_{out}}\right)}_{<0} \end{aligned}$$

So $\exists k_i \in \mathbf{N}$ such that $y_i(k_i) < 0$ (and subsequently $\delta_i(k_i) < 0$); and conse-

quently, we can also conclude that $|y_i(k)| \leqslant 1$ for $k \geqslant k_i$ until the D-ZIZO state machine is in Zoom-Out state.
Hence, from the above analysis it follows that there exists a finite time k_{catch} at which all components of the vector $\delta(k) = (\delta_1(k), ..., \delta_\mu(k))^T$ have changed their sign and $y(k_{catch}) \in \mathcal{B}^{ext}$. This completes the proof.

Remark i) If the D-ZIZO algorithm is in ZO mode; while $y(k) \in \mathcal{B}^{ext}$, then $y(k)$ will decrease until at the time instant k_{catch}, we have $y(k) \in \mathcal{B}^u$. At this time, we have $\delta(k_{catch}) = \mathcal{B}^u$; and therefore, the D-ZIZO algorithm switches to ZI mode.
ii) It is interesting to note that the bigger C_{out} is, the faster the signal is caught. However, taking a big value for C_{out} implies a big value for $\Delta(k)$. This results in a larger excursion of the solution of $y(k)$ from its equilibrium.

Now, we show that if the algorithm is in Zoom-In mode, at some time k, i.e., $y(k) \in \mathcal{B}^{ext}$, then $y(k+1) \in \mathcal{B}^{ext}$, at time $k+1$.

Lemma 4 (Invariance of $\mathcal{B}^{ext}$ during Zoom-In mode) *Assume that the algorithm is in Zoom-In mode with $y(k) \in \mathcal{B}^{ext}$, and that the initial values of $\Delta(0)$ and the number of quantization levels/words M_i is constrained by the inequality* (85)*, with $C_{in} > 0$ satisfying*

$$\max_{1 \leqslant i \leqslant \mu} \left(\frac{|\lambda| + \kappa}{M_i} \right) < C_{in} < 1. \tag{89}$$

Then, $y(k+1) \in \mathcal{B}^{ext}$.

Proof According to (83) and (84), the error equation in Zoom-In mode gives:

$$y_i(k+1) = \frac{|\lambda|}{C_{in}}(y_i(k) - \delta_i(k)) + \frac{\kappa}{C_{in}}(y_{i+1}(k) - \delta_{i+1}(k)). \tag{90}$$

$$y_\mu(k+1) = \frac{|\lambda|}{C_{in}}(y_\mu(k) - \delta_\mu(k)). \tag{91}$$

With $y(k) \in \mathcal{B}^{ext}$ we have $|y_i(k) - \delta_i(k)| \leqslant \frac{1}{2}$. Then, using (90), for $1 \leqslant i \leqslant \mu$, we get

$$|y_i(k+1)| \leqslant \frac{|\lambda|}{C_{in}}|y_i(k) - \delta_i(k)| + \frac{\kappa}{C_{in}}|y_{i+1}(k) - \delta_{i+1}(k)| \leqslant \frac{|\lambda|}{2C_{in}} + \frac{\kappa}{2C_{in}} \leqslant \frac{M_i}{2}. \tag{92}$$

Also, from (91) and (89) it follows that

$$|y_\mu(k+1)| \leqslant \frac{M_\mu}{2}. \tag{93}$$

That is, $y(k+1) \in \mathcal{B}^{\text{int}}$ with $\mathcal{B}^{\text{int}}$ as defined earlier. From condition (89), it follows that $\mathcal{B}^{int} \subseteq \mathcal{B}^{ext}$; and therefore, together with the constraint on the value of C_{in}, we have that $y(k+1) \in \mathcal{B}^{ext}$.

Now in the following lemma, we show that transitions from Zoom-In mode to Dwell-Time mode preserves invariance property of $\mathcal{B}^{ext}$.

Lemma 5 (Transition from Zoom-In to Dwell-Time) *Suppose that the algorithm switches to Dwell-Time mode at time k, and $y(k) \in \mathcal{B}^{ext}$. Then, in this mode at time $k+1$, we also have $y(k+1) \in \mathcal{B}^{ext}$.*

Proof The algorithm behavior in Dwell-Time mode can be analyzed along the same lines of Lemma 4 with C_{in} replaced by 1, and $y(k) \in \mathcal{B}^{ext}$.

We next analyze the transition condition $\mathcal{C}_\mathcal{T}$. Towards this goal, let k_{DT} be the time instant when the state machine enters to Dwell-Time state from Zoom-In mode. Also, let $S_{(i,k_{DT})}$ be the sign of $\delta_i(k_{DT})$; and define the condition $\mathcal{C}_\mathcal{T}$ as follows:

$$\mathcal{C}_\mathcal{T} = \text{true if} \{k = k_{DT} + \nu - 1\} \wedge \{\exists i, 1 \leqslant i \leqslant \mu : |\sum_{j=k-\nu+1}^{k} \delta_i(j)| = \frac{M_i - 1}{2}\nu\}$$

Transitions from Dwell-Time to either Zoom-Out, or Zoom-In depend on the condition $\mathcal{C}_\mathcal{T}$. In the following lemma, we investigate the cases where this transition conditions are satisfied.

Lemma 6 (Transition condition $\mathcal{C}_\mathcal{T}$) *Suppose that we have the inequality $1 < |\lambda| < M_i$, and also that κ is chosen sufficiently small such that:*

$$|\lambda| + \kappa < M_i,\ 1 \leqslant i \leqslant \mu. \tag{94}$$

Also, suppose that the duration of the Dwell - Time ν satisfies

$$\nu = \max(\nu_i), \quad (\nu_i - 1) \in \mathbf{N} \geqslant l_i$$

where

$$l_i = \frac{\ln\left(M_i + |\lambda| - 2 - \kappa\right)}{\ln(|\lambda|)} - \frac{\ln\left(M_i - |\lambda| - \kappa\right)}{\ln(|\lambda|)}. \tag{95}$$

Then, we obtain the following condition:

$$\mathcal{C}_{\mathcal{T}} \Rightarrow y(k_{DT}) \notin \mathcal{B}^{ext}. \tag{96}$$

Proof We start by assuming that $k = k_{DT}$ is the instant when Dwell-Time mode begins. In what follows the objective is to prove that (96) by showing that

$$\text{if } y(k_{DT}) \in \mathcal{B}^{ext} \Rightarrow \mathcal{C}_{\mathcal{T}} \text{ is false,}$$

which is equivalent to say that:
If $y(k_{DT}) \in \mathcal{B}^{ext}$, then $\forall i \quad (1 \leqslant i \leqslant \mu)$, $|\sum_{j=k_{DT}}^{k_{DT}+\nu-1} \delta_i(j)| \neq \frac{M_i-1}{2}\nu$.
We consider each component $y_i(k)$ separately and determine $\nu_i - 1$ as follows:

$$\begin{aligned} (\nu_i - 1) \in \mathbf{N} &> l_i \\ \nu &= \max_{1 \leqslant i \leqslant \mu} \nu_i. \end{aligned}$$

If we decompose each component y_i and each $\nu_i - 1$ corresponds to an upper bound of the maximal time such that the following conditions are verified:

$$y(k_{DT}) \in \mathcal{B}^{ext} \tag{97}$$

$$\mathcal{S}_{(i,k_{DT})} \sum_{j=k_{DT}}^{k_{DT}+\nu_i-2} \delta_i(j) = (\nu_i - 1)\frac{M_i - 1}{2} \tag{98}$$

We need to show that at $k_{DT} + \nu_i - 1$, it is impossible to have $\mathcal{S}_{(i,k_{DT})}\delta(k_{DT} + \nu_i - 1) = \frac{M_i-1}{2}$, which is equivalent to have $\mathcal{S}_{(i,k_{DT})}y_i(k_{DT} + \nu_i - 1) > \frac{M_i-2}{2}$. Thus, in what follows, we find conditions under which the following inequality $\mathcal{S}_{(i,k_{DT})}y_i(k_{DT}+\nu_i-1) \leqslant \frac{M_i-2}{2}$ holds. To reach this goal, consider $y_i(k_{DT}+\nu_i-1)$; and suppose that the equation (97) is verified. Using Lemma 5, we know that if $y(k_{DT}) \in \mathcal{B}^{ext}$, then during all Dwell - Time period, we have $y(j) \in \mathcal{B}^{ext}$, $\forall j \in [k_{DT}, k_{DT} + \nu - 1]$. Thus, we can conclude that $|y_{i+1}(j) - \delta_{i+1}(j)| \leqslant 1/2$.

From this conclusion and the error equation (83) it follows that:

$$\mathcal{S}_{(i,k_{DT})}y_i(k_{DT}+\nu_i-1) \leqslant |\lambda|^{\nu_i-1}|y_i(k_{DT})| - \left(\frac{M_i-1}{2}\right)|\lambda|\sum_{j=0}^{\nu_i-2}|\lambda|^j + \frac{\kappa}{2}\sum_{j=0}^{\nu_i-2}|\lambda|^j.$$

But, we have $|y_i(k_{DT})| \leqslant M_i/2$ (since $y(k_{DT}) \in \mathcal{B}^{ext}$). Thus, if we want to have $\mathcal{S}_{(i,k_{DT})}y_i(k_{DT}+\nu_i-1) \leqslant \frac{M_i-2}{2}$ it is sufficient that

$$\frac{M_i-2}{2} \geqslant |\lambda|^{\nu_i-1}\frac{M_i}{2} - \frac{M_i-1}{2}|\lambda|\left(\frac{|\lambda|^{\nu_i-1}-1}{|\lambda|-1}\right) + \frac{\kappa}{2}\left(\frac{|\lambda|^{\nu_i-1}-1}{|\lambda|-1}\right).$$

It can be shown after a few calculations that this condition is true if

$$(\nu_i-1) \in \mathbf{N} \geqslant l_i = \frac{\ln\left(M_i+|\lambda|-2-\kappa\right)}{\ln(|\lambda|)} - \frac{\ln\left(M_i-|\lambda|-\kappa\right)}{\ln(|\lambda|)}$$

To conclude, we make the choice of $\nu = \max(\nu_i)$ with $\nu_i - 1 \geqslant l_i$.

In normal operation, there is a continuous transition between ZI and DT modes which results in a contraction of the estimation error $\tilde{z}(k)$. From Lemma 4 it follows that when the algorithm enters to ZI mode at time k_{catch}, $y(k)$ remains in $\mathcal{B}^{ext}$ for all $k \geqslant k_{catch}$. If $\delta(k_{catch}+1) \in \mathcal{B}^u$, the algorithm stays in ZI mode; otherwise, it switches to DT mode. But, because of the invariance property of $\mathcal{B}^{ext}$ during ZI mode, we have $y(k_{DT}) \in \mathcal{B}^{ext}$; and therefore, in normal situations, condition $\mathcal{C}_{\mathcal{T}}$ is never activated. Hence, the D-ZIZO algorithm always switches between DT mode and ZI mode in normal situations.

In fact, condition of Lemma 6, can be used to detect abnormal situations where, due to some unmodeled disturbances, $y(k_{DT})$ leaves $\mathcal{B}^{ext}$. In those situations, the algorithm needs to switch to ZO mode. This procedure is described next.

5.3.2 Transition to ZO due perturbations

Starting from ZI mode, the event $\delta(k) \notin \mathcal{B}^u$ triggers the DT mode. In order to check condition $\mathcal{C}_{\mathcal{T}}$, the system must remain in DT for at least ν samples, unless we have some k during that period such that $|\delta_i(k)| < \frac{M_i-1}{2}$ for all i (which would mean that the system has returned to $\mathcal{B}^u$ and the ZI is activated). If this is not the case, we would remain at DT until the ν samples have elapsed, and then, condition $\mathcal{C}_{\mathcal{T}}$ would be evaluated for all components, with the following decision map:

- If $\mathcal{C}$ holds, a perturbation has occurred and ZO mode should be activated.
- Otherwise, switch to ZI.

Recoding for disambiguation

In order to consider all possible cases, a slight fix must be done to the coding algorithm. In fact, (96) is a one-way implication, and it might happen that $\mathcal{C}_{\mathcal{T}}$ is false and still $y(k_{DT}) \notin \mathcal{B}^{ext}$. So, even without fulfilling $\mathcal{C}_{\mathcal{T}}$ we must be able to detect the quantizer overload and switch to ZO mode. This is tackled by using the fact that the sender (encoder) can directly detect from the measures that $y_i(k_{DT}) \notin \mathcal{B}^{ext}$ for some i; in that case, even if the straight coding sequence should not result in $\mathcal{C}_{\mathcal{T}}$, the sequence of $\delta_i(k)$ transmitted during Dwell-Time should be transformed for it to fulfill the condition $|\sum_{j=k-\nu+1}^{k} \delta_i(j)| = \frac{M_i-1}{2}\nu$. With that fix, the receiver will be properly aware that it should switch to ZO mode.

Now, we are ready to show the global stability using the proposed algorithm. This is shown in the following theorem:

5.3.3 Main stability result

Theorem 5.1 *Let the number of words M_i satisfy the inequality* (94). *To build the algorithm, we must introduce two scalars C_{out}, C_{in} which are respectively constrained by* (86) *and* (89).

Then, for all initial conditions $\tilde{z}(0)$,

- $\exists k_{catch} > 0$ *such that* $\forall k \geqslant k_{catch}$, $y(k) \in \mathcal{B}^{ext}$
- $\tilde{z}(k)$ *converges to* 0
- *The system is globally stable and this can be realized under the condition on the channel rate R, given as follows:*

$$\prod_{i=1,|\lambda_i|>1}^{n} \lceil |\lambda_i| \rceil < 2^R = \prod_{i=1,M_i\neq 0}^{n} M_i. \tag{99}$$

Proof The system is described by the equation:

$$x(k+1) = (\boldsymbol{A} - \boldsymbol{BK})x(k) + \boldsymbol{BKT}(k)\tilde{z}(k)$$

Since $\boldsymbol{A}-\boldsymbol{BK}$ is Schur, then if we prove that $\tilde{z}(k)$ converges to 0, we obtain global stability. The adaptive quantization law, D-ZIZO, provides this property. Lemma 3 proves that there exists a finite time k_{catch} such that $y(k) \in \mathcal{B}^{ext}$, $\forall k \geqslant k_{catch}$ and $\Delta(k_{catch})$ is finite. Lemma 4 and Lemma 5 imply respectively that in Zoom - In mode and Dwell - Time mode, $\mathcal{B}^{ext}$ is invariant. With Lemma 6, at the end of Dwell - Time mode, the condition $\mathcal{C}_{\mathcal{T}}$ is never activated (in normal conditions) due to the invariance property of $\mathcal{B}^{ext}$. Therefore, the adaptive quantization law always switches between Dwell - Time mode and Zoom - In mode. If we decompose this switching, each cycle is composed of ν samples in Dwell - Time mode with $\Delta(k+1) = \Delta(k)$ and at least one sample in Zoom - In mode with $\Delta(k+1) = C_{in}\Delta(k)$. Hence, we obtain the following inequality for all $k > k_{catch}$:

$$\|\tilde{z}(k)\|_\infty \leqslant \frac{M_i}{2} C_{in}^{\frac{k-k_{catch}}{\nu+1}} \|\Delta(k_{catch})\|_\infty, \quad C_{in} < 1$$

Thus, $\tilde{z}(k)$ converges to 0.
Now, if a perturbation occurs such that the condition $\mathcal{C}_{\mathcal{T}}$ is activated (or explicitly coded at the sender), the algorithm leaves the DT mode, and then this process will start over following the condition of Lemma 6.

5.4 The D-ZIZO algorithm in the presence of system noise

This far, the analysis has been based on the noiseless system model (65). In order to take into account additive disturbances entering the system and their effect on the stability of the D-ZIZO algorithm, the system and error equations will be rewritten as follows:

$$\begin{aligned} x(k+1) &= \boldsymbol{A}x(k) + \boldsymbol{B}u(k) + s(k) \\ \hat{x}(k+1) &= (\boldsymbol{A}-\boldsymbol{BK})\hat{x}(k) + \boldsymbol{A}\hat{\tilde{x}}(k) \\ \tilde{z}(k+1) &= \boldsymbol{T}^{-1}(k+1)\boldsymbol{AT}(k)(\tilde{z}(k) - \hat{\tilde{z}}(k)) + \boldsymbol{T}^{-1}(k+1)s(k) \end{aligned}$$

where $s(k)$ is the additive noise. Before entering the analysis, two situations must be distinguished: *i*) That of bounded input noise on the system, i.e. $||s(k)|| < S$ and *ii*) unbounded additive disturbances. The main difference, is that in *i*, as shown in this section, an appropriate choice of the system parameters will guarantee that ZO mode will be executed at startup in order to catch the initial state, and it will not be triggered anytime later, while in *ii*), Zoom - Out stages may be required at any time due to state deviations provoked by time-limited noise bursts.

As we saw in previous section, in that case, some conditions (e.g., $\mathcal{C}_{\mathcal{T}}$) derive from these bursts such that the overall dynamics does not result in total loss of stability.

5.4.1 Bounded noise

The infinity norm of $\boldsymbol{T}(k)$ is bounded; and hence the bound on $s(k)$ immediately implies that $w(k) \stackrel{\triangle}{=} \boldsymbol{T}^{-1}(k+1)s(k)$ is bounded as

$$||w(k)||_{\infty} < W$$

and the error equation is rewritten as

$$\tilde{z}(k+1) = F(\lambda)(\tilde{z}(k) - \hat{\tilde{z}}(k)) + w(k)$$

The analysis will be focused on the error-to-quantizer ratio as in previous sections, whose dynamics is

$$y(k+1) = D^{-1}(k+1)\tilde{z}(k+1) = D^{-1}(k+1)(F(\lambda)(\tilde{z}(k) - \hat{\tilde{z}}(k)) + w(k)) \tag{100}$$

$$= D^{-1}(k+1)F(\lambda)D(k)(y(k) - \delta(k)) + D^{-1}(k+1)w(k) \tag{101}$$

$$= G(\lambda)(y(k) - \delta(k)) + D^{-1}(k+1)w(k) \tag{102}$$

In the following sections we will assume that in the noisy case the D-ZIZO modes are DT, ZI, ZO as in the standard algorithm, and that the switching conditions are left unchanged.

Transition from ZO to ZI with noise: Assume that the systems starts in ZO mode. We will show that there is a finite time, in which the systems switches to

ZI by analyzing he evolution of $y(k)$ along a Zoom-Out stage:

$$\begin{aligned} y(k+1) &= G(\lambda)(y(k)-\delta(k)) + D^{-1}(k+1)w(k) \qquad (103)\\ \|y(k+1)\|_\infty &= \|G(\lambda)\|_\infty \|y(k)-\delta(k)\|_\infty + \|D^{-1}(k+1)w(k)\|_\infty \\ &\leqslant \frac{|\lambda|+\kappa}{C_{out}}\|y(k)\|_\infty + \frac{W}{\Delta_1(k)C_{out}} \\ &= \left(\frac{|\lambda|+\kappa}{C_{out}}\right)^{k+1}\|y(0)\|_\infty + \frac{W}{\Delta_1(0)C_{out}^{k+1}}\sum_{j=0}^{k}(|\lambda|+\kappa)^j \\ &= \left(\frac{|\lambda|+\kappa}{C_{out}}\right)^{k+1}\|y(0)\|_\infty + \frac{W}{\Delta_1(0)C_{out}^{k+1}}\left(\frac{1-(|\lambda|+\kappa)^{k+1}}{1-|\lambda|-\kappa}\right) \end{aligned}$$

Now by choosing $C_{out} > |\lambda| + \kappa$, we ensure that all elements in this expression tend to zero; and hence, we conclude that after some time $y(k+1)$ enters $\mathcal{B}^o$ and the algorithm enters the Zoom - In mode.

Invariance of $\mathcal{B}^{ext}$ in ZI mode: In order to check this property, it will be assumed that the system has entered the Zoom - In stage with an initial value of $\Delta(k_{catch})$. The time evolution of $y(k)$ is described as

$$\begin{aligned} y(k+1) &= G(\lambda)(y(k)-\delta(k)) + D^{-1}(k+1)w(k) \\ y_i(k+1) &= \frac{1}{C_{in}}\left(|\lambda|(y_i(k)-\delta_i(k)) + \kappa(y_{i+1}(k)-\delta_{i+1}(k))\right) \\ &+ \frac{w_i(k)}{C_{in}\Delta(k)}, \quad \forall i = 1\ldots\mu-1 \\ y_\mu(k+1) &= \frac{1}{C_{in}}|\lambda|(y_\mu(k)-\delta_\mu(k)) + \frac{w_\mu(k)}{C_{in}\Delta(k)} \end{aligned}$$

Now using the bound $y(k) \in \mathcal{B}^{ext} \Rightarrow |y_i(k)-\delta_i(k)| \leqslant 1/2$ we have

$$|y_i(k+1)| \leqslant \frac{1}{2C_{in}}\left(|\lambda| + \kappa + 2\frac{W}{\kappa^\mu \Delta_1(k)}\right), \quad \forall i = 1\ldots\mu$$

and the invariance of $\mathcal{B}^{ext}$ is ensured by making $|y_i(k+1)| < M_i/2$. This can be only attained if the latter expression is upper bounded, for which $\Delta_1(k)$ should be lower bounded, i.e. a lower limit must be set for the quantization step by constraining the Zoom In operation to $\Delta_1(k) \geqslant \Delta_{min}$ for all k. This is the price to be paid in terms of quantization resolution in the presence of noise, which

is reasonable enough as the presence of noise eventually carry variations in the steady state, rendering infinite resolution impractical.

With this analysis, the necessary data-rate condition can be stated regardless of the noise power as

$$|\lambda| < M_i \;\; \forall i = 1 \dots \mu$$

because if this condition is fulfilled, the following bound (from above)

$$|y_i(k+1)| \leqslant \frac{1}{2C_{in}} \left(|\lambda| + \kappa + 2\frac{W}{\kappa^{\mu}\Delta_{min}} \right) < \frac{M_i}{2} \; \forall i = 1 \dots \mu \tag{104}$$

will be satisfied with the appropriate choice of C_{in}, κ and Δ_{min},

Invariance of $\mathcal{B}^{ext}$ in DT mode: If the previous bound holds for $C_{in} < 1$, it will consequently be true for $C_{in} = 1$, which corresponds to the Dwell-Time mode of operation.

Condition for entering the ZO mode: This far we have proved that $\mathcal{B}^{ext}$ is an invariant both in ZI and DT modes. The transition from DT to ZO mode will be triggered by quantizer saturation ($|y_i(k)| \notin \mathcal{B}^{ext}$) only in abnormal cases, for instance due to a temporary disturbance increase above the upper bound W or to a loss of estimator synchronization (this will be discussed in the next section).

In order for the receiver to detect such event, a sequence of $\delta_i(k)$ must be unambiguously related to its occurrence. As in the noiseless case, we will prove that

$$\mathcal{C}_{\mathcal{T}} \Rightarrow y(k) \notin \mathcal{B}^{ext}$$

where the condition $\mathcal{C}_{\mathcal{T}}$ is defined as

$$\mathcal{C}_{\mathcal{T}} = \text{true if } \; \{k = k_{DT} + \nu - 1\} \wedge \left\{ \exists i, 1 \leqslant i \leqslant \mu : \Big| \sum_{j=k-\nu+1}^{k} \delta(j) \Big| = \frac{M-1}{2}\nu \right\}$$

which is equivalent to say that if $y(k_{DT}) \in \mathcal{B}^{ext}$,
then $\forall i \quad (1 \leqslant i \leqslant \mu)$, $|\sum_{j=k_{DT}}^{k_{DT}+\nu-1} \delta_i(j)| \neq \frac{M_i-1}{2}\nu$. We consider each component $y_i(k)$ separately and determine $\nu_i - 1$ as follows:

$$\begin{aligned} (\nu_i - 1) \in \mathbf{N} \;\; &> \;\; l_i \\ \nu \;\; &= \;\; \max_{1 \leqslant i \leqslant \mu} \nu_i. \end{aligned}$$

where each ν_i corresponds to an upper bound of the maximal time such that the following conditions are verified:

$$y(k_{DT}) \in \mathcal{B}^{ext} \tag{105}$$

$$\mathcal{S}_(i,k_{DT}) \cdot \sum_{j=k_{DT}}^{k_{DT}+\nu_i-2} \delta_i(j) = (\nu_i - 1)\frac{M_i - 1}{2}. \tag{106}$$

We will show that at $k_{DT}+\nu_i-1$, it is impossible to have $\mathcal{S}_(i,k_{DT})\delta(k_{DT}+\nu_i-1) = \frac{M_i-1}{2}$ which is equivalent to have $\mathcal{S}_(i,k_{DT})y_i(k_{DT}+\nu_i-1) > \frac{M_i-2}{2}$.

Thus, in what follows, we will find conditions under which the inequality $\mathcal{S}_(i,k_{DT})y_i(k_{DT}+\nu_i-1) \leqslant \frac{M_i-2}{2}$ holds. For this, it will be assumed that equations (105) and (106) are verified along the period $\forall j \in [k_{DT}, k_{DT}+\nu-2]$. From previous arguments, we know that if $y(k_{DT}) \in \mathcal{B}^{ext}$, then during all the Dwell - Time period, we have $y(j) \in \mathcal{B}^{ext}$, $\forall j \in [k_{DT}, k_{DT}+\nu-2]$. Thus, we can conclude that $|y_{i+1}(j) - \delta_{i+1}(j)| \leqslant 1/2$. From this fact and the error equation considering noise (103) it follows that:

$$\mathcal{S}_(i,k_{DT})y_i(k_{DT}+\nu_i-1) \leqslant |\lambda|^{\nu_i-1}|y_i(k_{DT})| - \left(\frac{M_i-1}{2}\right)|\lambda| \sum_{j=0}^{\nu_i-2} |\lambda|^j + \left(\frac{W}{\Delta_i(k_{DT})} + \frac{\kappa}{2}\right) \sum_{j=0}^{\nu_i-2} |\lambda|^j.$$

And under the assumption $|y_i(k_{DT})| \leqslant M_i/2$, and using the lower bound $\Delta_1(k) \geqslant \Delta_{min}$ proposed in the previous analysis for the noisy case, we have that the sufficient condition for $\mathcal{S}_(i,k_{DT})y_i(k_{DT}+\nu_i-1) \leqslant (M_i-2)/2$ thus violating $\mathcal{C}_{\mathcal{T}}$ turns into

$$|\lambda|^{\nu_i-1}\frac{M_i}{2} - \frac{M_i-1}{2}|\lambda| \left(\frac{|\lambda|^{\nu_i-1}-1}{|\lambda|-1}\right) + \left(\frac{|\lambda|^{\nu_i-1}-1}{|\lambda|-1}\right)\left(\frac{W}{\kappa^i\Delta_{min}} + \frac{\kappa}{2}\right) \leqslant \frac{M_i-2}{2}.$$

From above equation and by a direct calculation, it follows that

$$\nu_i = \nu \in \mathbf{N} \geqslant 1 + \frac{\ln\left(1 + \frac{|\lambda|+M_i+2-\kappa-\frac{2W}{\kappa^i\Delta_{min}}-\kappa}{M_i-|\lambda|-\kappa-\frac{2W}{\kappa^i\Delta_{min}}}\right)}{\ln(|\lambda|)} = \cdots \tag{107}$$

$$1 + \frac{\ln\left(1 + \frac{2(1+|\lambda|)}{M_i-|\lambda|-\kappa-\frac{2W}{\kappa^i\Delta_{min}}}\right)}{\ln(|\lambda|)}. \tag{108}$$

Note that to have above inequality, we need to assume that $M_i > |\lambda| + \kappa + \frac{2W}{\kappa^i\Delta_{min}}$.

With this choice, if $y_i(k_{DT}) \in \mathcal{B}^{ext}$, it is impossible to have a ν-long sequence of $\delta_i(k)$ fulfilling $\mathcal{C}_\mathcal{T}$. However, the backwards implication $y_i(k_{DT}) \notin \mathcal{B}^{ext} \Rightarrow$ remains uncertain. The solution is again to recode the $\delta_i(k)$ signals at the encoder side as $\mathcal{C}_\mathcal{T}$ whenever the event $y_i(k_{DT}) \notin \mathcal{B}^{ext}$ is detected (see Section 5.3.2). With that fix, the ZO mode will be triggered and the system will recover from time-limited unbounded disturbances (i.e. after an unbounded disturbance or burst, sufficient time must elapse, possibly with W-bounded noise, in order to recover the ZI mode and approach the attainable limit set).

5.5 Robustness to packet losses

A final fix to the D-ZIZO algorithm will be done in order to deal with the abnormal situation of packet losses. A lost or corrupted packet results in a bad reception of $\delta(k)$ at some instants k. For this, we will distinguish between the data and variables computed at the sender (superscript s) and their counterparts as perceived by the receiver (superscript r) whenever they differ. The state estimation dynamics turns into

$$\begin{aligned}\hat{x}^s(k+1) &= (\boldsymbol{A} - \boldsymbol{BK})\hat{x}^s(k) + \boldsymbol{AT}(k)D^s(k)\delta^s(k)\\ \hat{x}^r(k+1) &= (\boldsymbol{A} - \boldsymbol{BK})\hat{x}^r(k) + \boldsymbol{AT}(k)D^r(k)\delta^r(k)\end{aligned}$$

where $\delta^s(k) = [\delta_1^s(k), \ldots, \delta_\mu^s(k)]^T$ and $\delta^r(k) = [\delta_1^r(k), \ldots, \delta_\mu^r(k)]^T$. The estimation divergence is computed as

$$\hat{x}^e(k) = \hat{x}^r(k) - \hat{x}^s(k) = \sum_{j=0}^{k-1}(\boldsymbol{A} - \boldsymbol{BK})^{k-j}\boldsymbol{AT}(j)\underbrace{\left(D^r(j)\delta^r(j) - D^s(j)\delta^s(j)\right)}_{e(j)}.$$

and the error dynamics at the sender side will be affected by this divergence according to

$$\tilde{z}^s(k+1) = \boldsymbol{T}^{-1}(k+1)\boldsymbol{A}\boldsymbol{T}(k)(\tilde{z}^s(k) - \hat{\tilde{z}}^s(k)) + \boldsymbol{T}^{-1}(k+1)s(k) - \boldsymbol{T}^{-1}(k+1)\boldsymbol{B}\boldsymbol{K}\hat{x}^e(k)$$

However, boundedness of $\hat{x}^e(k)$ depends on boundedness of $e(j)$ and this is only guaranteed if both sender and receiver remain in ZI-DT modes. The main issue is that ZO modes may be triggered not only at the sender when the $\hat{x}^e(k)$ disturbance is large, but *anytime* at the receiver as a result of a corrupted $\delta^r(k)$ sequence (e.g. a sequence corresponding to $\mathcal{C}_\mathcal{T}$). Whatever the case is, unsynchronized ZO modes make the term $e(j)$ drift according to $D^r(k) = C_{out}^l D^r(k)$ where l is the number of times that the receiver has been unduly in ZO. As l is obviously unbounded (e.g. due to a corrupted sequence of all $\delta(k) = (M_i - 1)/2$ for all k), we have that $\hat{x}^e(k)$ is unbounded.

This difficulty is easily addressed by slightly fixing the algorithm. First, as long as the disturbance remains bounded in such a way that

$$\|\boldsymbol{T}^{-1}(k+1)(s(k) - \boldsymbol{B}\boldsymbol{K}\hat{x}^e(k))\|_\infty < W \;\; \forall k$$

with W the bound used for parameter tuning, the system will alternate naturally between ZI and DT. When, for the above reasons, the sender detects $|y(k_{DT})| \notin \mathcal{B}^{ext}$, it should transmit the sequence $\mathcal{C}_\mathcal{T}$ and both parts will enter ZO. A useful fact is that the stability proofs do not change if these ZO modes start always from predefined values, say, $\Delta_1(0) = \Delta_{min}$ and $\hat{x}_0(0) = 0$, both in receiver and transmitter. This will produce full resynchronization at ZO stages.

However, the mode synchronization at ZO is reliable only if both systems are at the present time in ZI mode. For instance, if the receiver is already in ZO, it will not obey the $\mathcal{C}_\mathcal{T}$ sequence. As the sender ignores the mode of the receiver, a safe recovery procedure is required to ensure that a number of error-free consecutive transmissions, recover full synchronization.

Assume that at time instant k the sender detects $|y(k_{DT})| \notin \mathcal{B}^{ext}$. By considering the 3x3 combined-state machine of Table 5.5, we see that the desirable position to trigger ZO is from 9, but in reality, any could be active. So, in case of saturation, the sender must do as follows,

1. Stop its Zoom machine
2. Issue a sample with the minimal values of $\delta_i(k)$ for all i (e.g. $\delta_i(k) = 0$ for

		Sender		
		ZO	DT	ZI
Receiver	ZO	1	2	3
	DT	4	5	6
	ZI	7	8	9

Table 6: Loss of synchronization in Zoom modes.

M=3) in order to drive the receiver to ZI mode[7].

3. Once position 9 is secured, a ν-long sequence of $\pm(M_i - 1)/2$ with the sign of the estimation error values would drive the receiver to ZO mode, recovering at position 1.

Then, as long as $\nu + 1$ consecutive samples are transmitted without errors, the synchronization is recovered via the normal operation of ZO.

Remark It is important to recall that this recovery procedure works as long as no packet loss occurs for a sufficiently long period of time, which may be computed in terms of the initial deviation of the estimators. Hence, the packet loss assumption is not a strictly random one, as it requires a deterministic behavior during that period. This is consisting with existing results where it is stated that it is impossible to guarantee stability in this type of systems with a strictly random (nonzero-erasure probability) channel, see for instance [73].

[7]For this case we assume that the Dwell-Time is canceled the first time a vector with non-extreme values of $\delta_i(k)$ is received instead of waiting for the whole ν-sequence.

6 Conclusions and further work

The conclusions drawn form the presented work is divided in four parts, as the contents of the document itself.

The first part proposes a novel cross-layer protocol for control applications over WSNs (TREnD), which satisfies application requirements on reliability and latency while minimizing energy consumption. In addition, it posed and solved an optimization problem to select the protocol parameters by a simple algorithm. The experimental results showed that TREnD achieves reliable and timely transmission of packets, ensuring low node duty cycle and load balancing. Moreover, TREnD outperformed some existing solutions in terms of reliability and energy efficiency.

The second part deal with the problem of robust model predictive power control within a wireless CDMA cellular network in the presence of uncertain channel fading and interference has been considered. The problem has been formulated as an open-loop min-max MPC problem in a decentralised fashion. The efficacy of the proposed robust power control law has been illustrated by various numerical test scenarios carried out on a CDMA network simulation model. The results, achieved in terms of the robust SINR tracking, reduction in transmit power, reduced occurrence of outage events, and improvements in the observed standard deviation of the tracking error, indicate that the min-max MPC exhibits superior performance when compared to other approaches.

The third part proposes a novel mechanism to configure 802.11 networks based on the dynamic selection of the contention window and retry limit parameters. This mechanism is designed with the twofold objective of maximizes the energy efficiency and provides minimum QoS levels. Extensive numerical results show that our algorithm achieves better energy efficiency and QoS performance than default 802.11 configurations. We also proves that our strategy achieves similar energy efficiency than other optimization mechanisms and outperforms it in terms of and QoS performance. Additionally, it provides new analytical expressions for energy consumption and energy efficiency which take into account the erroneous channel effect and can used for both active and power saving mode.

The fourth part introduces a new adaptive differential coding algorithm for systems controlled over digital channels subject to limited bit rate constraint. As shown, the proposed algorithm provides the global stability for general multivariable systems; while it improves transient behavior and reaches the rate theoretical limits under constant length coding. These are obtained by introducing a Dwell - Time state in addition of ZI and ZO classical modes. For future, it will be inter-

esting to consider more complicated systems, such as partially observed systems.

A Refinement for energy expression

A.1 power consumption

In order to decompose the total energy in detail, paper [34] considers an analytical model of 802.11 where timeline is divided into six kinds of slots.

1) Idle, 2) Successful reception of packet destined for the tagged station l, 3) Successful reception of packet not destined for the tagged station l 4) Reception of a collided packet, 5) Successful transmission of a packet by the tagged station l y 6) Colliding transmission of a packet by tagged station l.

We extend this energy decomposition by including the three additional kinds of slots which represent the energy wasted on transmitting or receiving an error affected packet. Then, we define the extra slots as: : 7) Erroneous transmission of a packet by tagged station l. , 8) Reception of error affected packet destined for the tagged station l, y 9) Reception of error affected packet not destined for the tagged station l. The energy consumed by each kind and its probability of occurrence are listed below:

(1) Idle slot, probability: $\tau(1-\tau)^n$

(2) Successful reception of packet destined for the tagged station l, probability: $(1-p_e)\tau(1-\tau)^{n-1}$

(3) reception of packet not destined for the tagged station l, probability: $(1-p_e)(n-2)\tau(1-\tau)^{n-1}$

(4)) Reception of a collided packet, probability: $(1-\tau)(p_c-(n-1)\tau(1-\tau)^{n-2})$

(5) Successful transmission of a packet by the tagged station l, probability: $(1-p_e)\tau(1-p_c)$

(6) Colliding transmission of a packet by tagged station l, probability: τp_c

(7) Erroneous transmission of a packet by tagged station l, probability: $p_e\tau(1-p_c)$

(8) Reception of error affected packet destined for the tagged station l con probability: $p_e\tau(1-\tau)^{n-1}$

(9) Reception of error affected packet not destined for the tagged station l. probability: $p_e(n-2)\tau(1-\tau)^{n-1}$

Putting all terms together the average energy consumption per slot can as(18).

Being J_σ, $J_s^{rx}(l)$, $J_s^{rx}(\sim l)$,J_c^{rx}, J_s^{tx}, J_c^{tx}, J_e^{tx} y J_e^{rx} the energy consumed in each kind of slot. These values can be obtained from (110).

$$\begin{aligned}
J_\sigma &= \rho_\sigma SLOT \\
J_s^{rx}(l) &= \rho_{rx}T_{DATA} + \rho_\sigma(SIFS+\delta) + \rho_{tx}T_{ACK} + \rho_\sigma(\delta+DIFS) \\
J_s^{rx}(\sim l) &= \rho_{rx}T_{DATA} + \rho_\sigma(SIFS+\delta) + \rho_{rx}T_{ACK} + \rho_\sigma(\delta+DIFS) \\
J_c^{rx} &= \rho_{rx}T_{DATA} + \rho_\sigma(EIFS+\delta) \\
J_s^{tx} &= \rho_{tx}T_{DATA} + \rho_\sigma(SIFS+\delta) + \rho_{rx}T_{ACK} + \rho_\sigma(\delta+DIFS) \\
J_c^{tx} &= \rho_{tx}T_{DATA} + \rho_\sigma(EIFS+\delta) \\
J_e^{tx} &= J_c^{tx} \\
J_e^{rx} &= J_c^{rx}
\end{aligned} \tag{110}$$

Where ρ_σ, ρ_{rx}, ρ_{tx} and ρ_{psm} is the power (Watts) consumed in idle, transmit, receive and sleep state, respectively. T_{DATA} represents the time taken to send a data packet of size P, T_{ACK} is the time taken to send ACK packet, and δ is the propagation delay.

A.2 Energy efficiency

We solve the equation $dE_f/d\tau = 0$ using the expression $E[J_{ts}]$ given in 18 with the aim of calculating the optimal probability τ_{opt}^e accurately. After deriving and some algebra, we get:

$$\begin{aligned}
(p_e-1)PL(1-\tau)^n \Big[&-J_\sigma(1-\tau)^n + J_c^{tx}(n-1)\tau^2 \\
&+J_c^{rx}(-1+(1-\tau)^n - n(\tau-1)\tau+\tau^2)\Big] = 0
\end{aligned} \tag{111}$$

Note that p_e is a common factor which can be cancelled. It means that optimal probability τ_{opt}^e does not depend on the probability p_e. We can solve this equation

analytically by making the common assumption $\tau << 1$. Then

$$\frac{1}{2}\Big[-2J_c^{tx} + J_c^{rx}(n-2)(n-1) \\ +2n(J_c^{tx} + J_\sigma - 2J_\sigma n)\Big]\tau^2 + 2n\tau J_\sigma - J_\sigma = 0 \quad (112)$$

Solving the equation for τ and after some algebra, we canwrite the optimal probability τ_{opt}:

$$\tau_{opt}^e = \frac{1}{n + \frac{\sqrt{J_\sigma(n-1)(2J_c^{tx} + (n-2)J_c^{rx} - 2nJ_\sigma)}}{\sqrt{2}J_\sigma}} \quad (113)$$

Assuming that the term $n \cdot J_c^{rx}$ is dominant and approximating $n-1$ and $n-2$ as n we get:

$$\tau_{opt}^e = \frac{1}{n}\frac{1}{1 + \sqrt{\frac{J_c^{rx}}{2J_\sigma}}} \approx \frac{1}{n}\sqrt{\frac{2J_\sigma}{J_c^{rx}}} \approx \frac{1}{n}\sqrt{\frac{2J_\sigma}{\rho_{rx}T_s}} \quad (114)$$

which is the result found in [90]. We compares both expression in Fig. 31. Serrano's expression underestimate the maximal energy efficiency due to it provides an optimal transmission probability lower than the real one.

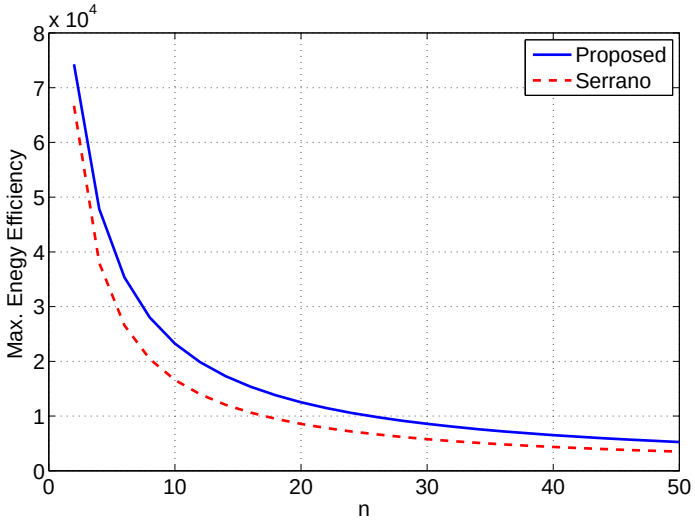

Figure 31: Maximum energy effiency resulting from appling the two possible expressions of τ^e_{opt}. The packet error probability is 0.5.

B Modelling q under big buffer size assumption

Assuming a M/M/1/k queue of length k with Markovian arrival and departure, we can define the probability that the queue is nonempty q according to [58]:

$$q = 1 - p_0 = \frac{f_s\overline{T}_{svc} - (f_s\overline{T}_{svc})^{k+1}}{1 - (f_s\overline{T}_{svc})^{k+1}} \tag{115}$$

Where fs is the packet arrival rate and ,$\overline{T}_{svc}$ is the average service time. These alternative expressions consider the queue waiting time which is relevant if the stations' buffer size is not negligible.

References

[1] A. Bonivento, C. Fischione, L. Necchi, F. Pianegiani, and A. Sangiovanni-Vincentelli. System Level Design for Clustered Wireless Sensor Networks. *IEEE Trans. on Industrial Informatics*, August 2007.

[2] Ö. B. Akan and F. Akyildiz. Event-to-Sink Reliable Transport in Wireless Sensor Networks. *IEEE Trans. on Networking*, 13, 2005.

[3] S.M.M. Alavi and M.J. Hayes. Robust power control for cdma cellular communication networks using quantitative feedback theory. pages 5080–5085, 2007.

[4] S. Ariyavisitakul and L.F Chang. Signal and interference statistics of a cdma system with feedback power control. *IEEE Transactions on Communications*, 41(11):1626–1634, 1993.

[5] S. Azuma and T. Sugie. Optimal dynamic quantizers for discrete - valued input control. *Automatica*, 44:396–406, 2008.

[6] S. Baek and B. D. Choi. Performance analysis of power save mode in ieee 802.11 infrastructure wireless local area network. *Journal of Industrial and Management Optimization*, 5(3):481–492, 2009.

[7] J. Bailleul and P.Antsaklis. Control and communication challenges in networked real time systems. *Proceedings of the IEEE*, 95:9–28, 2007.

[8] A. Banchs, X. Perez-Costa, and D. Qiao. Providing throughput guarantees in ieee 802.11e wireless lans. In *Proceedings of the 18th International Teletraffic Congress (ITC-18)*, pages 1001–1010, 2003.

[9] G. Bianchi. Performance analysis of the ieee 802.11 distributed coordination function. *IEEE Journal on Selected Areas in Communications*, 18(3):535–547, 2000.

[10] Giuseppe Bianchi, Luigi Fratta, and Matteo Oliveri. Performance evaluation and enhancement of the csma/ca mac protocol for 802.11 wireless lans. In *IEEE International Symposium on Personal, Indoor and Mobile Radio Communications (PIMRC)*, volume 2, pages 392–396, 1996.

[11] L. Bononi, M. Conti, and E. Gregori. Runtime optimization of ieee 802.11 wireless lans performance. *IEEE Transactions on Parallel and Distributed Systems*, 15(1):66–80, 2004.

[12] B.Picasso, F. Gouaisbaut, and A. Bicchi. Construction of invariant and attractive sets for quantized input linear systems. In *Conference on Decision and Control*, 2002.

[13] R.W. Brockett and D. Liberzon. Quantized feedback stabilization of linear systems. *IEEE Transactions on Automatic Control*, 45(7):1279–1289, July 2000.

[14] Nicolas Burri, Pascal von Rickenbach, and Roger Wattenhofer. Dozer: ultra-low power data gathering in sensor networks. In *ACM IPSN 2007*, 2007.

[15] F. Calì, M. Conti, and E. Gregori. Dynamic tuning of the ieee 802.11 protocol to achieve a theoretical throughput limit. *IEEE/ACM Transactions on Networking*, 8(6):785–799, 2000.

[16] E.F. Camacho and C. Bordons. *Model predictive control*. Springer Verlag, 2004.

[17] C. Canudas-de-Wit, F. Rubio, J. Fornes, and F. Gómez-Estern. Differential coding in networked controlled linear systems. *American Control Conference. Silver Anniversary ACC. Minneapolis, Minnesota USA*, June 2006.

[18] M. M. Carvalho, C. B. Margi, K. Obraczka, and J. J. Garcia-Luna-Aceves. Modeling energy consumption in single-hop ieee 802.11 ad hoc networks. In *13th International Conference on Computer Communications and Networks (ICCCN 2004).*, pages 367–372, 2004.

[19] D. S. Chan, T. Berger, and R. Bridgelall. Energy efficiency of csma protocols for wireless packet switched networks. In *IEEE Wireless Communications and Networking Conference (WCNC 2004)*, volume 1, pages 447–452, 2004.

[20] S. Yu Chang. Energy-delay analysis of wireless networks over rayleigh fading channel. In *Wireless Telecommunications Symposium*, pages 197–201, 2005.

[21] P. Chatzimisios, A. C. Boucouvalas, and V. Vitsas. Ieee 802.11 packet delay-a finite retry limit analysis. In *IEEE Global Telecommunications Conference 2003 (GLOBECOM '03)*, volume 2, pages 950–954, 2003.

[22] P. Chatzimisios, A. C. Boucouvalas, and V. Vitsas. Performance analysis of ieee 802.11 dcf in presence of transmission errors. In *IEEE International Conference on Communications*, volume 7, pages 3854–3858, 2004.

[23] P. Chatzimisios, V. Vitsas, and A. C. Boucouvalas. Throughput and delay analysis of ieee 802.11 protocol. In *Networked Appliances, 2002. Liverpool. Proceedings. 2002 IEEE 5th International Workshop on*, pages 168–174, 2002.

[24] B. Chen, K. Jamieson, H. Balakrishnan, and R. Morris. Span: An Energy-Efficient Coordination Algorithm for Topology Maintenance in Ad Hoc Wireless Networks. *MobiCom*, 2001.

[25] X. Chen, H. Zhai, X. Tian, and Y. Fang. Supporting qos in ieee 802.11 e wireless lans. *IEEE Transactions on Wireless Communications*, 5(8):2217–2227, 2006.

[26] L. Chisci, R. Fantacci, L. Mucchi, and T. Pecorella. A queue-based approach to power control in wireless communication networks. *IEEE Transactions on Wireless Communications*, 7(1):128–134, 2008.

[27] R. G. Cole and J. H. Rosenbluth. Voice over ip performance monitoring. *ACM SIGCOMM Computer Communication Review*, 31(2):9–24, 2001.

[28] F. Daneshgaran, M. Laddomada, F. Mesiti, and M. Mondin. A model of the ieee 802.11 dcf in presence of non ideal transmission channel and capture effects. In *IEEE Global Telecommunications Conference, 2007 (GLOBECOM '07)*, pages 5112–5116, 2007.

[29] D.F Delchamps. Stabilizing a linear system with quantized state feedback. *IEEE Transactions on Automatic Control*, 35, no 8:916–924, Aug. 1990.

[30] J.C. Delvenne. An optimal quantized feedback strategy for scalar linear systems. *IEEE Transactions on Automatic Control*, 51:298–303, 2006.

[31] D. J Deng, C. H Ke, H. H Chen, and Y. M Huang. Contention window optimization for ieee 802.11 dcf access control. *IEEE Transactions on Wireless Communications*, 7(12):5129–5135, 2008.

[32] P. Di Marco, P. Park, C. Fischione, and K. H. Johansson. A Cross-Layer Protocol for Wireless Sensor Networks in Control and Automation. Technical report, Royal Institute of Technology (KTH), August 2009.

[33] N. Elia and S.-K. Mitter. Stabilization of linear systems with limited information. *IEEE Transactions on Automatic Control*, 46(9):1384–1400, September 2001.

[34] M. Ergen and P. Varaiya. Decomposition of energy consumption in ieee 802.11. In *IEEE International Conference on Communications, 2007. ICC '07.*, pages 403–408, 2007.

[35] F. Fagnani and S. Zampieri. Stability analysis an synthesis for scalar linear systems with a quantized feedback. *IEEE Transactions on Automatic Control*, 48:1569–1584, 2003.

[36] E. Felemban, C.-G. Lee, and E. Eylem. MMSPEED: Multipath Multi-SPEED Protocol for QoS Guarantee of Reliability and Timeliness in Wireless Sensor Networks. *IEEE Trans. on Mobile Computing*, 5(6), June 2006.

[37] E. Ferro and F. Potortì. Bluetooth and wi-fi wireless protocols: A survey and a comparison. *IEEE Wireless Communications*, 12(1):12–26, 2005.

[38] G.J. Foschini and Z. Miljanic. Simple distributed autonomous power control algorithm and its convergence. *IEEE Transactions on Vehicular Technology*, 42(4):641–646, 1993.

[39] M. Fu and L. Xie. The sector bound approach to quantized feedback control. *IEEE Trans. On Automatic Control*, 50:1698–1711, 2005.

[40] D. Gay, P. Levis, and D. Culler. Software Design Patterns for TinyOS. *LCTES*, 2005.

[41] F. Gómez-Estern, C. Canudas-de-Wit, F. Rubio, and J. Fornes. Adaptive delta-modulation coding in networked controlled systems. *American Control Conference, New York, USA*, June 2007.

[42] F. Gunnarsson and F. Gustafsson. Control theory aspects of power control in umts. *Control Engineering Practice*, 11(10):1113–1125, 2003.

[43] P. Havinga and G. Smit. Energy-efficient TDMA medium access control protocol scheduling. In *Asian International Mobile Computing Conference (AMOC 2000)*, pages 1–9. Citeseer, 2000.

[44] J. P. Hespanha, P. Naghshtabrizi, and Yonggang Xu. A survey of recent results in networked control systems. *Proceedings of the IEEE*, 2007.

[45] M. Heusse, F. Rousseau, R. Guillier, and A. Duda. Idle sense: An optimal access method for high throughput and fairness in rate diverse wireless lans. In *Computer Communication Review*, volume 35, pages 121–132, 2005.

[46] M. Hirsch and S. Smale. *Differential Equations, Dynamical Systems, and Linear Algebra*. San Diego, CA: Academic, 1974.

[47] R. P. F. Hoefel. A mac and phy analytical cross-layer model for energy consumption in ieee 802.11 networks. In *Telecommunications Symposium, 2006 International*, pages 237–242, 2006.

[48] IEEE, 3 Park Avenue, New York, USA. *IEEE 802.15.4*, 2006.

[49] J.-P. Hespanha , A. Ortega , and L. Vasudevan . Towards the control of linear systems with minimum bit–rate. In *15th Int. Symp. Mathematical Theory of Networks and Systems (MTNS)*, Notre Dame, IL, USA, 2002.

[50] S. Jagannathan, M. Zawodniok, and Q. Shang. Distributed power control for cellular networks in the presence of channel uncertainties. *IEEE Transactions on Wireless Communications*, 5(2):540–549, 2006.

[51] J. Jaglin, C. Canudas de Wit, A. Farhadi, and F. Gómez-Estern. Dwell - time robust adaptive delta modulation signal coding for networked control systems. In *submitted to 50th IEEE Conference on Decision and Control*, 2011.

[52] J. Jaglin, C. Canudas de Wit, and C. Siclet. Delta modulation for multivariable centralized linear networked controlled systems. In *Control and Decision Conference, Cancun, Mexico*, 2008.

[53] Y. Jihwang and A. Agrawala. Packet error model for the ieee 802.11 mac protocol. In *14th IEEE Proceedings on Personal, Indoor and Mobile Radio Communications, 2003. PIMRC 2003.*, volume 2, pages 1722–1726 vol.2, 2003.

[54] E. S Jung and N. H. Vaidya. Improving ieee 802.11 power saving mechanism. *Wireless Networks*, 14(3):375–391, 2008.

[55] S. Kandukuri and S. Boyd. Optimal power control in interference-limited fading wireless channels with outage-probability specifications. *IEEE Transactions on Wireless Communications*, 1(1):46–55, 2002.

[56] S.R. Kao, C.-Y. Venkatesh. Stabilization of linear systems with limited information multiple input case. In *American Control Conference*, 2002.

[57] Sukun Kim, Rodrigo Fonseca, Prabal Dutta, Arsalan Tavakoli, David Culler, Philip Levis, Scott Shenker, and Ion Stoica. Flush: a reliable bulk transport protocol for multihop wireless networks. In *ACM SenSys 2007*, 2007.

[58] L. Kleinrock. *Queueing systems, volume 1: theory*. John Wiley & Sons, 1975.

[59] A.N. Kolmogorov. New metric invariant of transitive dynamical systems and endomorphisms of lebesgue spaces. *Doklady of Russian Academy of Sciences*, 119:861–864, 1958.

[60] S. Koskie and Z. Gajic. Signal-to-interference-based power control for wireless networks: A survey, 1992-2005. *Dynamics of Continuous, Discrete and Impulsive Systems Series B: Applications and Algorithms*, 13(2):187–220, 2006.

[61] M. Laddomada, F. Mesiti, M. Mondin, and F. Daneshgaran. On the throughput performance of multirate ieee 802.11 networks with variable-loaded stations: Analysis, modeling, and a novel proportional fairness criterion. *IEEE Transactions on Wireless Communications*, 9(5):1594–1607, 2010.

[62] B.-K. Lee, Y.-H. Chen, and B.-S. Chen. Robust $\mathcal{H}_\infty$ power control for cdma cellular communication systems. *IEEE Transactions on Signal Processing*, 54(10):3947–3956, 2006.

[63] Q. Li and M. Van Der Schaar. Providing adaptive qos to layered video over wireless local area networks through real-time retry limit adaptation. *IEEE Transactions on Multimedia*, 6(2):278–290, 2004.

[64] Y. S. Liaw, A. Dadej, and A. Jayasuriya. Performance analysis of ieee 802.11 dcf under limited load. In *2005 Asia-Pacific Conference on Communications*, volume 2005, pages 759–763, 2005.

[65] D. Liberzon. On stabilization of linear systems with limited information. *IEEE Transactions on Automatic Control*, 48(2):304–307, February 2003.

[66] D. Liberzon and D. Nesic. Input to state stabilization of linear systems with quantized state measurements. *IEEE Transactions on Automatic Control*, Volume 52 no. 5:767–781, 2007.

[67] J. Liu, D. Yuan, S. Ci, and Y. Zhong. Nonlinear optimization for energy efficiency in ieee 802.11a wireless lans. *Computer Communications*, 29(17):3455–3466, 2006.

[68] I. Lopez, C.T. Abdallah, and C. Canudas-de-Wit. Compensation schemes for a delta-modulation-based ncs. *ECC'07 KOS, Greece*, 2007.

[69] E. Anderson M. Buettner, G. Yee and R. Han. X-MAC: A Short Preamble MAC Protocol For Duty-Cycled Wireless Sensor Networks. In *4th ACM Conference on Embedded Sensor Systems (SenSys)*, November 2006.

[70] M. Zuniga, B. Krishnamachari. Analyzing the transitional region in low power wireless links. *IEEE SECON*, 2004.

[71] D. Malone, P. Clifford, and D. J. Leith. Mac layer channel quality measurement in 802.11. *IEEE Communications Letters*, 11(2):143–145, 2007.

[72] David Malone, Ken Duffy, and Doug Leith. Modeling the 802.11 distributed coordination function in nonsaturated heterogeneous conditions. *IEEE/ACM Transactions on Networking*, 15(1):159–172, 2007.

[73] A.S. Matveev and A.V. Savkin. Comments on control over noisy channels and relevant negative results. *IEEE Transactions on Automatic Control*, 50:2105–2110, 2005.

[74] P. Minero, M. Franceschetti, S. Dey, and G. Nair. Data rate theorem for stabilization over time varying feedback channels. *IEEE Transactions on Automatic Control*, 54:243–255, 2009.

[75] Moteiv. *Tmote Sky Data Sheet*, 2006.

[76] G.N. Nair and R.J. Evans. Stabilization with data rate limited feedback: Tightest attainable bounds. *System and Control Letters*, 41:49–56, 2000.

[77] G.N. Nair, F. Fagnani, S. Zampieri, and R.J. Evans. Feedback control under data rate constraints: An overview. *Proceeding of the IEEE*, 95:108–136, 2007.

[78] Qiang Ni, T. Li, Thierry Turletti, and Yang Xiao. Saturation throughput analysis of error-prone 802.11 wireless networks. *Wireless Communications and Mobile Computing*, 5(8):945–956, 2005.

[79] O. Younis and S. Fahmy. HEED: A Hybrid, Energy-efficient, Distributed Clustering Approach for Ad Hoc Sensor Networks. *IEEE Trans. on Mobile Computing*, 3(4), Oct.-Dec. 2004.

[80] C. Oliveira and P. Pardalos. A Survey of Combinatorial Optimization Problems in Multicast Routing. *Computers and Operations Research*, Aug. 2005.

[81] Technologies Inc. OPNET. http://www.opnet.com/, 2010.

[82] P. Park, C. Fischione, A. Bonivento, K. H. Johansson, and A. Sangiovanni-Vincentelli. Breath: a Self-Adapting Protocol for Wireless Sensor Networks. *IEEE SECON*, June 2008.

[83] P. Patras, Albert Banchs, and Pablo Serrano. A control theoretic approach for throughput optimization in ieee 802.11e edca wlans. *Mobile Networks and Applications*, 14(6):697–708, 2009.

[84] D.M. De La Peña, T. Álamo, D.R Ramírez, and E.F. Camacho. Min-max model predictive control as a quadratic program. *IET Control Theory and Applications*, 1(1):328–333, 2007.

[85] F. De Pellegrini, D. Miorandi, S. Vitturi, and A. Zanella. On the use of wireless networks at low level of factory automation systems. *IEEE Transactions on Industrial Informatics*, 2(2):129–143, 2006.

[86] J.G. Proakis. *Digital Communications*. McGraw-Hill, Inc. Series in electrical and computer engineering, 2001.

[87] T.S. Rappaport et al. *Wireless communications: principles and practice*, volume 207. Prentice Hall PTR New Jersey, 1996.

[88] I. Rec. G. 109, 1999. ITU-T Recommendation G. 109, 1999. Definition of categories of speech transmission quality. *International Telecommunication Union, CH-Geneva*.

[89] K. Sakakibara, H. Nakagawa, and J. Yamakita. Analysis of energy consumption of ieee 802.11 dcf under non-saturation conditions. In *1st International Symposium on Wireless Pervasive Computing*, page 6, 2006.

[90] P. Serrano, A. Garcia-Saavedra, M. Hollick, and A. Banchs. On the energy efficiency of ieee 802.11 wlans. In *Wireless Conference (EW), 2010 European*, pages 932–939, 2010.

[91] Pablo Serrano, Albert Banchs, P. Patras, and A. Azcorra. Optimal configuration of 802.11e edca for real-time and data traffic. *Vehicular Technology, IEEE Transactions on*, PP(99):1–1, 2010.

[92] Y. Sharon and D. Liberzon. Input - to - state stabilization with minimum number of quantization regions. In *Conference on Decision and Control*, 2007.

[93] Md A. R. Siddique and J. Kamruzzaman. Performance analysis m-retry beb based dcf under unsaturated traffic condition. In *IEEE Wireless Communications and Networking Conference, WCNC*, 2010.

[94] E. I. Silva, G. C. Goodwin, D. E. Quevedo, and M. S. Derpich. Optimal noise shaping for networked control systems. In *European Control Conference*, 2007.

[95] Ya.G. Sinai. On the notion of entropy of a dynamical system. *Doklady of Russian Academy of Sciences*, 124:768–771, 1959.

[96] F. Stann and J. Heidemann. RMST: Reliable Data Transport in Sensor Networks. In *IEEE SNPA*, 2003.

[97] S. Tatikonda and S. K. Mitter. Control under communications constraints. *IEEE Transactions on Automatic Control*, 49(7):1056–1068, July 2004.

[98] I. Tinnirello and A. Sgora. A kalman filter approach for distinguishing channel and collision errors in ieee 802.11 networks. In *IEEE Global Telecommunications Conference, 2008. IEEE GLOBECOM 2008.*, pages 1–5, 2008.

[99] A. L. Toledo, T. Vercauteren, and X. Wang. Adaptive optimization of ieee 802.11 dcf based on bayesian estimation of the number of competing terminals. *IEEE Transactions on Mobile Computing*, 5(9):1283–1296, 2006.

[100] W. Heinzelman, A. Chandrakasan, and H. Balakrishnan. An Application-Specific Protocol Architecture for Wireless Microsensor Networks. *IEEE Trans. on Wireless Communications*, Oct. 2002.

[101] W. Zhang, M. S. Braniky, S. M. Phillips. Stability of Networked Control Systems. *IEEE Control Systems Magazine*, 2001.

[102] C. Wang and W. Tang. A probability-based algorithm to adjust contention window in ieee 802.11 dcf. In *2004 International Conference on Communications, Circuits and System*, volume 1, pages 418–422, 2004.

[103] Xiaodong Wang and D. P. Agrawal. Analysis and optimization of energy efficiency in 802.11 distributed coordination function. In *IEEE International Conference on Performance, Computing, and Communications, 2004*, pages 707–712, 2004.

[104] A. Willig. Recent and emerging topics in wireless industrial communications: A selection. *IEEE Transactions on Industrial Informatics*, 4(2):102–122, 2008.

[105] A. Willig. Recent and Emerging Topics in Wireless Industrial Communication. *IEEE Trans. on Industrial Informatics*, 4,2, May 2008.

[106] A. Willig, K. Matheus, and A. Wolisz. Wireless technology in industrial networks. *Proceedings of the IEEE*, 93(6):1130–1151, 2005.

[107] H. Witsenhausen. A minimax control problem for sampled linear systems. *IEEE Transactions on Automatic Control*, 13(1):5–21, 1968.

[108] W.S. Wong and R.W. Brockett. Systems with finite communication bandwidth constraints, ii,: Stabilization with limited information feedback. *IEEE Transactions on Automatic Control*, 44, no 5:1049–1053, May 1999.

[109] Yang Xiao and Y. Pan. Differentiation, qos guarantee, and optimization for real-time traffic over one-hop ad hoc networks. *IEEE Transactions on Parallel and Distributed Systems*, 16(6):538–549, 2005.

[110] R.D. Yates. A framework for uplink power control in cellular radio systems. *IEEE Journal on Selected Areas in Communications*, 13(7):1341–1347, 1995.

[111] J. Yin, X. Wang, and D. P. Agrawal. Energy efficiency evaluation of wireless lan over bursty error channel. In *IEEE Global Telecommunications Conference, 2005. GLOBECOM '05.*, volume 6, pages 5 pp.–3632, 2005.

[112] A. Zanella and F. Pellegrini. Mathematical analysis of ieee 802.11 energy efficiency. In *Proc. WPMC*. Sept, 2004.

[113] H. Zhai, X. Chen, and Y. Fang. How well can the ieee 802.11 wireless lan support quality of service? *IEEE Transactions on Wireless Communications*, 4(6):3084–3094, 2005.

[114] J. Zhu and A. O. Fapojuwo. A new call admission control method for providing desired throughput and delay performance in ieee802.11e wireless lans. *IEEE Transactions on Wireless Communications*, 6(2):701–709, 2007.

[115] M. Zorzi and R.R. Rao. Energy and Latency Performance of Geographic Random Forwarding for Ad hoc and Sensor Networks. *IEEE WCNC'03*.